1990

Characterization of mono- and multi-molecular assemblies at glassy carbon and noble metals by ex situ and in situ infrared external reflection spectroscopy

Scott Marlan Stole
Iowa State University

Order Number 9110570

Characterization of mono- and multimolecular assemblies at glassy carbon and noble metals by *ex situ* and *in situ* infrared external reflection spectroscopy

Stole, Scott Marlan, Ph.D.

Iowa State University, 1990

U·M·I
300 N. Zeeb Rd.
Ann Arbor, MI 48106

Characterization of mono- and multi-molecular assemblies at glassy carbon and noble metals by ex situ and in situ infrared external reflection spectroscopy

by

Scott Marlan Stole

A Dissertation Submitted to the
Graduate Faculty in Partial Fulfillment of the
Requirements for the Degree of
DOCTOR OF PHILOSOPHY

Department: Chemistry
Major: Analytical Chemistry

Approved:

Signature was redacted for privacy.

Signature was redacted for privacy.

In Charge of Major Work

Signature was redacted for privacy.

For the Major Department

Signature was redacted for privacy.

For the Graduate College

Iowa State University
Ames, Iowa

1990

TABLE OF CONTENTS

DEDICATION

This dissertation is dedicated to my wife, Donna, who supported me through the difficult times, and who rejoiced with me when things went well. She deserves much of the credit for this work, and I will be eternally grateful to her for all she has done.

GENERAL INTRODUCTION

In recent years, interest in the chemistry and physics of interfaces has led to the emergence of a vigorous area of research which utilizes characterization methodologies from a variety of disciplines (1-6), including contact angle measurements, ellipsometry, infrared spectroscopy (IRS), scanning tunneling microscopy (STM), electrochemistry, Auger electron spectroscopy (AES), electron microscopy, ultraviolet photoelectron spectroscopy (UPS), X-ray photoelectron spectroscopy (XPS), low energy electron diffraction (LEED), and electron energy loss spectroscopy (EELS). Central to this emergence is the recognition that interfacial phenomena play critical roles in the fabrication and performance of a variety of technologically significant materials and surface processes, for example, adhesion, corrosion control, tribology (friction and wear), biocompatibility, catalysis, and microelectronics. For instance, the development of strategies to enhance adhesion at the fluoropolymer-metal interface promises to advance the large scale integration of microelectronic devices. In contrast, schemes to reduce bacterial adhesion are critical to the implantation of complex prosthetic devices, such as joint replacements and artificial hearts. Consequently, furthering the understanding of the interactions between the substrate and the adsorbate is critical to the development of a multitude of products and applications.

On a more fundamental level, the technological developments made and the information gleaned from these applications will serve to increase an understanding of the chemical and physical interactions which occur at interfaces. For example, the attribution of a nominally simple macroscopic property such as wetting to a precise microscopic description is enormously difficult at present. More involved interfacial phenomena and processes are characterized by a correspondingly increased level of complexity. As a consequence, the development of models to describe accurately interfacial properties demands a systematic examination of each of the fundamental components that affect the properties and hence, the performance characteristics of an interface. Specific questions include:

1. What is the chemical identity of the surface species?
2. What is the mode of attachment of the analyte to the surface (i.e., ionically or covalently bonded)?
3. How is a film of the adsorbate spatially organized on the surface? (i.e., commensurate or non-commensurate, densely or loosely packed, crystalline or amorphous, etc.)
4. How does the morphology of the substrate effect the integrity of the adsorbed film?
5. What is the effect of the surrounding environment on the molecular order of an adsorbed film?

6. How do the above effect the function and long-term performance of the interface?
7. What levels and distributions of surface structures are necessary to achieve the desired performance?

The search for answers to these questions poses one of the most formidable challenges in interfacial science today. Not only is it necessary to develop an integrated approach to construct and to control the architecture of the surface microstructure, but the capability to characterize these structures at a molecular level, i.e., composition, spatial orientation, surface coverage, and reactivity, must also be achieved. Furthermore, while information from all types of surface methodologies must be incorporated into any phenomenological description of the interface, it is also essential to characterize these systems in the environment in which they are utilized, insuring a direct correlation between the interfacial structure and its performance.

Infrared spectroscopy (IRS), like other vibrational spectroscopies, provides information regarding the identity or chemical functionality of a species in terms of 'group frequencies' that can be directly related to those of known samples. In addition, by the careful application of classical electromagnetic theory, IRS can provide a description of the spatial arrangement (orientation) of an adsorbate. It is also important to note that, while providing a wealth of information about these systems, many of the surface physics

techniques are not directly applicable to investigations of interfaces in the laboratory atmosphere or in contact with solution. These techniques, which include EELS, XPS, AES, and LEED, require ultra-high vacuum conditions to attain usable electron mean free path lengths. Careful transfer experiments have recently permitted an *in vacuo* characterization of electrode surfaces after the adsorption of an analyte from solution with these techniques (7-9). However, the integrity of the sample may be compromised as a result of its removal from the electrochemical cell.

This dissertation describes the utilization of infrared external reflection spectroscopy (IR-ERS) as a means of elucidating many of the aforementioned interfacial properties of polymer films and mono- and multimolecular films at both semiconducting glassy carbon and conducting noble metal surfaces. Theory of the reflection phenomenon and its applicability to the acquisition and interpretation of these spectra is presented along with a discussion of previous investigations using this method. The sections following describe the utilization of these methods as part of a multidisciplinary examination of a polymer film coated at glassy carbon, and monolayer films at gold and silver, both in the laboratory ambient and under a solvent layer. A discussion of the future of these methodologies concludes the manuscript.

SECTION I. INTRODUCTION TO THE PRINCIPLES GOVERNING THE ACQUISITION OF INFRARED EXTERNAL REFLECTION SPECTRA OF MONO- AND MULTI-MOLECULAR FILMS ON SEMICONDUCTING AND CONDUCTING MATERIALS

INTRODUCTION

The basis for applying IR-ERS to the characterization of thin films on surfaces was originally developed by Greenler (10-11), and by Francis and Ellison (12). These efforts defined the dependence of a reflection spectrum on the optical properties of the adsorbate and metal substrate, and on the angle of incidence and polarization of the incident light. This chapter first summarizes these earlier works and provides a general description of the properties of electromagnetic radiation and the boundary conditions that govern its passage from one medium to another. Examples are then given to illustrate the utility of IR-ERS for probing the composition and spatial arrangement of thin polymeric films and monomolecular assemblies at surfaces with a high reflectivity (i.e., metals).

PROPAGATION OF ELECTROMAGNETIC RADIATION

The instantaneous magnitude of the oscillating electric field vector, $\hat{\mathbf{E}}$, which is found from the time-dependent solutions of Maxwell's equations for a uniform isotropic medium is:

$$\hat{\mathbf{E}} = E^{\circ} \exp\left[i\left(\omega t - \frac{2\pi \hat{n}}{\lambda} \mathbf{s}\cdot\mathbf{r}\right)\right] \qquad (1)$$

where the complex refractive index of the medium is defined as $\hat{n} = n + ik$, with n being the real refractive index of the medium, and k the absorption index. The term E^0 is the maximum amplitude of the wave, λ is the wavelength in a vacuum, ω is the angular frequency, $\mathbf{s}$ is a unit vector in the direction of propagation, and $\mathbf{r}$ is a position vector. The wavelength is related to the angular frequency by $\omega = 2\pi c/\lambda = 2\pi\nu$, where ν is the radiation frequency. As shown in Eq. 1, $\hat{\mathbf{E}}$ is typically treated as a complex-valued function of time t and is treated in terms of the spatial coordinates x, y, and z. This figuration is more convenient for mathematical manipulations than the use of a real-valued trigonometric function. An expression similar to Eq. 1 can also be written for the magnetic field vector, $\hat{\mathbf{H}}$. Thus, the periodicity of both the electric and magnetic fields are defined in time and space by λ.

It should also be noted that the refractive index is related to the dielectric constant, $\hat{\varepsilon}$, by:

$$\hat{n} = \sqrt{\mu\hat{\varepsilon}} \qquad (2)$$

and the magnetic permeability, μ, equals unity at optical frequencies. Therefore, since $\hat{n}$ is complex, $\hat{\varepsilon}$ for absorbing materials is also complex and can be written as:

$$\hat{\varepsilon} = \varepsilon' - i\varepsilon'' \qquad (3)$$

where ε' and ε'' are linked to n and k as:

$$\varepsilon' = n^2 - k^2 \qquad (4)$$

$$\varepsilon'' = 2nk. \qquad (5)$$

For infrared spectroscopy, the optical properties of each phase are, therefore, completely defined by a set of optical functions: n and k, or ε' and ε''. Physically, ε' and ε'' are related to the frequency dependent polarizability and the conductivity of the medium, respectively. A single complex function, as in either of the following equations, completely defines the optical properties of a homogeneous isotropic medium at any wavenumber, $\bar{\nu}$:

$$\hat{n}(\bar{\nu}) = n(\bar{\nu}) + ik(\bar{\nu}) \qquad (6)$$

$$\hat{\varepsilon}(\bar{\nu}) = \varepsilon'(\bar{\nu}) + i\varepsilon''(\bar{\nu}). \qquad (7)$$

OPTICAL THEORY FOR REFLECTION SPECTROSCOPY

In a reflection spectroscopy experiment, electromagnetic radiation interacts with more than one optical medium. In its simplest approximation, such an experiment can be depicted as a stratified medium with two optically isotropic phases that are separated by a plane boundary, as shown in Figure 1. The entry phase is transparent, whereas the optical functions of the second phase may be complex. It is useful at this juncture to define the axes and planes which will be used in the following discussion. If the surface of the substrate is denoted as the x-y plane with the z-axis oriented along the surface normal, then the path of the incident light is defined as the x-z plane. Light polarized parallel to the x-z plane is denoted as p-polarized and light perpendicular to this plane is denoted as s-polarized. The angle of incidence is measured from the surface normal. The mean square electric field (MSEF) at the surface along each of the axes is denoted as E_t, and the incident MSEF is denoted as E_t^0, where $t = x$, y, or z respectively.

An n-phase stratified medium representing a multilayered system is given is Figure 2. An example of such a system is a polymer film at a Au surface in contact with H_2O. This system would be composed of 5 phases: air (or N_2), the window material, H_2O, the polymer film, and the Au substrate. The characteristics of the three- and n-phase media are defined by the optical functions of each phase j as:

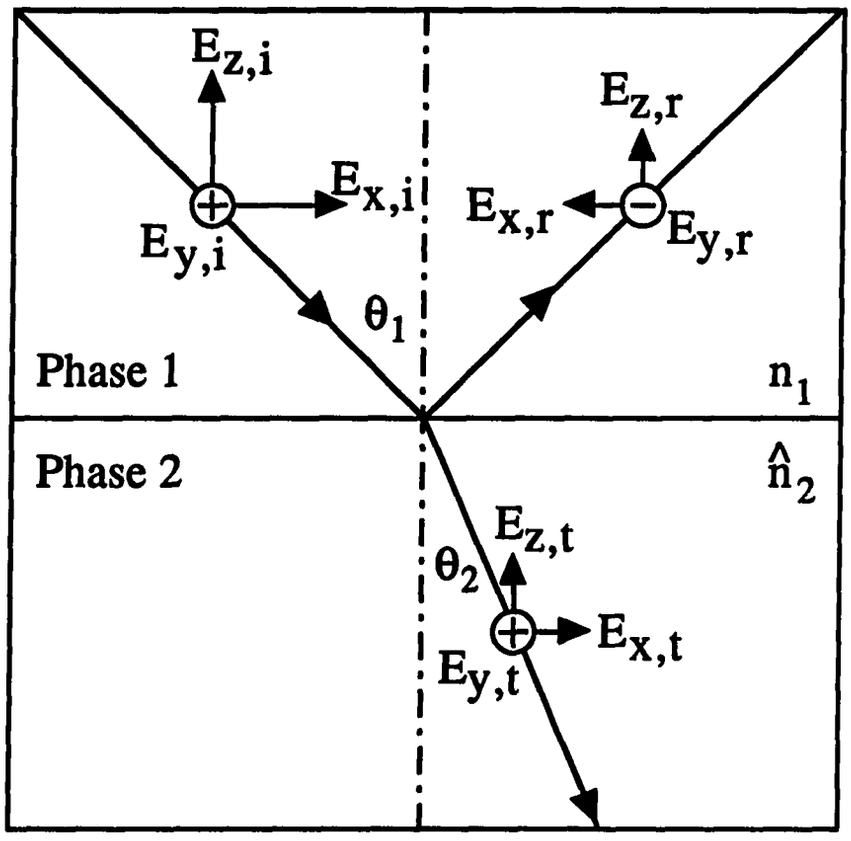

Figure 1. The electric field vectors for plane-polarized light incident at a phase boundary in a two-phase medium. The subscripts x, y, and z represent the direction of the vectors relative to the surface normal and i, r, and t indicate "incident," "reflected," and " transmitted," respectively

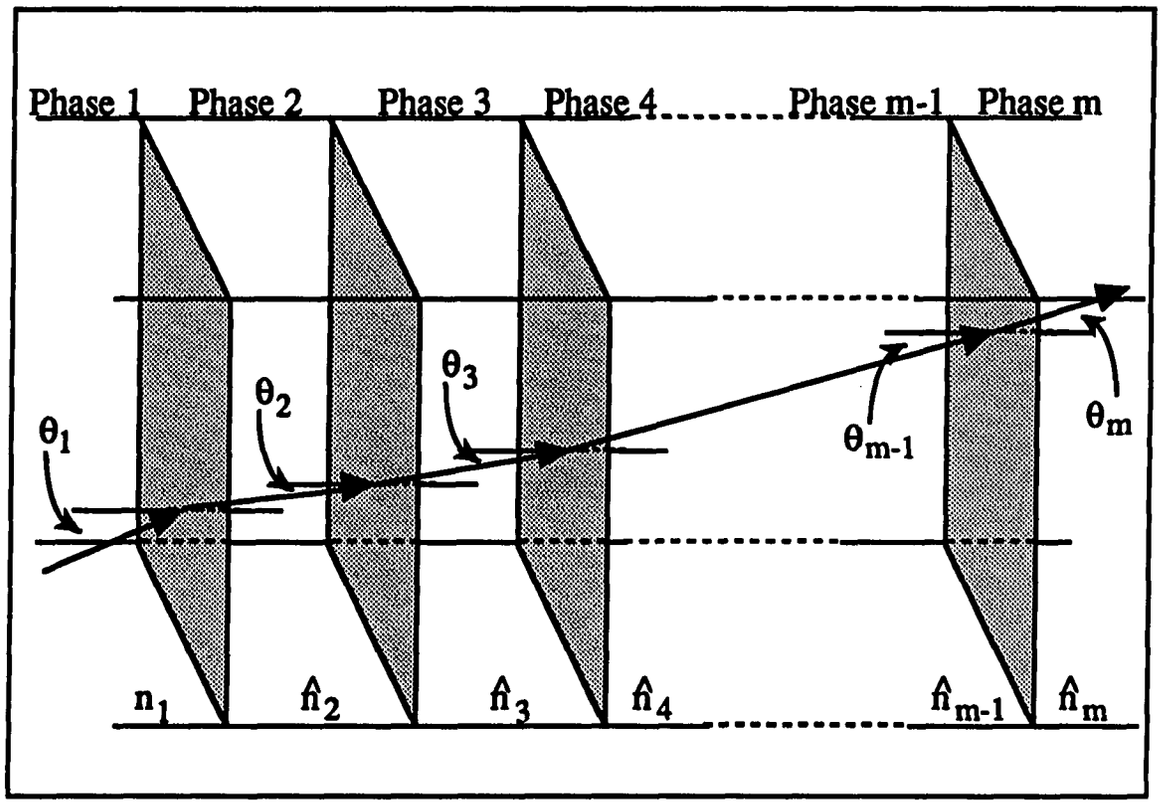

Figure 2. Radiation incident upon an *m*-phase medium. Rays for reflected light are omitted for clarity

$$\hat{n}_j = n_j + ik_j \tag{8}$$

and the thicknesses of the intermediate phases d_j.

The Fresnel coefficients quantify the magnitudes of the transmitted and reflected waves emanating from a phase boundary. These coefficients are defined as the ratio of the complex amplitudes of the electric field vectors of the incident wave to those of the reflected or transmitted wave, and are a function of the angle of incidence and polarization of the incident beam. Before calculating these coefficients, it is useful to define the refractive coefficient ξ_j for phase j as:

$$\xi_j = \hat{n}_j \cos\hat{\theta}_j \tag{9}$$

If phase j is absorbing, then $\hat{\theta}_j$ is complex. By Snell's law, ξ_j can be related to the angle of incidence and real refractive index of phase 1 as:

$$\xi_j = \left(\hat{n}_j^2 - n_1^2 \sin^2\theta_1\right)^{1/2} \tag{10}$$

The complex Fresnel coefficients for reflection, r_{jk}, and transmission, t_{jk}, at the boundary of phases j and k for radiation polarized parallel and perpendicular to the plane of propagation are then given as:

$$r_{\perp jk} = \frac{\xi_j - \xi_k}{\xi_j + \xi_k} \qquad t_{\perp jk} = \frac{2\xi_j}{\xi_j + \xi_k} \tag{11}$$

$$r_{\parallel jk} = \frac{\hat{n}_k^2\xi_j - \hat{n}_j^2\xi_k}{\hat{n}_k^2\xi_j + \hat{n}_j^2\xi_k} \qquad t_{\parallel jk} = \frac{2\hat{n}_j\hat{n}_k\xi_j}{\hat{n}_k^2\xi_j + \hat{n}_j^2\xi_k}. \tag{12}$$

Again, μ for all phases equals unity. These coefficients were derived from Maxwell's equations by applying the continuity requirements of $\hat{\mathbf{E}}$ and $\hat{\mathbf{H}}$ at the phase boundary.

MEAN SQUARE ELECTRIC FIELD STRENGTHS AT A REFLECTING INTERFACE

In a reflection spectroscopy experiment, the sensitivity of the measurement is a function of the optical properties of the substrate, and the angle of incidence and polarization of the incident light. For an in situ experiment, such as one to examine the interactions of solvent with a monolayer film, the sensitivity is further affected by the thickness and optical properties of the solvent and electrolyte (13-17).

In air, the detectability of a thin film is governed to a large extent by the boundary conditions imposed by the free electrons of the substrate. The electrical resistivity for metals is very low (2.35 $\mu\Omega$-cm for Au (18)), leading to a high infrared reflectivity (near unity). The dependence of the reflectivity, and hence, the intensity of the MSEF at the surface is elucidated by examining the relationships between an oscillating $\hat{\mathbf{E}}$ and the free conductive electrons in a metal. From the standpoint of physical optics, a reflecting metal surface acts as a collection of charges that are free to move within the metal but are prevented from escaping the confines of the substrate. The incident radiation gives rise to an oscillating electric field vector $\hat{\mathbf{E}}$ at the surface which interacts with the metal as follows: the component of $\hat{\mathbf{E}}$ parallel to the surface induces an image dipole in the metal that opposes, equally and oppositely, the incident field (Figure 3a), whereas, the component of $\hat{\mathbf{E}}$ perpendicular to the surface induces an

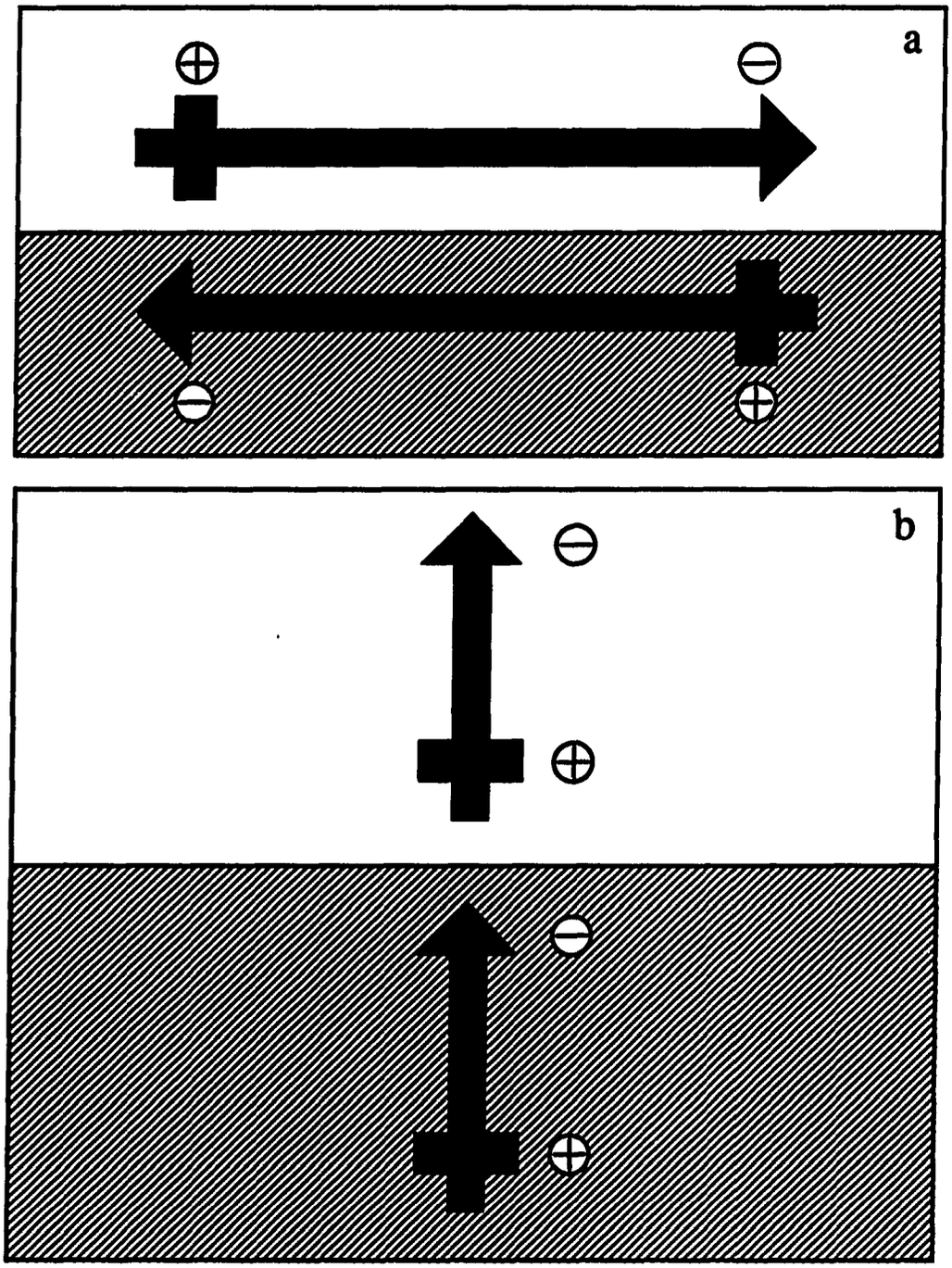

Figure 3. Orientation of the image dipole in a metal juxtaposed with the external electric field arising from the incident radiation for the component of radiation (a) parallel to, and (b) perpendicular to the metal surface

image dipole that is aligned with the incident component (Figure 3b). The phase change of the reflected wave then results from the orientational difference between the incident electric field and the induced image dipole.

Figure 4 illustrates the phase shift for light polarized both perpendicular to and parallel to the plane of propagation at a large angle of incidence at a metal surface. For *s*-polarized light, the incident $\hat{\mathbf{E}}$ is parallel to the surface, leading to a phase shift of ~180°, as discussed above. This holds for all angles of incidence and serves to nullify effectively the MSEF intensity parallel to the surface in the x and y directions. Conversely, *p*-polarized light at incident angles other than 0° has a portion of its electric field oriented perpendicular to the surface. The induced dipole in the metal also has a component aligned along the surface normal which reinforces the electric field at the surface by constructive superposition, serving to enhance the MSEF intensity along the z-axis. At normal incidence, the MSEF will be effectively zero, but as the incident angle approaches near-grazing conditions, the MSEF normal to the surface increases to ~3.4 times that of the incident radiation. Therefore, the absorbance by a thin film at a metal will be at a maximum at grazing angles of incidence with *p*-polarized light.

Calculations of the electric field intensity due to the superposition of the incident and reflected beams reveal quantitatively the effect of many of the experimental parameters on a reflection spectrum. The boundary conditions imposed by electromagnetic

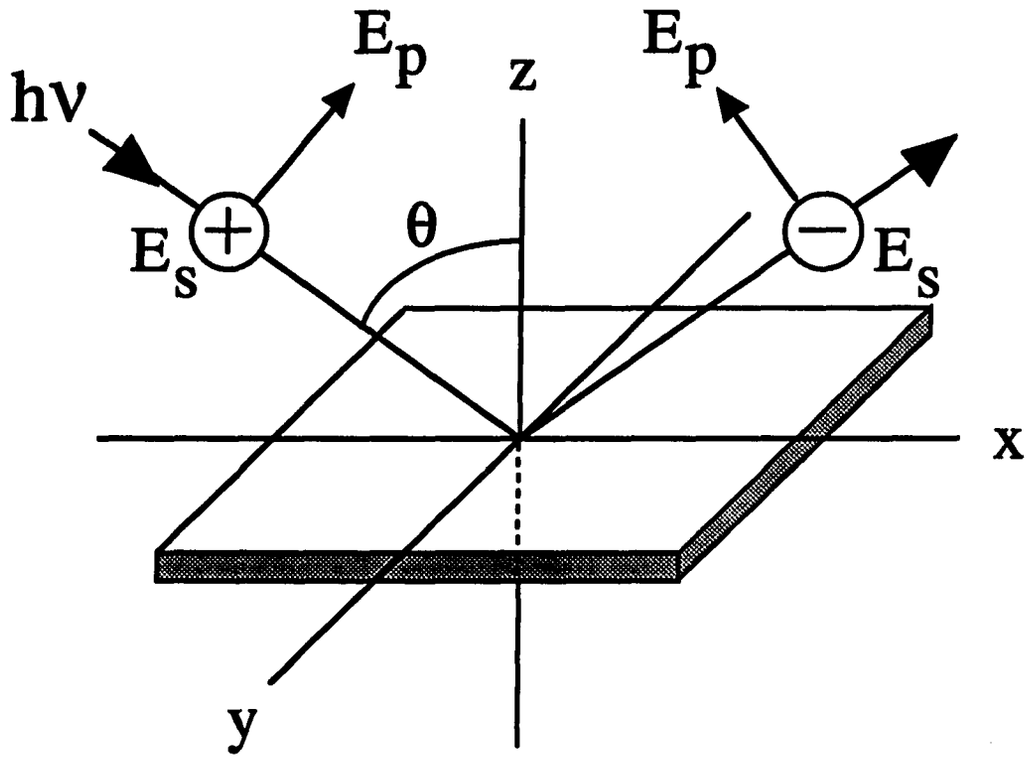

Figure 4. A representation of the phase change upon reflection for perpendicular-polarized light (E_p), and parallel-polarized light (E_s)

theory define the MSEF of the standing wave at each phase boundary; the value of which is strongly dependent on the optical properties of the substrate, the angle of incidence, and the polarization of the incident light. To foster an understanding of the effects of these experimental parameters, it is instructive to examine the MSEF in a two-phase optical medium. Since there is little energy dissipation (absorption) in a thin film such as a monolayer, the attenuation of the MSEF by the film is insignificantly small and can be neglected. In other words, for monolayers and thin polymeric films, calculations describing a two-phase system accurately represent those for a three-phase system. Values for MSEFs are generally expressed as the ratio of the MSEF in the j^{th} phase, $\langle E_j^2 \rangle$, to that of the incident plane wave in phase 1, $\langle E_1^{ot2} \rangle$. The following equations define the value of each component of the relative MSEF in the incident phase:

$$\frac{\langle E_{\perp 1}^2 \rangle}{\langle E_{\perp 1}^{ot2} \rangle} = (1 + R_\perp) + 2R_\perp^{1/2} \cos\left[\delta_\perp^r + 4\pi\left(\frac{z}{\lambda}\right)\xi_1\right] \tag{13}$$

$$\frac{\langle E_{\parallel 1x}^2 \rangle}{\langle E_{\parallel 1x}^{ot2} \rangle} = \cos^2\theta_1 \left\{(1 + R_\parallel) - 2R_\parallel^{1/2} \cos\left[\delta_\parallel^r + 4\pi\left(\frac{z}{\lambda}\right)\xi_1\right]\right\} \tag{14}$$

$$\frac{\langle E_{\parallel 1z}^2 \rangle}{\langle E_{\parallel 1z}^{ot2} \rangle} = \sin^2\theta_1 \left\{(1 + R_\parallel) + 2R_\parallel^{1/2} \cos\left[\delta_\parallel^r + 4\pi\left(\frac{z}{\lambda}\right)\xi_1\right]\right\} \tag{15}$$

A comparison of the results of these calculations using different experimental parameters provides a means to select conditions for high detectability.

It is helpful to visualize the intensities of the three components of the electric field as a function of distance from the substrate. These calculations are based on experimentally determined values of the optical constants of the substrates and apply Maxwell's equations as per the formulizations of Hansen (19, 20). The programs were written by D. D. Popenoe in conjunction with his research and their use is acknowledged. Figure 5a shows the MSEF for 2000 cm^{-1} light at an angle of incidence of 82° from 0-10,000 Å from the Air/Au interface. Dashed lines are superimposed on the data to demonstrate deviation from linearity as a function of distance from the interface. The net electric field can be envisioned as a standing wave with a node at the Air/Au interface with an effective intensity along E_x and E_y, of zero, leading to the infrared surface selection rule (vide infra). Figure 5b shows the same calculation for the light incident at glassy carbon at 60° from the surface normal. As discussed, due to the inability of the semiconducting material to mirror equally and oppositely the electric fields along E_x and E_y, these components have a finite magnitude at the interface and are free to interact with surface adsorbates aligned along these axes.

Figure 6 shows the calculated MSEFs for the light incident at glassy carbon from 0-100,000 Å from the interface. It is evident that

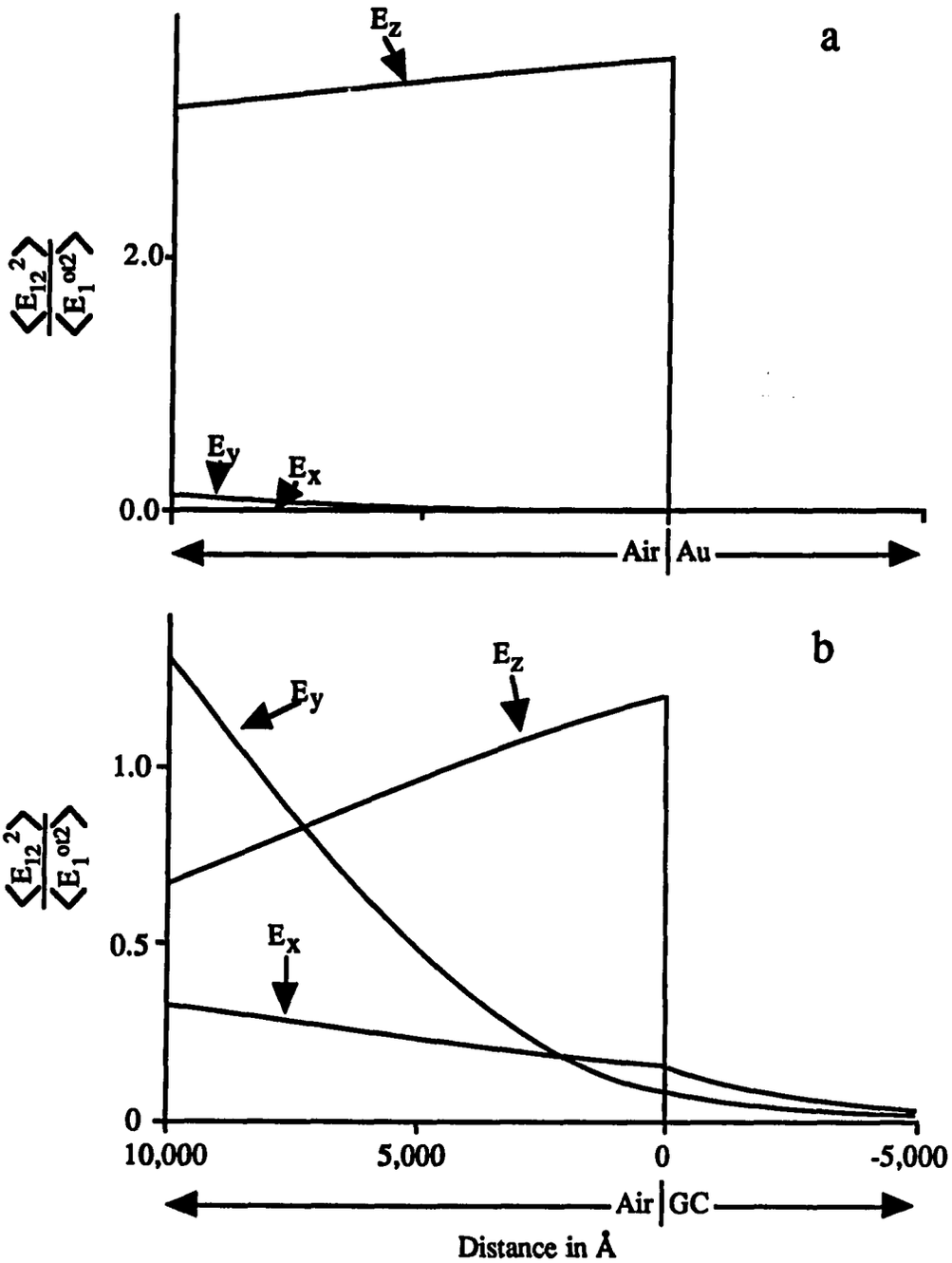

Figure 5. Plot of the MSEF at 2000 cm^{-1} vs. distance from the surface for (a) Au at an angle of incidence of 82° and (b) glassy carbon at an angle of incidence of 60°

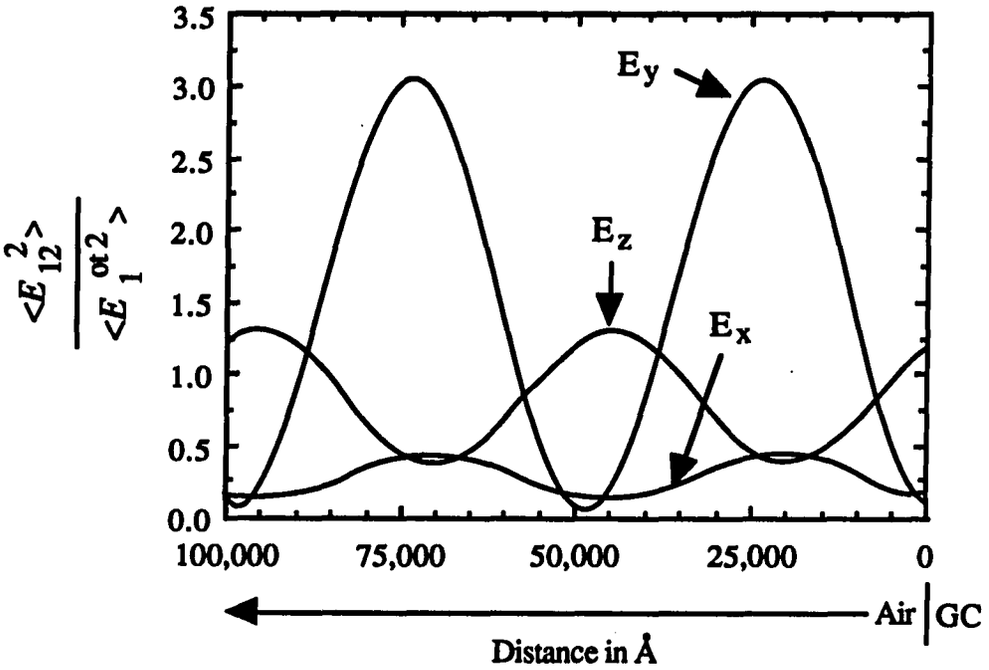

Figure 6. Plot of MSEF at 2000 cm^{-1} vs. distance from the surface at an angle of incidence of 60° at glassy carbon from 0 to 100,000 Å

quantitation of materials of thicknesses greater than 2000 Å is complicated by the sinusoidal periodicity of the MSEF components. Consequently, absorbance will not increase linearly with film thickness. Integration of the net MSEF intensity that is within the confines of the surface adsorbate is required to correct for this effect. For films less than 2000 Å, however, since the MSEF deviates only slightly from linearity (Figure 5b), absorbances can be correlated to film thickness directly to within a few percent.

A plot of the MSEF at an air/Au interface at 2000 cm^{-1} is shown in Figure 7. As follows from the discussion of boundary conditions, this plot provides insights as to how the high reflectivity of a metal influences the detectability of a surface film. The optical constants for Au were interpolated from a previous study (21). For highly reflecting materials, such as gold, the MSEF at the surface along E_z reaches a maximum value ~3.4 times that of E_z^0 at an angle of incidence of ~79°. The magnitudes of E_x and E_y are essentially zero at all angles of incidence. This net intensity of the MSEF exclusively along E_z gives rise to the infrared surface selection rule (22) which states that only those infrared active modes of an adsorbed species which have a component of their transition dipole oriented along the surface normal will be excited by the incident radiation.

To summarize, for the absorption of light of wavenumber $\bar{\nu}$ by a molecule immobilized at an air-metal interface, three conditions must be met:

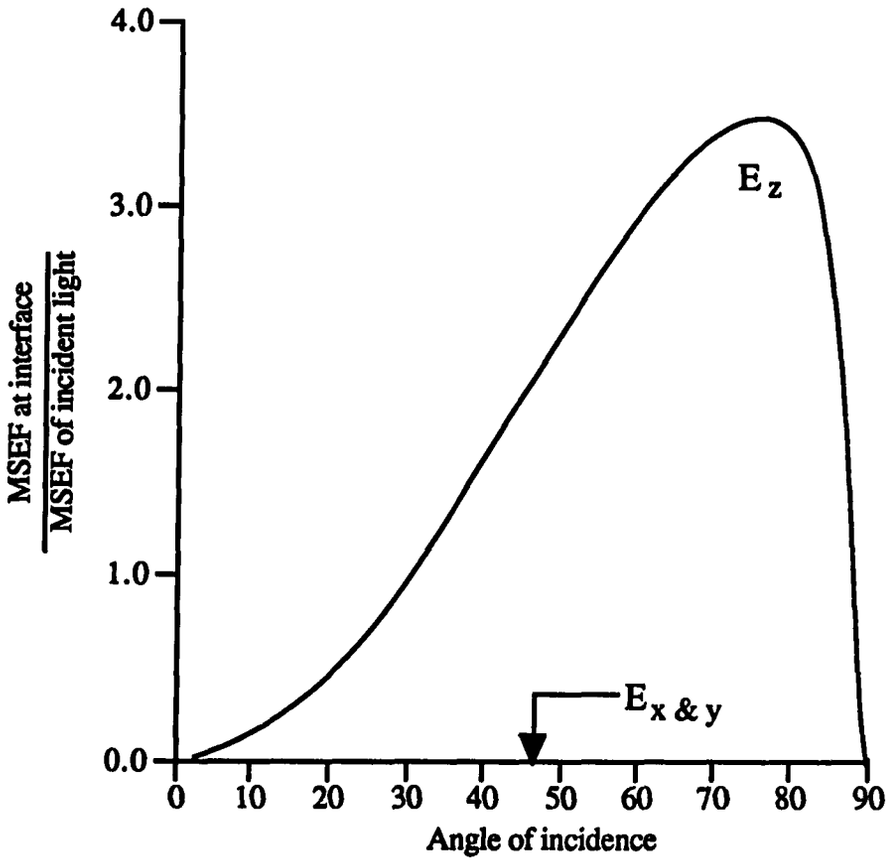

Figure 7. The mean square electric field at 2000 cm^{-1} as a function of angle of incidence and polarization at the air/Au interface (14)

(1) The molecule must have a nonzero transition dipole moment at $\bar{\nu}$.

(2) The magnitude of the MSEF at the interface must be nonzero (with conditions for high detectability at large angles of incidence and *p*-polarized light).

(3) The transition dipole moment must have a component oriented along the surface normal.

OPTICALLY INDUCED BAND SHAPE DISTORTIONS

For poorly reflecting semiconducting materials, such as the polished glassy carbon used in these experiments, E_z reaches a maximum at an angle of incidence of 60° with a value ~1.2 times that of E_z^o (23). In contrast to reflection at metallic surfaces, at semiconductors, E_x and E_y have nonzero magnitudes due to the inability of the substrate to mirror, equally and oppositely, the incident electric field. The use of a polarizer aligned along the plane of incidence (*p*-polarization) removes contributions to the spectrum due to E_y. Band shape distortions in the reflection spectrum arise from changes in the reflectivity at the phase 1/phase 2 boundary and from the period of the MSEF in phase 2. Distortions arising from changes in reflectivity are more pronounced at less conductive materials, such as glassy carbon, than at good conductors, such as Au. One must be cognizant of the fact that these distortions occur to some extent at all reflective surfaces, however, and must be considered before attributing the differences in spectral features between reflection and transmission spectra to chemical phenomena.

As an example of band distortions, plots of the real and imaginary parts of the refractive index for the C=O stretch of cellulose acetate are shown in Figure 8. For small values of k_2, the reflectivity R_{12}, which is the square of the Fresnel reflectance coefficient, is directly proportional to n_2. Thus the relative contribution of R_{12} to the reflection spectrum of an organic film is greater on the low-energy

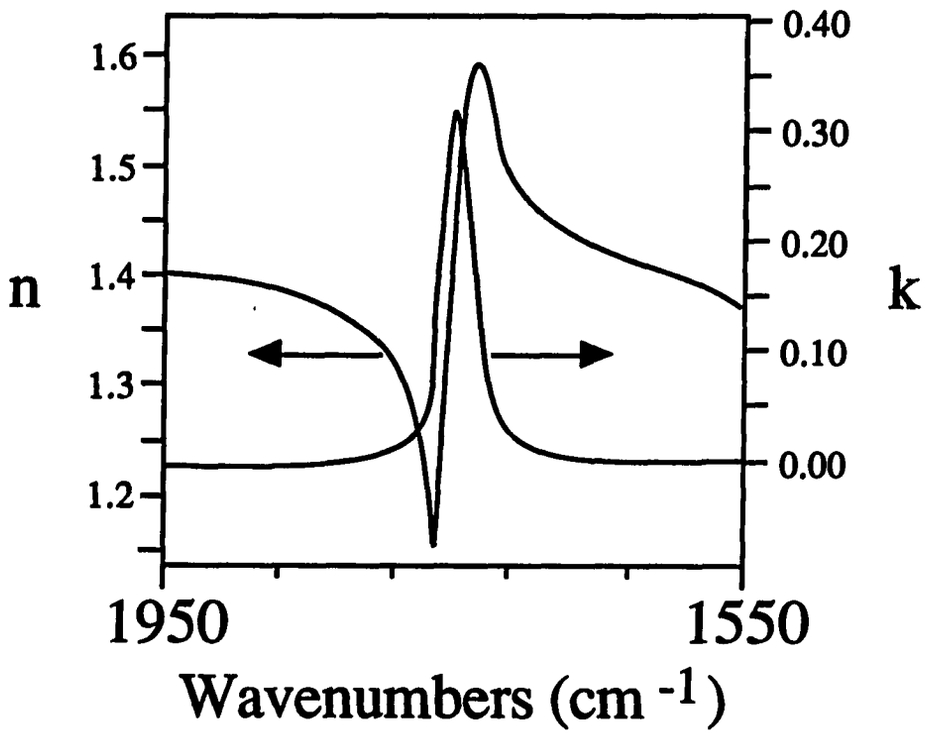

Figure 8. Complex refractive index for cellulose acetate in the carbonyl stretching region

side of the k_2 maximum. This results in a band with an absorbance maximum that is shifted toward higher energies and has an asymmetric shape (Figure 9a). These distortions increase as the thickness of the film increases and the reflectivity of the substrate decreases, as shown in Figures 9b-c (23-24). Furthermore, the variation of R_{12} also alters the MSEF in phase 2; that is, the greater R_{12}, the lower the MSEF available to interact with the oscillators in phase 2.

Band shapes and intensities of external reflection spectra are also distorted by the period of the MSEF in phase 2. For small values of k_2, the period of the standing wave in phase 2 is given by:

$$x = 1/\left(2\bar{\nu}n_2 \cos \theta_1\right) \qquad (16)$$

where x represents the distance between adjacent nodes or antinodes. This equation shows that x is inversely proportional to both $\bar{\nu}$ and n_2. Thus, as $\bar{\nu}$ increases, the standing wave contracts (x decreases), concentrating the MSEF in phase 2. In contrast, a decrease in $\bar{\nu}$ expands the standing wave (x increases); this reduces the MSEF in phase 2.

These considerations indicate that the band shapes and intensities of infrared reflection spectra are a strong function of the relative reflectivity of the substrate and of the thickness and complex refractive index of phase 2. The consideration of these optical effects

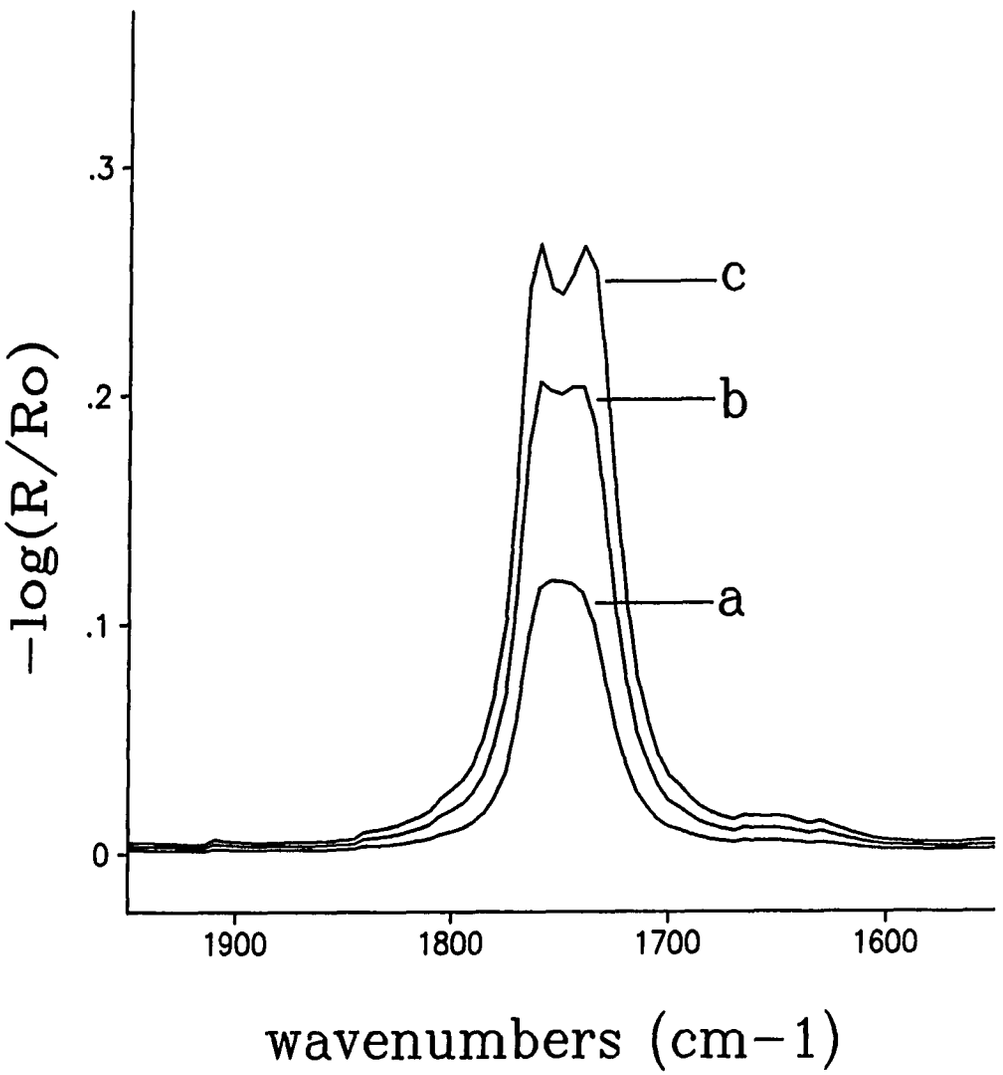

Figure 9. Calculated absorption/reflection bands for cellulose acetate at glassy carbon at 60° angle of incidence for films of the following thicknesses: (a) 100 nm, (b) 200 nm, (c) 300 nm

is relevant to the qualitative interpretation of infrared reflection spectra of thin polymer films at all types of reflective surfaces. Furthermore, a quantitative assessment of such effects, based on comparisons of observed and calculated spectra, provides a means to determine the *average* spatial orientation of an organic monomolecular surface structure. These calculations will be discussed in Section IV.

SECTION II. A HISTORICAL OVERVIEW OF THE LITERATURE FOR EX SITU AND IN SITU INFRARED EXTERNAL REFLECTION SPECTRA OF THIN FILMS

INTRODUCTION

Infrared external reflection spectroscopy has been utilized in many investigations to probe the molecular composition at the surface, thereby elucidating the behavior of the adsorbate under a particular set of conditions. Substrates have ranged from metals to water, and adsorbates have spanned the gamut from organic to inorganic, and polymer to mono- and submonolayer films. This section will discuss briefly several of these applications and will list some other examples of each method. The initial portion will be concerned with the detection of polymer films at the surface, the next will deal with the ex situ investigation of monolayer films under a variety of conditions, and the last section will be concerned with the various methodologies for the in situ examination of adsorbates at a surface. To follow the theme of this dissertation, research involving the utilization of transmission and attenuated total reflectance methods to examine these films will not be discussed. Further, the discussion will be limited to metallic and semiconducting materials as substrates.

THIN POLYMER FILMS MEASURED BY EX SITU IRS

The standard experimental arrangement for the acquisition of infrared external reflection spectra of thin organic films at conducting and semiconducting substrates is shown schematically in Figure 10. Here, the incident light passes through a polarizer to select that component which is in the plane of propagation (*p*-polarized). The light strikes the substrate at an angle θ, the value of which is determined from the reflectivity of the substrate as discussed in the previous chapter. The signal is then reflected from the substrate onto the detector and ratioed to the reflected radiation from a bare substrate.

Polymer Film at a Metal Substrate

An example of the utility of infrared external reflection spectroscopy for the examination of polymer films at metals is found in reference (25). Yang et al. used this technique to probe the orientational characteristics of electropolymerized poly(3-methylthiophene) at a Pt electrode as a function of thickness. This polymer shows considerable chemical and electrochemical stability in the presence of both moisture and oxygen, therefore, it has potential for a variety of applications. Examinations of thiophenes by ultra high vacuum techniques (electron energy loss spectroscopy, thermal desorption spectroscopy, near edge X-ray absorption fine structure spectroscopy) have shown that these molecules tend to adhere to the

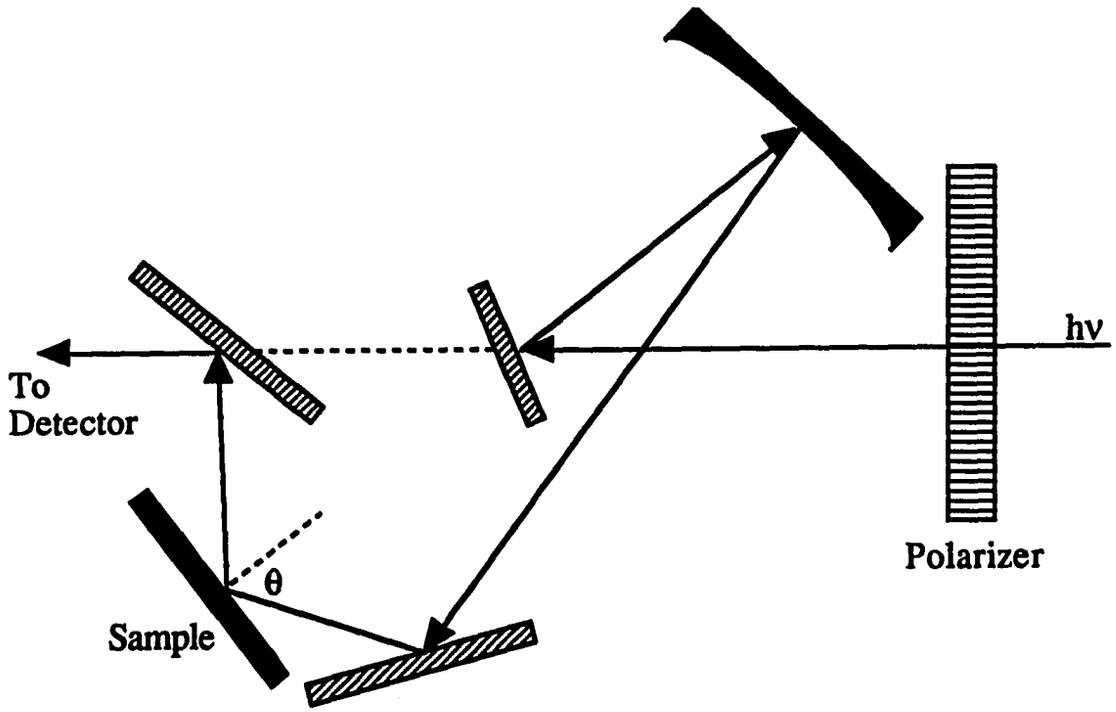

Figure 10. Standard optical arrangement for infrared external reflection spectroscopy

metal with the ring parallel to the surface. These authors were concerned with the long-range order of the film as the thickness of the polymer was increased.

The acquisition of reflection spectra at grazing incidence (~80-85° from the surface normal) maximizes the MSEF along the *z*-axis, thereby optimizing the interaction with the surface adsorbate. Utilizing the infrared surface selection rule, and being cognizant of the directions of the various dipole moments in the adsorbate, Yang et al. were able to conclude that, for thin films (200 Å), the molecules are indeed oriented mostly parallel to the surface through interactions between the π electrons of the ring and the metal. This was evidenced by a lack of response from those modes which are oriented in the plane of the molecule. Those modes which are out of the plane of the molecule showed a relatively large response which is also in agreement with the model. As the polymer thickness was increased to several hundred angstroms, the absorbance for the in-plane modes increased at a faster rate than those from the out-of-plane modes, suggesting that, at long range, the molecules orient with a larger degree of tilt relative to the surface normal. This implies that the ordering of the film diminishes with increasing thickness.

Other examples from the literature for the use of this technique to explore polymer films at metals are cited in the references (25-44).

Polymer Film at a Semiconductor

The extension of this technique to non-metallic surfaces introduces several experimental concerns which must be dealt with in order to extract both qualitative and quantitative data from the adsorbate. Distortions of band-shapes and shifting of peak centers to higher energy from the "normal" transmission spectrum can arise due to the low reflectivities of the substrates (see Section I). Porter et al. (23) developed methodologies, based on classical electromagnetic theory, to calculate the optical effects observed in the data and to predict the band shapes of the expected reflection spectrum based on the optical constants of the free-standing film and the substrate. When semiconducting materials, such as glassy carbon, are used as substrates, the angle of incidence at which the MSEF is optimized is at ~60° from the surface normal, compared to the grazing incidences used at metals. The details of the phenomena determining these distortions were discussed in Section I. This paper demonstrated that spectra calculated from classical theory can model the bandshapes and intensities observed experimentally to better than 93%, and that the inherent differences in the reflection spectrum relative to its transmission analog can and should be predicted prior to assigning those differences to chemical phenomena alone.

Other Examples

Other examples from the literature concerning the IR external reflection spectroscopy of polymer films can be found in the

references. Various problems have been explored including the effects of ultra-violet radiation, heat, and weathering on the molecular structure of polymer films (45-58), the biocompatibility of polymer materials for use as prosthetic devices (59-60), and the characterization of inorganic films at surfaces (61-63). This list represents an overview only and is not intended to be fully inclusive.

MONOLAYER FILMS MEASURED BY EX SITU IRS

The same principles which govern the acquisition of polymer film spectra can be applied to the spectra of monolayer films. Monolayers have proven to be useful both as models of more complex systems, such as biomembranes, and as organized probes of the fundamental interactions at the metal/adsorbate interface. Examples of the use of IR external reflection spectroscopy to probe these interactions are discussed in the following section.

CO at Platinum

Carbon monoxide is a relatively simple molecule that has been used extensively as a probe to explore the adsorption mechanism at a metal surface (64-82). At Pt, the characteristic absorption/reflection bands are strongly dependent on the mode of attachment to the surface, with the on-top C-O stretch occurring at ~2100 cm^{-1} and the bridge-bonded C-O stretch appearing at ~1850 cm^{-1}. An absorption band at ~475 cm^{-1} due to the Pt-CO stretch has also been studied (65). The peak position and shape of this band are also dependent on surface coverage and bonding type. In this report, Malik and Trenary investigated the effects of surface coverage and temperature on the infrared external reflection spectrum of the Pt-CO bond. They observed a shifting of the Pt-CO absorption band to higher energy from 474 cm^{-1} to 478 cm^{-1} for coverages from the lowest measurable amount to 0.19 monolayers, followed by a decrease to 466 cm^{-1} at

saturation. A broadening of the band after coverages of 0.2, which they attribute to the on-set of adsorption at the bridge sites as opposed to only the on-top sites, was also observed. They propose that adsorption proceeds from the regularly spaced islands of ($\sqrt{3}$ x $\sqrt{3}$)R30° at low coverage to a c(4 x 2) structure at higher coverages. Some band-width increase from inhomogeneous broadening due to disorder in the more densely populated surfaces may also occur.

Langmuir-Blodgett Thin Solid Films at a Metal

The use of IR-ERS to examine Langmuir-Blodgett monolayer films at metallic substrates has been well documented in the literature (83-88). A specific example where the technique was utilized to elucidate the molecular orientation of the structure is found in reference 84. Here, Mumby et al. were concerned with the preparation of an isotropic monolayer film devoid of internal stresses great enough to cause cracking upon polymerization. This can arise from segregation of monomer components prior to polymerization. The species of interest was poly(octadecyl-methacrylate) deposited on a purified water layer from dichloromethane, followed by subsequent evaporation of the solvent. The monolayer was transferred under constant surface pressure to an IR transparent material and also to an evaporated Al mirror. As was previously mentioned, upon reflection, those modes oriented along the surface normal will be preferentially excited by the incident radiation, while those parallel to the surface will not. The effect is reversed for transmission, where only those

modes parallel to the surface will be observed. The data show that the monolayer adheres to the surface via the carbonyl, with the alkyl chain oriented mostly normal to the surface.

Organic Monolayer Films at a Metal

An example of the application of infrared external reflection spectroscopy to the examination of a nonpolymerizing organic monolayer film at a metal surface can be found in reference (89). Schlotter et al. examined the orientational properties of a self-assembled monolayer of arachidic acid at Ag and compared this with the properties of a multilayer of cadmium arachidate formed at a Langmuir-Blodgett trough. Self-assembly will be discussed in a later section. Calculations based on the relative intensities of the hydrocarbon stretching bands, as compared to a transmission spectrum of the bulk material, demonstrated that these monolayers form at Ag with an orientation that is mostly normal to the surface. Further, peak positions indicate that the monolayer is predominantly crystalline in nature, in a trans zig-zag conformation. The absence of a band for the carbonyl indicates that the head-group attaches to the Ag as a carboxylate salt.

Differences between the self-assembled monolayer and the LB multilayer are manifested in the methyl and carboxylate modes. Differences in the methyl modes are due to the local environments of these groups in the two layers. The LB multilayers were formed by a Y-type deposition, with each layer being formed alternatively in a

head-to-head and tail-to-tail arrangement, allowing interchain interactions between the methyl modes of each subsequent layer. For the self-assembled monolayer, the methyl modes only interact with the adjacent chains and the laboratory ambient. Consequently, environmental differences for the methyl group in the two systems lead to shifts and changes in the bandshapes relative to each other. The changes in the carboxylate stretches are due to frequency variations caused by differences in the counterion (i.e., Ag^+ vs. Cd^+). The similarities in the methylene modes, however, indicate that the layers formed by self-assembly are structurally similar to those formed by LB methods. More importantly, since these layers can be readily formed by self-assembly, thereby avoiding the preparative limitations of LB films, a wider variety of structures can be formed and subsequently tailored for more specific applications.

Polarization Modulation

Another important technique which is used to acquire infrared reflection spectra of an adsorbate at a metallic surface is polarization modulation. This method utilizes the fact that the *p*-polarized component of the incident light at a metal is sensitive to both surface adsorbates and all gaseous phases in the path of the incident radiation (i.e., CO_2, N_2, H_2O, etc.), while the *s*-polarized component is oblivious to the surface species, yet equally sensitive to the other adsorbers. A photoelastic modulator is used to alternate between the two polarizations and the data are collected into separate data files. The

ratio of these files provides the spectrum of the adsorbate only. The details of the experiment will be discussed at greater length later in this section. Research reports using this method can be found in the references (90-102).

Other Examples

Infrared external reflection spectroscopy has been utilized for a variety of other applications. Many examples in the literature stem from the evaluation of organic and inorganic adsorbates at the surface of a variety of catalysts (103-117). In addition, many reports examined the adsorption of organic and inorganic moieties at various other metals (118-138). The purpose for selecting IR-ERS as the test method varied from simple identification of the molecular structure to a detailed orientational analysis of the adsorbate. As has been shown, this method serves as a powerful tool to elucidate the structure and orientation of a surface without the need for elaborate ultra high vacuum techniques.

EXAMPLES OF IN SITU METHODOLOGIES

It has long been recognized that there are two major obstacles to overcome in order to probe molecular films in situ by infrared external reflection spectroscopy. The first is the strong solvent absorption which can obscure most or all of the measurable optical throughput. If the first is overcome, then the problem of detecting very small absorbances in the presence of the large background (solvent) absorbance arises. The solution for the first obstacle is to use an ultra-thin-layer cell, whereas the second is usually resolved by the application of an optical (polarization) or electrochemical modulation scheme which is coupled with phase-sensitive detection. Solution layer thicknesses for thin layer cells are typically ~0.5 - 5.0 μm but can be as large as 100 μm for certain applications (139-145). These cells function primarily in an external reflection mode; that is, as shown in Figure 11, the optical beam passes through an IR transparent window, propagates through a thin layer of solvent, interacts with the surface adsorbate, and is reflected at the electrode surface. Coupling the aforementioned modulation schemes with the many data acquisition and manipulation techniques now available makes it possible to detect low analytical signals and separate them from the strong solution absorbance.

In the material that follows in this section, the previous methodologies of the various in situ techniques for external reflection spectroscopy are discussed. The two most frequently used modulation

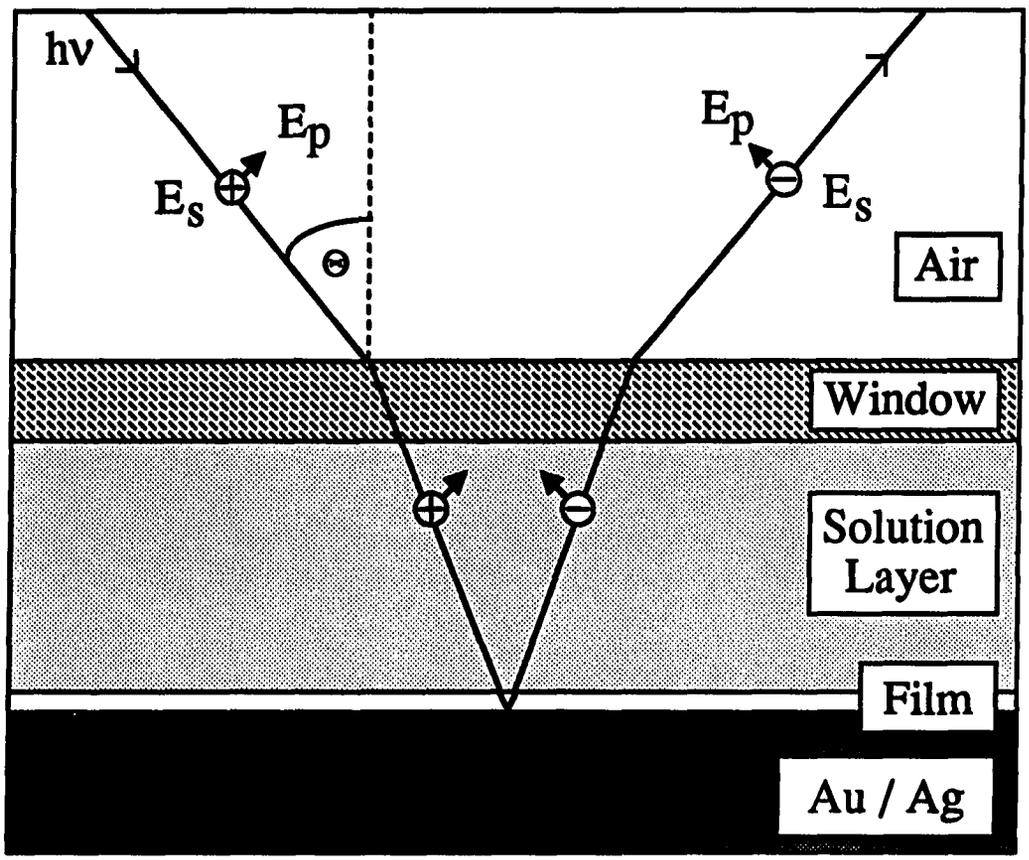

Figure 11. Schematic diagram for the propagation of light in an in situ infrared external reflection spectroscopy measurement

techniques employed for the phase-sensitive detection of electrogenerated surface species are discussed, followed by examples from the literature of problems explored by these techniques. Other approaches to the in situ applications of IRS to electrochemical problems are essentially variations of electrochemical or polarization modulation techniques, and will be discussed when appropriate.

ELECTROCHEMICAL MODULATION

Designs for three-electrode thin-layer spectroelectrochemical (SEC) cells for external reflection are shown in Figures 12 and 13. In these cells, the solution layer is confined between a flat IR transparent window and a cylindrical electrode. The window is mounted to the cell either with an epoxy resin or with an O-ring seal. The latter method is preferable to eliminate the possible contamination of the electrode and solution by the slow dissolution of the epoxy. The working electrode is mounted on a plunger constructed either from glass or Kel-F. Electrical connection to the working electrode is achieved through a channel in the plunger. The electrode surface is usually polished to a specular finish with an alumina slurry. As a final step, the plunger is inserted into the cell and polished concurrently to insure that all surfaces are parallel with each other (146-147).

There are two common designs for cell windows. The original cell design by Pons (14) used flat windows with IR transparent materials such as silicon, zinc selenide and calcium fluoride (Figure 12). In much of the early work (148), Si was used to gain access to vibrational modes at the low-energy portion of the mid-IR spectral region. This material is also relatively inert, with a high chemical stability in dilute acidic solutions. However, since Si is not transparent in the visible region, cell alignment and verification of solution filling or the observation of generated bubbles in the cell are problematic. Additionally, the high refractive index of this material

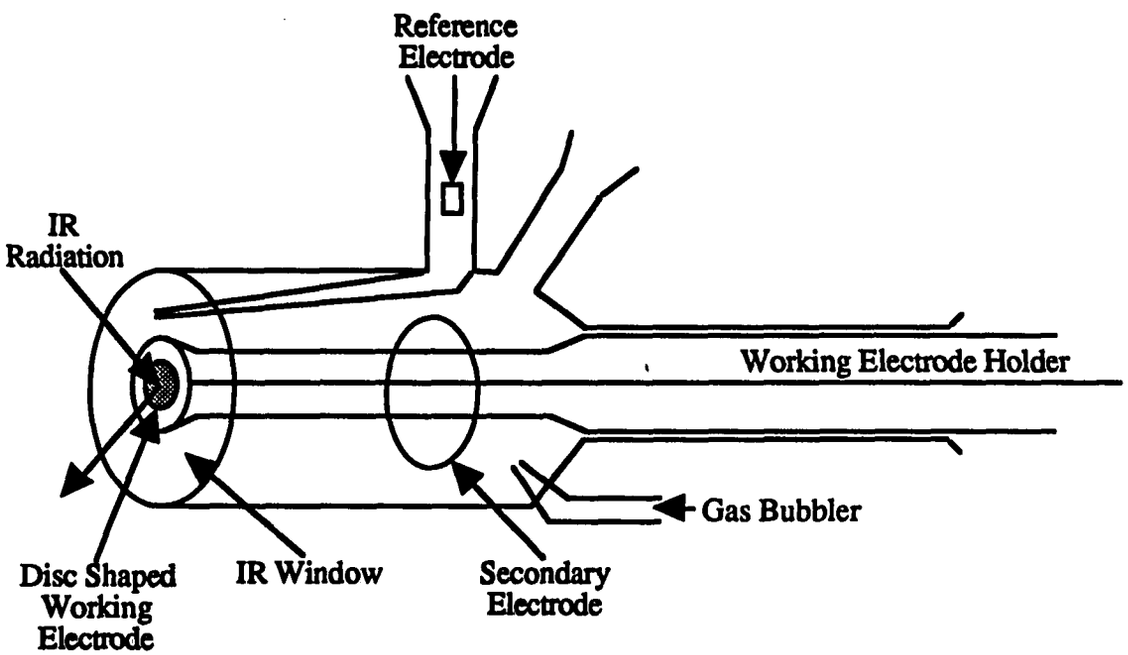

Figure 12. Schematic diagram of electrochemical infrared cell (14)

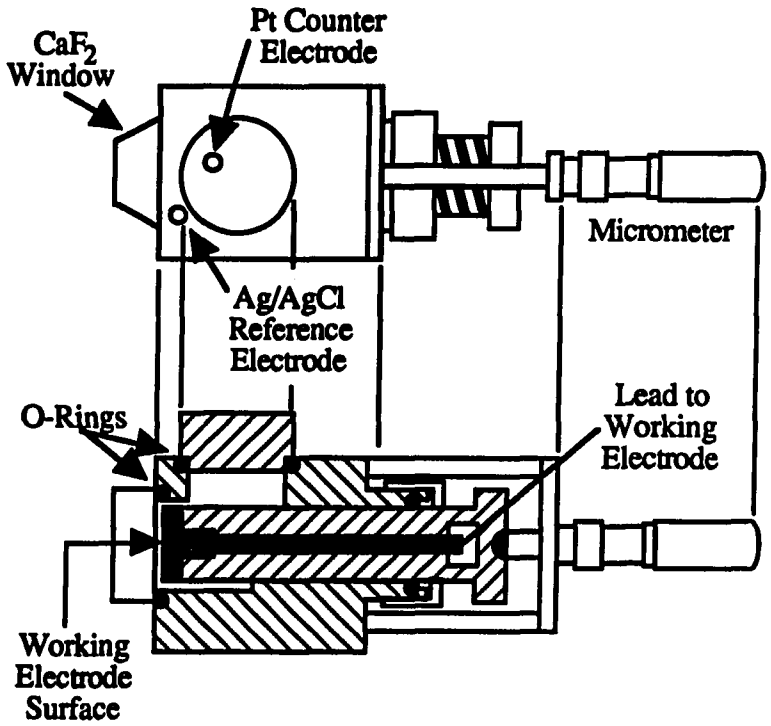

Figure 13. Top and side views of the thin-layer electrochemical cell with a CaF_2 window. The side view is shown as a cross-section (149)

produces a high front surface reflection loss. One approach to overcome these hindrances is to use materials such as CaF_2. This material is transparent in the visible spectral region, has a low refractive index, and is only slightly soluble in acidic solutions. A prismatic window design, as shown in Figure 13, minimizes the reflection losses for high refractive index materials.

An important experimental consequence results from the thin-layer configuration of these cells. This arises from the large uncompensated and nonuniform resistance of the thin solution layer, leading to a relatively long time constant for charging the electrode. Typical time constants are ~1-10 μs for a solution with 0.1-1.0 M aqueous electrolyte, a 10 μm solution thickness, and an electrode area of 0.3 cm^2 (141). Thus, distortions of the transient response can be expected in electrochemical modulation experiments that require the flow of large quantities of current.

Dispersive Spectrometers

The first successful in situ experimental application of infrared reflection spectroscopy to the characterization of a surface adsorbate involved the modulation of an applied voltage at a working electrode, monitoring the changes in molecular composition as a function of applied potential (13-17, 148). In this experiment, designated as EMIRS for electrochemically modulated infrared reflectance spectroscopy, the electrode potential undergoes an *ac* modulation between two potential limits, E_1 and E_2, where E_1 represents some

base potential and E_2 represents a potential where some change in the adsorbate composition has occurred. The spectrum is obtained by scanning the spectrometer slowly over the spectral range and integrating the signal from the monochromator, recording the difference between the detector response at the two potentials. This approach effectively discriminates against interferences from the bulk electrolytic solution (solvent and supporting electrolyte), and allows for the detection of fractional reflectance changes at the 10^{-5} level, which corresponds to changes in the properties of the adsorbate. The magnitude of the voltage change may alternate from a few tens to hundreds of millivolts. Modulation rates may vary from a few hertz to tens of hertz, depending on the response characteristics of the spectrometer and the electrochemical system. As a result of the time constant of the thin-layer cell, most applications are limited to a modulation frequency of a few hertz. Changes in the molecular composition or structure at the interface as a result of this modulation will be manifested as small *ac* changes in the reflectance signal and can be recovered by phase-sensitive detection with a lock-in amplifier. This is usually expressed as the difference between two single beam reflectivities, ratioed to the reflectivity at one of the applied potentials. The result is a difference spectrum, which is given as:

$$\frac{\Delta R}{R} = \frac{R_2\left(\bar{\nu}\right) - R_1\left(\bar{\nu}\right)}{R_1\left(\bar{\nu}\right)} \qquad (17)$$

where R_1 and R_2 are the reflectances at applied potentials E_1 and E_2, respectively. The normalization to $R_1(\bar{\nu})$ removes instrument functions such as the instrument energy throughput and detector responsivity, and turns a single beam spectrometer into a pseudo-dual beam spectrometer. For the small values of $\Delta R/R$ often encountered with spectral changes for adsorbates at monolayer surface coverages, this quantity is directly proportional to the more conventional optical absorbance.

The optical layout and a representative block diagram of the instrumentation used in the EMIRS technique is shown in Figure 14 (16, 148). This spectrometer features f/4 optics, providing a high energy throughput. A variety of detectors have been used, but liquid N_2 cooled InSb or HgCdTe photoconductive detectors provide the highest optical sensitivity; a key factor in low energy throughput measurements. For surface studies, a polarizer selectively passes *p*-polarized radiation. The spectrometer, cell, and detector chambers are purged with dry N_2 to minimize absorption by atmospheric H_2O and CO_2. The oscillator provides the input waveform to control the frequency and magnitude of the voltage waveform at the electrode. The signal processing, timing sequences, and operation of the monochromator are controlled by computer (148).

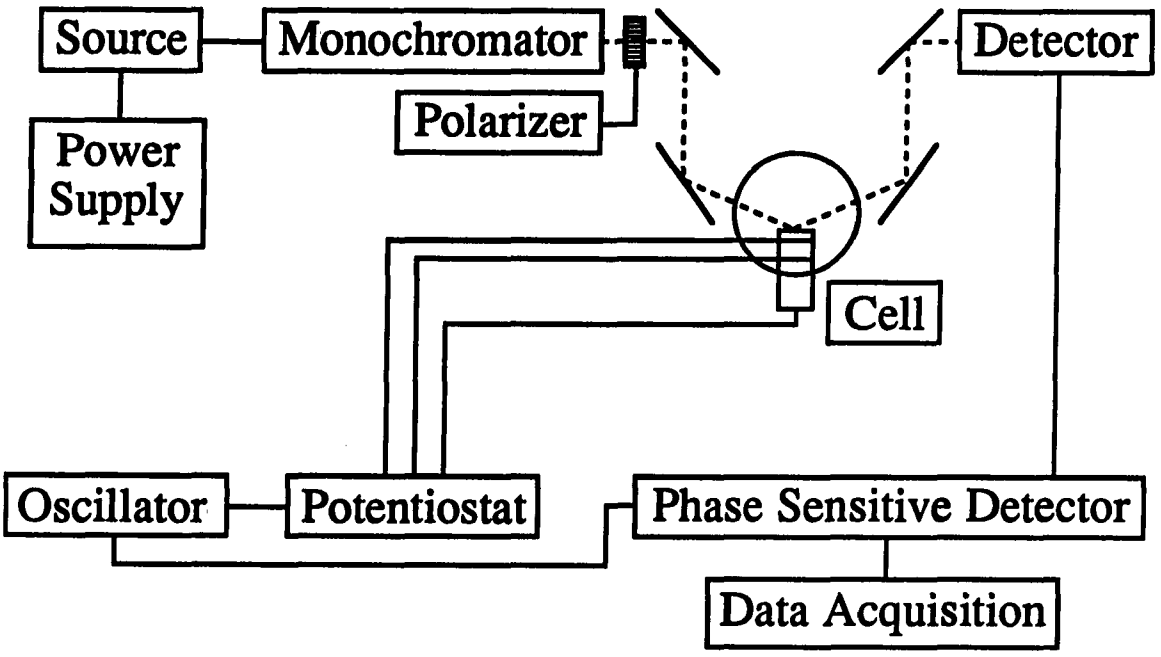

Figure 14. Block diagram of the instrumentation used for an EMIRS experiment (16)

Fourier Transform Infrared Spectrometers

It was not long after the development of EMIRS that efforts to exploit the throughput, multiplex, and resolution advantages of FT-IRS were undertaken (149-150). However, as it applies to studies in electrolytic solutions, the low noise discrimination per scan leads only to a comparable sensitivity with EMIRS. One of the causes of the loss of sensitivity is the limited dynamic range of the A/D converter. Most of the spectroscopic information is located in the wings of the interferogram, with the centerburst containing only overall spectral intensity information. As such, the dynamic range of the A/D is limited by the high amplitude of the centerburst, prohibiting the efficient sampling of the wings of the interferogram. Various gain-ranging techniques have been devised to overcome this limitation, and should be considered in the design of each experiment. In some instances, optical filters that pass only the bandwidth of interest may be useful to enhance sensitivity.

The basic mode of operation for IR-SEC utilizing an FT-IR is analogous to that of EMIRS, providing a difference spectrum between two potential limits, E_1 and E_2. When signal averaging over long periods of time, a small number of interferograms are collected successively at the two potential limits. In addition to other advantages (16), "block" co-addition effectively cancels long term electronic and mechanical drifts and reduces background signals from atmospheric H_2O and CO_2. This approach, which is termed SNIFTIRS for subtractively normalized interfacial Fourier transform infrared

spectroscopy, has been used for time resolved studies (151-152) and for obtaining interfacial spectra in the far IR region (153).

Polarization Modulation

An alternative method to obtain an *in situ* infrared spectrum at the electrochemical interface derives its surface sensitivity from the anisotropy of the MSEF at a metal surface. As discussed previously, with this technique (91, 150, 154) the polarization of the incident light is modulated between *p*- and *s*-polarization with a photoelastic modulator (PEM). For a ZnSe PEM, the modulation rate is 74 KHz. Since the intensity for *p*- and *s*-polarized light will, on the average, be attenuated to the same degree by any randomly oriented gas or liquid phase molecules, and since only *p*-polarized light is surface sensitive, modulation between the two polarizations yields an *ac* signal due only to the species at the electrode surface. With this technique, IR-SEC measurements can be performed without an alteration of the applied potential. This method assumes that the magnitudes of the *s*- and *p*-components remain proportionally constant. However, in those spectral regions where the solvent is strongly absorbing, the magnitudes of the two components are effected nonuniformly. The result is a disproportional contribution to the spectrum from the two components which gives rise to optical artifacts in the regions of solvent absorption. As a consequence, the acquisition of spectra for surface species whose absorption/reflection bands are shrouded by solvent absorption bands requires the potential to be stepped as in the

SNIFTIRS experiment, resulting again in a difference spectrum, and limiting the use of this technique to electroactive surface moieties.

The key instrumental component to the application of this technique is the PEM, the principles of which are well established (154). The PEM is essentially an IR transparent crystal with an isotropic refractive index. The device works by the application of a periodic strain with a piezoelectric transducer along one axis of the crystal and at the frequency of its fundamental longitudinal mode. The strain produces a periodic change in the refractive index of the crystal, resulting in a periodic phase retardation of the incident light with its polarization along the fundamental mode. This rotates the polarization of the incident beam. Thus, by orienting the stressed axis of the PEM 45° from the surface normal and by placing a fixed polarizer in the optical path to pass either *s*- or *p*-polarized light, the light incident on the electrode surface can be modulated between both polarizations.

A schematic diagram for processing the signal for IRRAS measurements that employ a FT-IRS is given in Figure 15. This electronic configuration splits the signal from the detector preamplifier into two channels which are each demodulated separately. One signal passes through the conventional circuitry of the instrument. This signal contains the normal single beam interferogram and equals the sum of the energy throughputs for *s*- and *p*-polarized light ($I_p + I_s$). In the other channel, the signal is demodulated at the PEM frequency and filtered to yield an

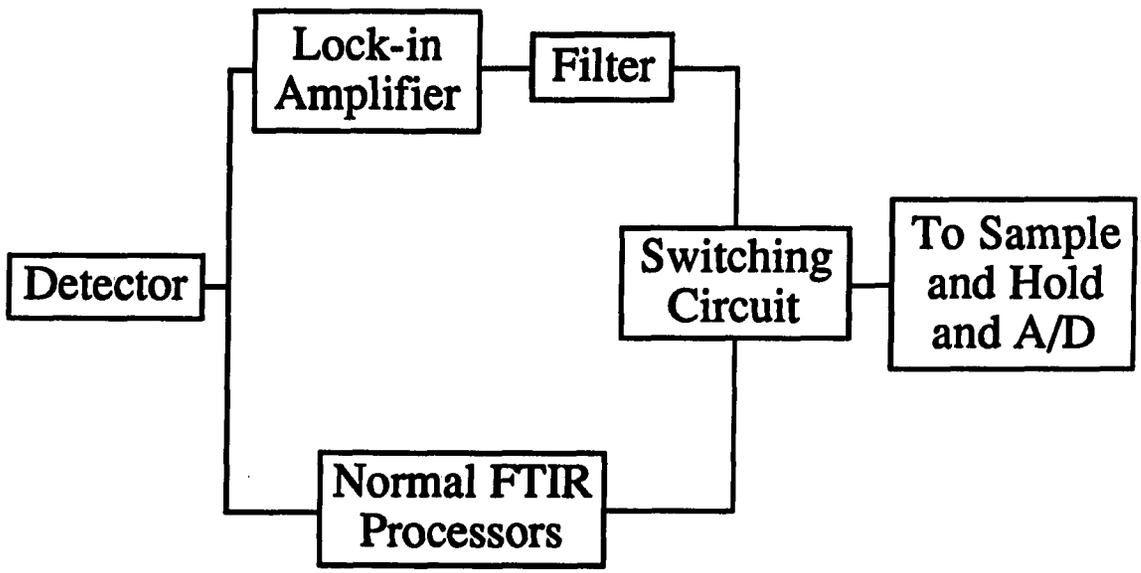

Figure 15. Schematic of the polarization-double-modulation FT-IRRAS signal processing arrangement. The signal from the detector preamplifier is split into two channels, and each channel is demodulated separately

interferogram that equals (I_p - I_s). After further software manipulation and Fourier transformation, the quotient of (I_p + I_s)/(I_p - I_s) provides a spectrum of the surface species. A block diagram of this instrument is shown in Figure 16. Further details of the basic principles, electrical circuitry, and data manipulation are available (150).

Origins of Band Shapes in Potential Modulation Spectra

Before continuing the discussion of the various modulation techniques, it is worthwhile to examine the underlying factors that govern the shapes of the spectral features observed with potential modulation techniques. One of the possible differences in reflectivity arises from a change in the dielectric function of a metal. This phenomenon, known as the electroreflectance effect, results from the dependence of the number of electrons near the surface of a metal on the applied potential. Since the reflectivity of metals is governed by the concentration of free electrons near the surface, a change in applied potential induces a change in reflectivity. In the ultraviolet and visible spectral regions, the electroreflectance effect can markedly complicate the interpretation of a difference spectrum. However, the effect usually leads to small structureless shifts in the baseline of a spectrum in the IR region that are of negligible significance. A difference spectrum may result from an absorption band that is present only at E_1 or E_2. Such changes could be caused by the dependence of the oscillator strength of a vibrational mode, the concentration of a species present in the solution or surface layer, or

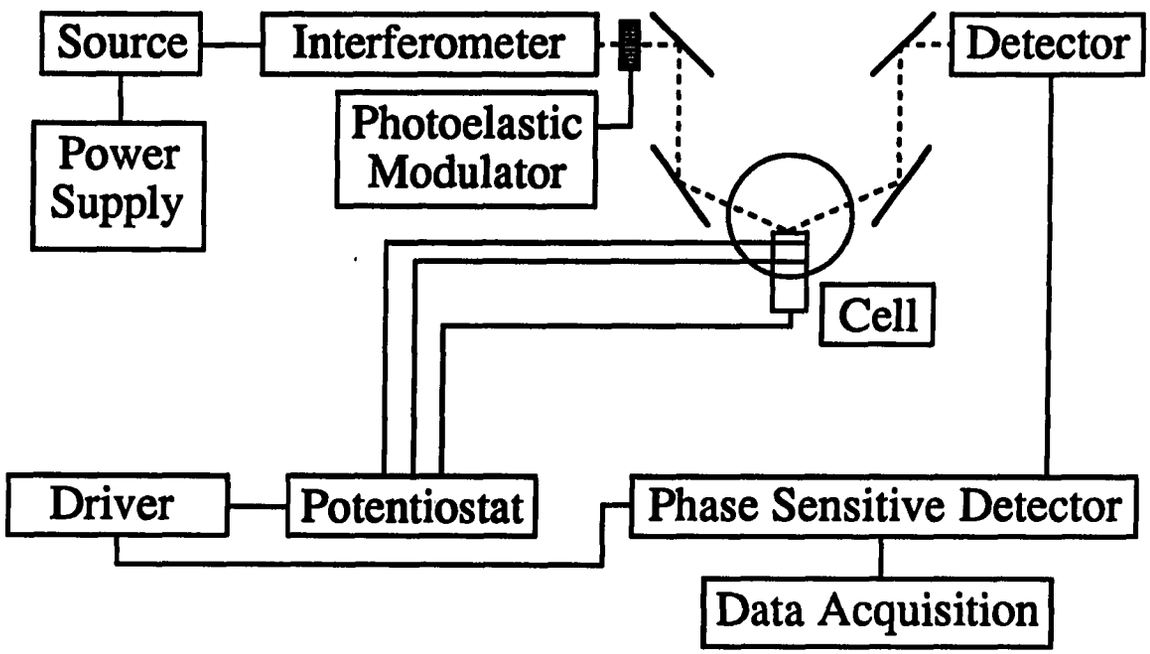

Figure 16. Block diagram of the instrumentation used for an IRRAS experiment (16)

the orientation of an adsorbate with respect to the surface normal as a function of the applied potential at the electrode. This latter case arises from the infrared surface selection rule. Bipolar features (i.e., those with positive and negative peaks) may be caused by a change in the position or shape of the band as a function of applied potential. Changes in the donation or withdrawal of electron density with applied potential between an adsorbate and an electrode may give rise to this spectral band shape. As is apparent, there are a variety of factors which can influence the shape of the observed spectral feature. However, in cases where a more detailed understanding of the origins of a band shape is required, the integration of a potential modulation spectrum should yield a reasonably interpretable "absolute" spectrum. The application of the polarization modulation technique also provides an opportunity to resolve such questions.

Specific Examples of the Use of In Situ IR-ERS

Adsorbed intermediates and poisons in the electrocatalytic oxidation of methanol at a platinum electrode

The immense interest in the electrocatalytic oxidation of small organic hydrocarbons stems from their potential as fuels for energy production. However, the development of such electrochemically based power sources has been greatly inhibited by the poisoning of the electrode surface as a result of the gradual adsorption of intermediates and/or products at active sites for the heterogeneous electron-transfer process. The elucidation of these reaction mechanisms and the

identification of these poison(s) are therefore of fundamental and practical importance toward increasing the catalytic activity and long-term stability of electrode materials.

The exact nature of the adsorbed species formed from the electrooxidation of fuel hydrocarbons such as methanol and ethanol has been the subject of extensive controversy since the early 1960s (155-159). The inability to identify accurately the structure of the adsorbate has led to the proposal of numerous mechanistic pathways for electrooxidation reactions. Of the previously cited studies, the electrocatalytic oxidation of methanol at a platinum electrode is an excellent example for illustrating the problem solving capability of infrared spectroelectrochemistry (IR-SEC). The two most commonly proposed intermediates of this reaction are COH_{ads} (157) and CO_{ads} (155). The controversy regarding the structure of the true adsorbed intermediate can be readily resolved with IR-SEC.

The earliest attempts at applying IR-SEC to deduce the structure of the adsorbed intermediate of the electrooxidation of methanol at platinum employed EMIRS (160). Here, linearly bonded =C=O (=C=O linked to one surface atom) was identified as the principle adsorbate with a strong spectral feature at ~2080 cm^{-1}. The presence of a bridge-bonded =C=O (=C=O linked to two surface atoms) was also evident from a spectral feature at ~1860 cm^{-1}.

These observations were confirmed in a subsequent study which utilized a different modulation techniques. This employed a variation of the potential modulation technique to construct an "absolute"

reflectance spectrum (161). With this technique, the change in reflectance is monitored at several fixed wavelengths during the imposition of a linear sweep of the electrode potential. Thus, by taking the difference between the reflectance at a given potential and that at a reference potential (a potential where the adsorbed species is absent), an accurate representation of an absorbance spectrum can be reconstructed. The spectrum corresponding to an electrode potential of 1.3 V (vs. NHE) exhibits a maximum for $\Delta R/R$ at ~2062 cm^{-1}, which is consistent with a linearly bonded CO intermediate.

Another confirmation of the nature of the adsorbate for the electrooxidation of methanol employed polarization modulation (162). However, the polarization of the incident light was accomplished with a rotating polarizer as opposed to a photoelastic modulator. These studies examined the relationships between the potential and the time dependence of the formation of the linearly bonded CO from methanol and its effect on electrocatalytic activity. The band intensity for the linearly bonded CO was greatly reduced as the applied potential became more negative, indicating that the formation of the adsorbate becomes more difficult as the initial coverage of adsorbed hydrogen increases. The dependence of the electrolysis rate on the coverage of the adsorbate shows that as CO is oxidatively removed from the surface by the application of an increasingly positive potential, the current for the oxidation of methanol increases dramatically. These results point to the role of adsorbed CO as a catalytic poison for the electrooxidation of methanol.

Molecular adsorption: Difluorobenzene at a polycrystalline platinum electrode

The adsorption of aromatic molecules at electrode surfaces has been a long-standing concern to electrochemists (7). Such studies have particular relevance to a variety of surface electrochemical processes, including electrocatalysis, chemical and clinical analysis, electroplating, etching, and passivation. Additionally, such studies promise to enhance a basic understanding of surface reaction kinetics, surface acid-base chemistry, and solvation at surfaces.

In many instances, aromatic molecules adsorb at a metal with the ring parallel to the surface, interacting through the π-orbitals. Based on analogous structures in organometallic chemistry, this type of bonding most likely occurs through the sigma-donation of electrons in the π-orbitals of the aromatic ring into vacant metal orbitals (163). Electron density is then returned to the empty π^*-orbitals of the adsorbate via d-π^* back-bonding. Such interactions should induce a decrease in the bond strength of the chemical bonds that are coupled strongly with these molecular orbitals, resulting in a shift of the affected vibrational modes to lower energy. In addition, by variation of the applied potential, the extent of the sigma-donation and d-π^* back bonding can be systematically addressed.

Pons and Bewick (164) studied the adsorption of p-difluorobenzene and its o- and m-substituted isomers at a polycrystalline platinum electrode with SNIFTIRS, examining the adsorption as a function of applied potential and solution

concentration. For p-difluorobenzene, twelve of the normal vibrations are active in the mid-infrared region. Ten of the modes undergo a change in their dipole moment in the plane of the aromatic ring, while two of the modes are perpendicular to the plane of the ring. Thus, based on the earlier discussion of the infrared surface selection rule, if the aromatic moiety adsorbs with the plane of the ring parallel to the surface, only the two modes orthogonal to the ring would be evident in the infrared reflection spectrum. In contrast, if the adsorbate adopted an orientation parallel to the surface, only those modes parallel to the ring would be excited. For instances where the adsorbate exhibits a random orientation at the surface, all twelve transitions would be observed, with the absorbance of each proportional to its orientation.

The difference spectrum for a 0.5 mM p-difluorobenzene solution in 1.0 M perchloric acid between +0.20 V and +0.40 V vs. NHE at Pt shows a spectrum with both positive and negative peaks. At the concentration and thin solution layer, the total quantity of p-difluorobenzene is slightly less than that required to form a closest-packed monolayer in a flat orientation relative to the electrode surface. Positive values of $\Delta R/R$ represent those modes which are present only at +0.20 V (i.e., solution phase species which adsorb onto the electrode surface) and the negative bands are for those modes present at +0.40 V (i.e., surface adsorbates). The observed bipolar shapes for some of the peaks are indicative of a potential-dependent adsorption process where the aromatic species adsorbs with the ring parallel to

surface. The study also demonstrated the effects of applied potential on the character of the spectra. Observations from these experiments indicate an increase in the donation of π-electron density from the adsorbate to the metal, consistent with the model of adsorption. Studies based on solution concentration demonstrated that as coverage increases, the adsorbate reorients from a flat to a skewed or perhaps randomly oriented surface structure.

Other examples

Potential modulation has been utilized to examine a multitude of electroactive moieties at electrode surfaces in aqueous and non-aqueous solvents (142, 145, 165-201). These experiments have primarily dealt with the adsorption of simple species such as CO and CH_3OH at Au or Pt, but have also examined more complex adsorbates such as isoquinoline and bisulfate. Polarization methods have also been used to explore redox probes in situ, however, as with potential modulation methods, the useful spectral windows are limited by the absorption bands of the solvents (202-206).

SECTION III. EVALUATION OF THE PERMSELECTIVE PROPERTIES OF A HYDROLYZED POLYMER FILM BY ELECTROANALYSIS AND INFRARED EXTERNAL REFLECTION SPECTROSCOPY

INTRODUCTION

Thin films of polymeric materials play a vital role in a wide variety of technological applications. This is due, in part, to the relative ease by which the chemical and physical properties of an interface can be modified by these materials to enhance or create a specific utility. Examples of such uses include electroanalysis (207-212), corrosion inhibition (213), lubrication (3), and biomaterials (4, 5). In addition, the structural integrity of many polymeric materials allows for their use as membranes (214-216) and as inert supports for chemically active moieties (217-218). To fully utilize the macroscopic properties, and hence, to maximize the effectiveness of these materials for such applications, an understanding of the processes which govern the chemical microstructure of the polymer must be developed.

Incentive for this work was two-fold. First, the importance of polymeric films in electrochemistry has increased with the development of surface modified electrodes. Here, the adherence of a polymer on the electrode imparts it with the chemical, physical, optical, and redox properties of the film, thereby tailoring the electrode's response to a specific application. The focus in this laboratory has been on the development, characterization, and application of thin polymer films to provide electrochemical selectivity based on molecular size and shape. A second interest is in the application of these films as porous supports for optical sensors (217).

To these ends, the permselective properties of hydrolyzed cellulose acetate have been utilized. These experiments probe the details of the hydrolysis and attempt to elucidate the mechanism of the reaction, to what extent the porosity and permselectivity of the film can be controlled, and what information can be acquired to aid in the design of other more selective interfaces.

This section presents the results of a detailed characterization of the structural evolution of a permselective film as a function of the extent of reaction. These films, coated on glassy carbon (GC), exhibit a marked change in permeability as alkaline hydrolysis is allowed to proceed. Infrared external reflection spectroscopy was utilized to monitor the hydrolysis of the film as the molecular composition changed from the acetate to the cellulosic form. These results are in qualitative agreement with electrochemical data obtained with cyclic voltammetry. The electrochemical measurements indicate a change in permselectivity as the hydrolysis proceeds, corresponding directly to changes in the infrared modes observed spectroscopically.

EXPERIMENTAL

Preparation of Glassy Carbon Substrates

A sheet of glassy carbon (GC-20, Tokai Carbon Co., Tokyo, Japan) was cut into approximately 2.5 by 2.5 cm squares and polished on one side with 600-grit Si powder, followed successively by 1, 0.3, and 0.05-μm alumina (Buehler Ltd., Evanston, IL) until a mirror-like finish was achieved. The substrates were rinsed in an ultrasonic bath (Branson Cleaning Equipment Co., Shelton, CT) with deionized water (Millipore Corp., Bedford, MA) between each step to remove residual alumina.

Preparation of Cellulose Acetate Films

Films were deposited on the glassy carbon substrates by flooding the surface with either a 2.5% or 1.0% (w/v) solution of cellulose acetate (Aldrich, Inc., Milwaukee, WI) in cyclohexanone and spinning at either 1000 rpm or 4000 rpm to form films with thicknesses of 170 ± 10 nm and 70 ± 10 nm respectively. The films were allowed to dry under a watch glass overnight. This cellulose acetate polymer contains 39.8% acetate by weight and represents an average of 2.45 acetyl groups per glucosidic unit. Film thicknesses were measured with an Alphastep surface profiler (Tencor Inst., Mountainview, CA) and represent the average of at least 3 measurements at several locations on the film. The uncertainty is reported as the range of the measurements.

Base hydrolysis of the films was achieved by immersion of the dried substrates in 0.070 M KOH at 25 °C with removal at intervals of 10 min. The hydrolysis was quenched in a stirred cold water bath. The substrates were then allowed to dry under a watch glass or were blown with dry N_2 before the analyses were performed.

Instrumentation

Cyclic voltammetric data were acquired with a BAS CV-27 potentiostat (Bioanalytical Systems, West Lafayette, IN) and is referenced to a Ag/AgCl electrode (saturated with KCl). An inert gasket material was utilized to maintain an effective electrode size of ~38 mm^2. Cyclic voltammograms are recorded as the first anodic sweep, with the cathodic trace removed for clarity.

Infrared spectra were obtained with a Nicolet 740 FT-IR (Nicolet Inst., Madison, WI) equipped with a liquid N_2 cooled, narrow-band HgCdTe detector. The spectrometer and sample compartment were purged with boiloff from liquid N_2. External reflection measurements were performed using a modified variable angle reflection accessory (Harrick Scientific, Ossining, NY) which had been set to an angle of incidence of 60°. Reflection spectra are presented as $-\log(R/R_o)$ vs. wavenumber, where R is the reflectivity of the coated substrate and R_o is that of the bare substrate, and are the ratio of 1024 sample to 1024 background scans at 4 cm^{-1} resolution. An aluminum wire grid polarizer on KRS-5 (Cambridge Physical Sciences) was

placed immediately before the accessory to select the *p*-polarized component.

Reagents

All reagents were used as received.

RESULTS AND DISCUSSION

Electrochemical Permeation Study

Impermeable, electrically insulating films of materials such as cellulose acetate form a substantial barrier to heterogeneous electron-transfer (219). This phenomenon is exponentially dependent on the separation between electroactive species and the underlying electrode surface. As has been demonstrated in the literature (209, 215, 220), a controlled base hydrolysis of these types of materials leads to an increase in the porosity of the films, and hence, to an increase in their permeation by electroactive probes.

In order to correlate the structural composition of the film (vide infra) with the observed changes in permeability, redox probes of varying sizes were selected. Aqueous solutions, with 0.05 M phosphate buffer (pH ≅ 7.4) as supporting electrolyte, were prepared of the following: 0.6 mM 1,4-hydroquinone, (HQ); 0.4 mM potassium ferrocyanide, ($K_4Fe(CN)_6 \cdot 3H_2O$) (J.T. Baker, Phillipsburg, NJ); and a 0.4 mM concentration of the cofactor nicotinamide adenine dinucleotide, (β-NADH) (Sigma Chemical Co., St. Louis, MO). The estimated molecular volumes of these probes (HQ: 190 $Å^3$; $Fe(CN)_6^{4-}$: 830 $Å^3$; β-NADH: 1050 $Å^3$) are estimated from tabulations of the Van der Waals and covalent radii for the species (221-222).

Cyclic voltammograms for the oxidation of the aforementioned redox pairs at glassy carbon are shown in Figure 17. Figure 17a shows the first oxidative sweep at polished, bare glassy carbon for all three

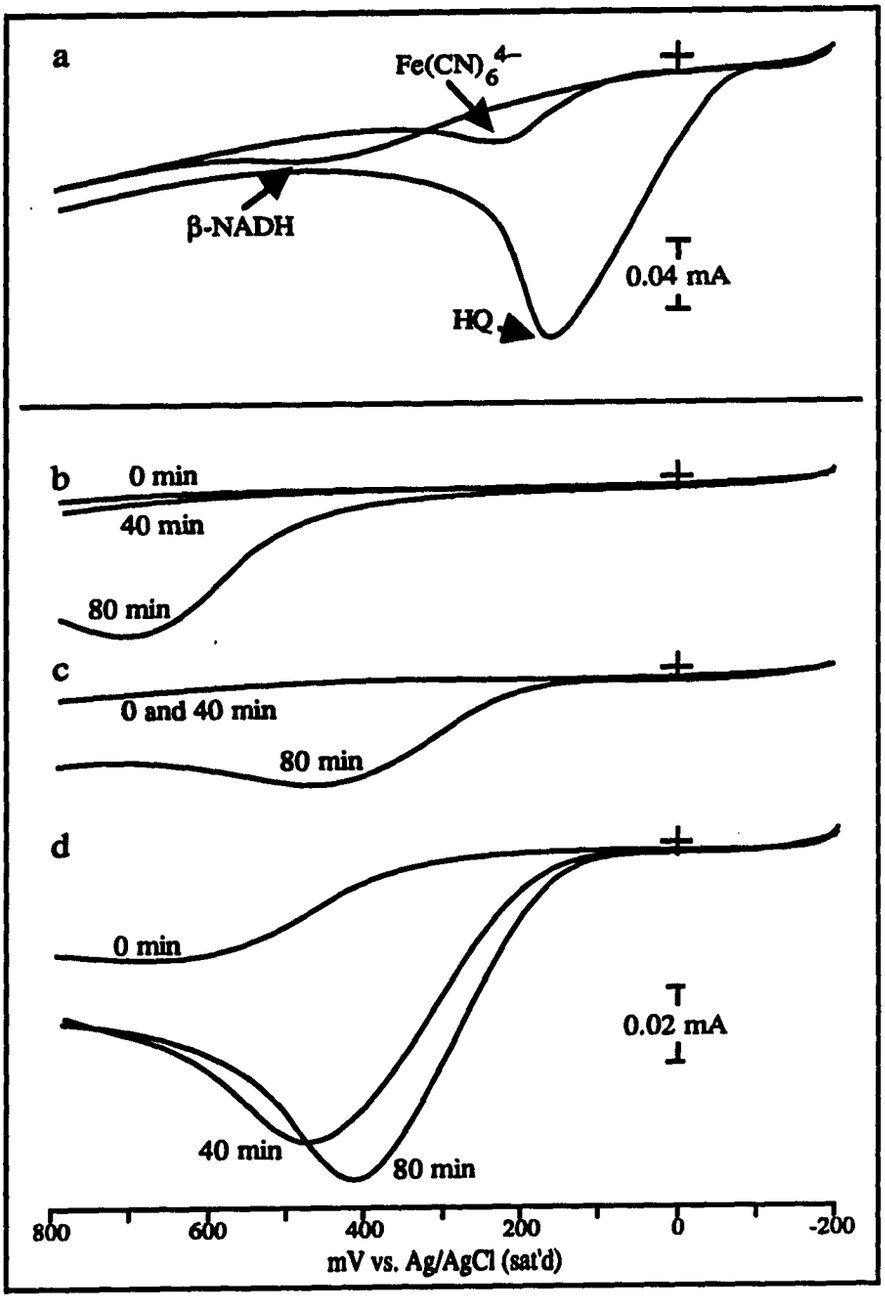

Figure 17. First sweep voltammograms for the test probes at (a) bare glassy carbon and (b-d) at cellulose acetate coated films at 0, 40, and 80 min of hydrolysis. (b) 0.4 mM β-NADH, (c) 0.4 mM $Fe(CN)_6^{4-}$, (d) 0.6 mM HQ

species. Figures 17b-d are the respective oxidations at cellulose acetate coated GC electrodes at 0, 40, and 80 min of hydrolysis as labeled. These films had nominal thicknesses of 170 ± 10 nm. The amount of charge passed during the forward sweep was determined by integration.

Figure 18 shows a plot of Q'_{ox} vs. hydrolysis time for the test species. Here, $Q'_{ox} = K'(Q_{ox}/n)$, where K' is the ratio of the concentrations of the analytes to the concentration of HQ, and n is the stoichiometric number of electrons involved in the oxidation, and Q_{ox} is the oxidative charge. The oxidations of HQ and β-NADH are two-electron processes while $Fe(CN)_6^{4-}$ proceeds through a one-electron process. The use of Q'_{ox} serves to normalize the charge passed for the three species to aid in direct comparison. Differences in the magnitudes of Q'_{ox} at longer hydrolysis times are likely attributable to the electrochemical kinetics involved in the oxidation.

Prior to hydrolysis (t = 0), films of cellulose acetate form an impermeable barrier to mass transport for the bulky β-NADH and $Fe(CN)_6^{4-}$ probes. This is attributed to the small free volume in the polymer which prevents these species from diffusing to the electrode surface. Some pathways through the film are present, however, which are sufficiently large to permit the smaller HQ molecule to pass to the electrode surface, allowing electron transfer to occur. Additionally, the response from the electrolysis may result, in part, from a partitioning of the HQ into the film (209), thereby limiting the utilization of this data in the development of a simple description of

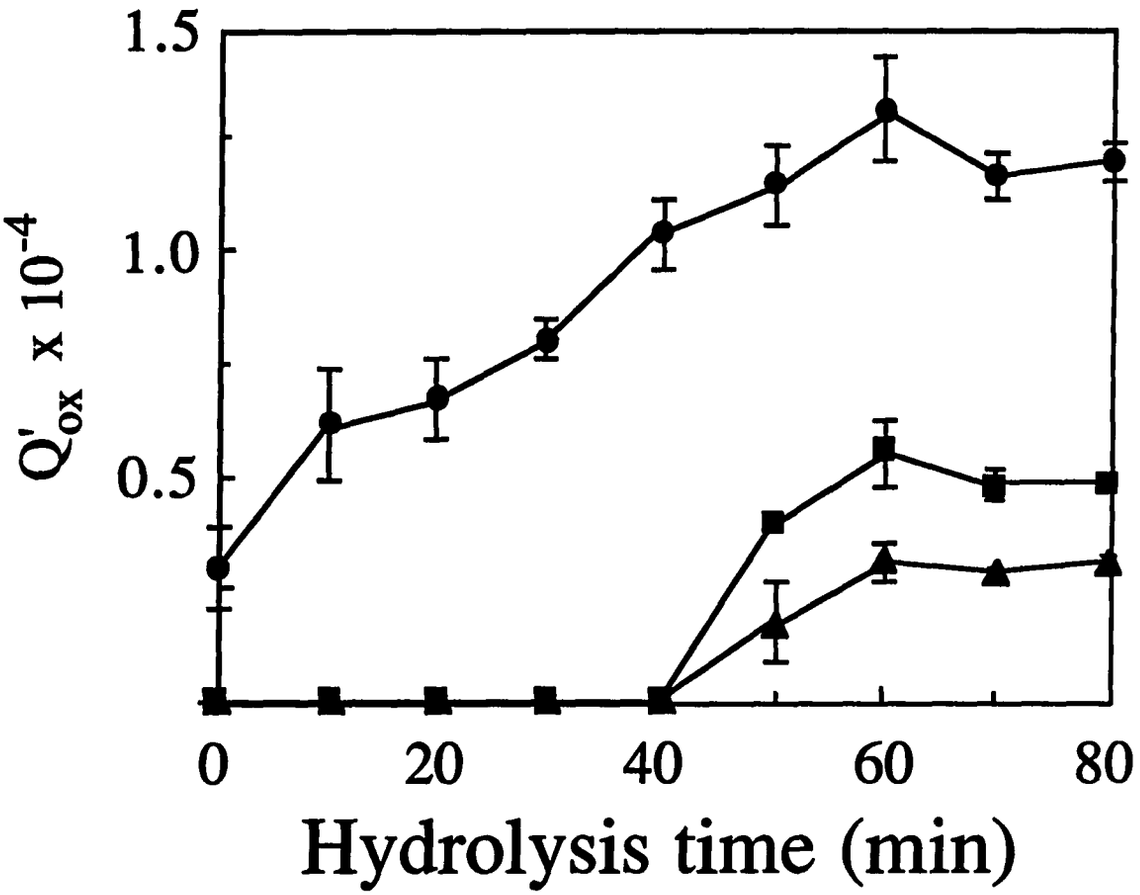

Figure 18. Normalized charge vs. hydrolysis time for a 170 ± 10 nm cellulose acetate film at glassy carbon. (●) Hydroquinone, (▲) β-NADH, (■) $Fe(CN)_6^{4-}$

the hydrolysis mechanism. The peak center for the oxidation wave is shifted significantly in the positive direction due to substantial potential drop across the resistive film. The amount of charge passed, Q'_{ox}, is also diminished.

As hydrolysis is allowed to proceed, permeation of the film by HQ gradually increases, indicating that the pathways through the film become larger or less obstructed. It is not until after 40 min of hydrolysis, however, that the film develops pores large enough to allow the passage of the bulky probes. After 60 min, permeation by all three test species reaches essentially a steady-state, where diffusion to the electrode surface within the channels proceeds unhindered. The total amount of charge passed is approximately 50% of that at the bare electrode. This is expected, however, since the cellulosic skeleton still remains on the surface, reducing the net electrode area. For this film thickness, the "threshold of permeability" for larger molecules to the surface occurs between 40 and 50 min of hydrolysis. Similar experiments using a 70 ± 10 nm film showed the same transport characteristics, however, the threshold occurred earlier, between 30 and 40 min.

Infrared External Reflection Spectroscopic Study

In an effort to understand the observed electrochemical permeation on a molecular level, infrared external reflection (IR-ER) spectra of the cellulosic films on GC were acquired at 10 min intervals as the hydrolysis proceeded. Figure 19a is a transmission spectrum of

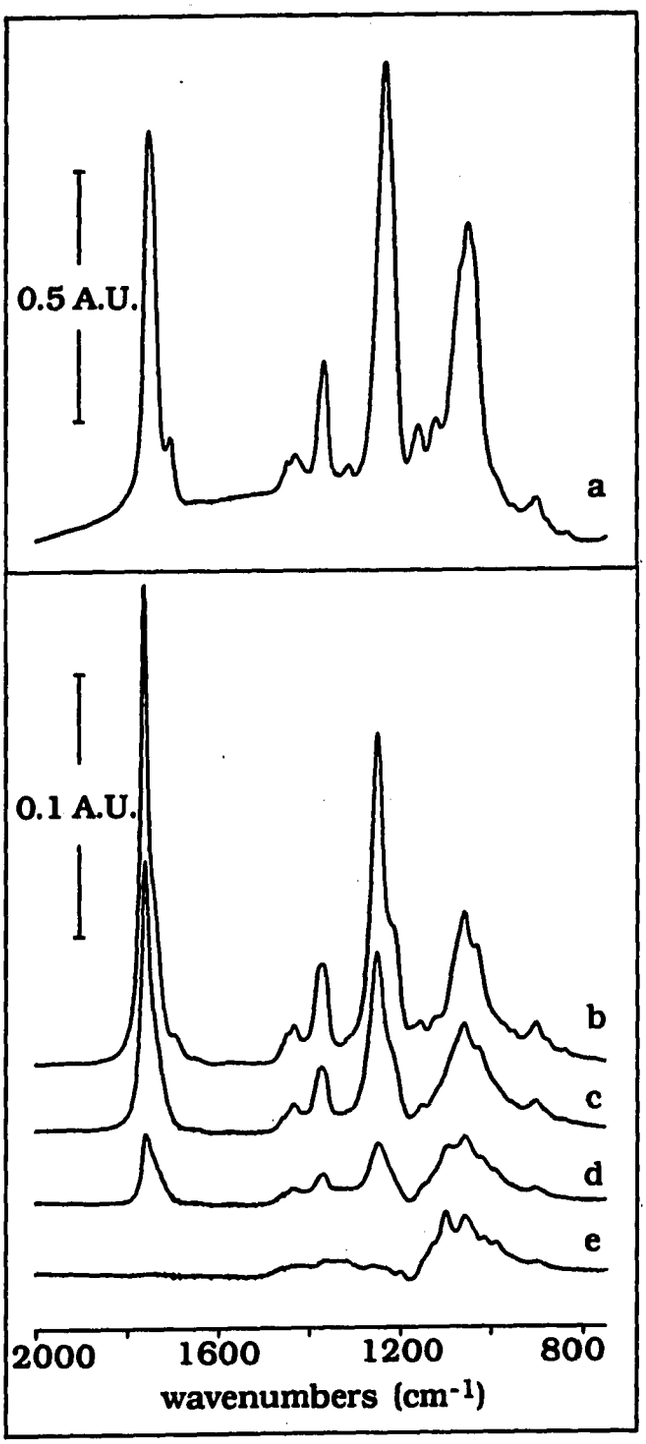

Figure 19. Infrared spectra for cellulose acetate films at Si (a) by transmission, and at glassy carbon (b-e) by external reflection at 60° for varying amounts of base hydrolysis: (b) 0 min; (c) 40 min; (d) 50 min; (e) 80 min

a 1.85 ± 0.01 μm film of cellulose acetate which was coated on a Si window. Based on previous work (223-225), the modes at 1760 cm^{-1} and 1234 cm^{-1} are assigned as ν(C=O) and ν(C-O) for the acetate functionality respectively. The small bands at 1440 cm^{-1} and 1365 cm^{-1} are probably due to the $-CH_3$ bending mode. A large cluster centered at 1050 cm^{-1} contains at least seven distinct bands (as determined from curvefitting analysis), which can be attributed to the primary and secondary C-OH stretches for the alcohol groups, the asymmetric and symmetric C-O-C stretches for the inter- and intra-ring ether linkages, and the O-C-C stretches for the ester group (226). The large extent of overlap for this cluster dictates only a qualitative discussion of its components (vide infra). Not shown in the Figure are the O-H stretching mode at ~3350 cm^{-1} and the C-H stretches for $\nu(CH_3)$ and $\nu(CH_2)$ between 3000 and 2800 cm^{-1}.

Figures 19b-e show the IR-ER spectra for a 170 ± 10 nm film of cellulose acetate on glassy carbon at an angle of incidence of 60° with p-polarized light at 0, 40, 50 and 80 min of hydrolysis. Distortions, caused by the residual s-polarization component, are readily observed in the reflection spectra as asymmetric band shapes. Decreases in intensity for the peaks associated with the acetate group are observed as a function of hydrolysis. The apparent shift to higher energy for the multiplet at 1050 cm^{-1} is most likely due to a decrease in intensity of the lower energy components of the band, corresponding to the acetate groups, and an increase in intensity for the higher energy bands; those which are attributable to the alcohol groups. Figure 20a

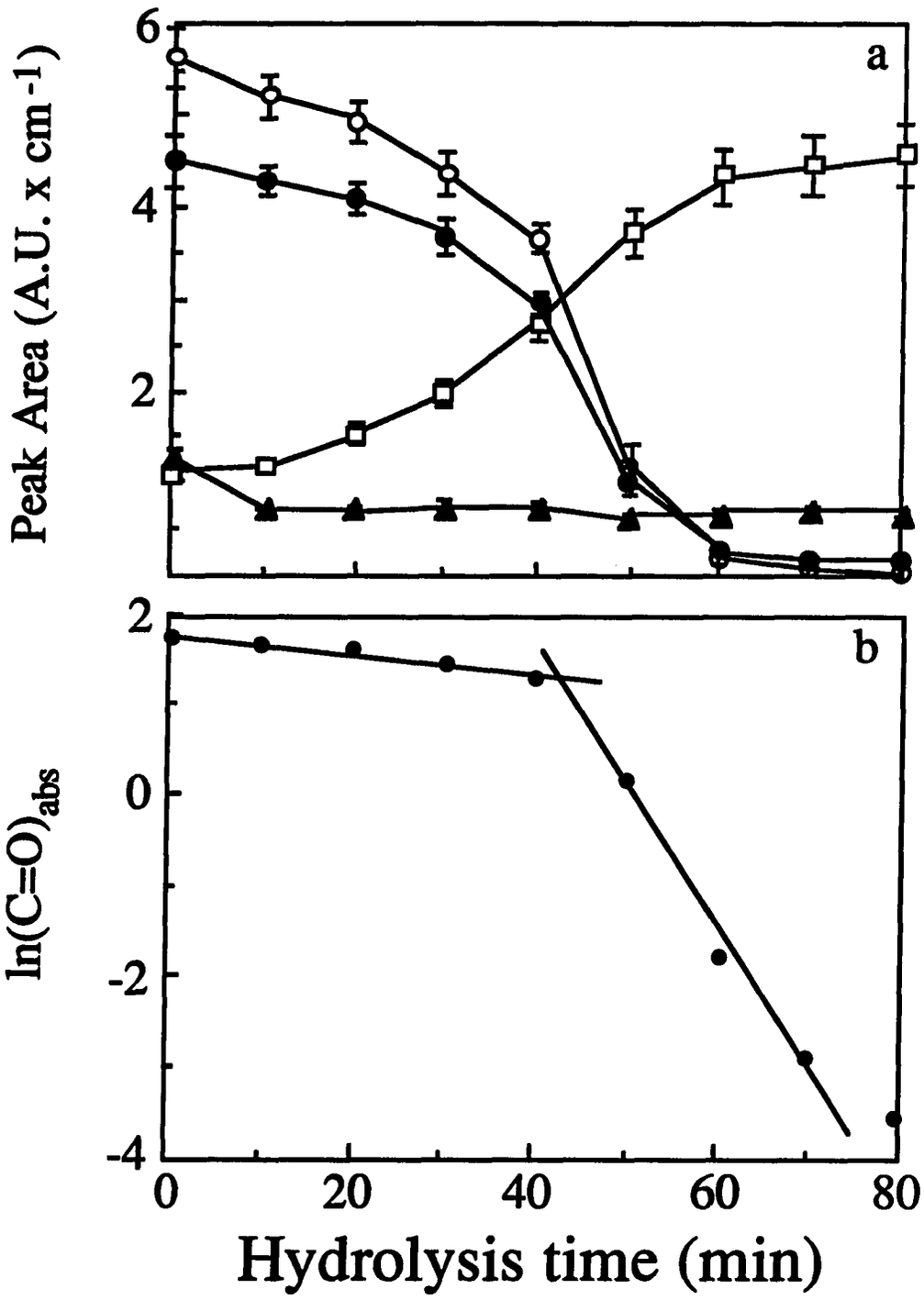

Figure 20. IR peak area vs. hydrolysis time for cellulose acetate at glassy carbon (a), (○) ν(C=O), (●) ν(C-O), (□) ν(OH), (▲) ν(CH_2), Pseudo first-order kinetics plot for hydrolysis (b)

is a plot of the integrated peak area for the prominent spectral features vs. hydrolysis time. Omitted from this plot are the peak areas for the individual components of the multiplet at 1050 cm^{-1}, as band assignments for these modes are made tentatively since peak positions in this region of the spectrum can vary substantially, and peak areas, as determined by curvefitting, are only approximate.

The reaction proceeds via a mechanism which is consistent with the hydrolysis of an ester; that is, acetate groups are replaced by hydroxyl groups. By 40 min, the integrated absorbances for the acetate marker bands have decreased by ~35%, and ν(OH) has increased accordingly. After 40 min, the reaction appears to proceed at an increased rate, resulting in the removal of an additional 45% of the acetate groups within 10 min and continuing until the hydrolysis is mostly complete at 80 min, with the film essentially the composition of cellulose. Long-term hydrolysis experiments (24 h) have shown that the weight of a cellulose acetate film decreases by ~47% as the reaction approaches completion. If weight loss was due only to the removal of the acetate functionalities, a loss of ~39% would be expected. This demonstrates that some of the glucosidic units of the polymeric chains must be cleaved and carried away into solution during the hydrolysis. This contribution to weight loss is small, however, when compared to that for the removal of the acetate groups.

The degree of crystallinity of a cellulose acetate film is known to be dependent on such preparation parameters as solvent, rotation rate, and the acetyl content of the bulk polymer (227). It can be

concluded, therefore, that the film is composed of several anisotropic regions, some of which are crystalline in nature and others which are more amorphous. Common to both, however, is the glucosidic backbone of the polymer. As hydrolysis proceeds, the hydroxide ion attacks the exposed surface of the chains, replacing the bulky acetate groups, and opening up microscopic pockets in the lattice, thereby increasing the surface area. As the acetate groups are removed, transport of the HQ molecule to the surface becomes less hindered, however, the pores in the film remain too small for the more massive probes to pass.

A plot of $\ln(C=O)_{abs}$ vs. hydrolysis time (Figure 20b) shows the pseudo first order rate constant for the reaction. The two distinct slopes are indicative of an A→B→C reaction mechanism (228), where "A" represents the initial, mostly crystalline film, "B" represents the film in a more amorphous state, and "C" represents the film after hydrolysis. A probable reaction scheme begins with the film representing a mostly crystalline structure which prevents mass transport to the electrode surface. The initial reaction, A→B, serves as an induction period, or a time when the film is solubilized by the base. As the film become softer (more amorphous) hydrolysis begins and acetate moieties are removed from the glucosidic backbone (B→C) opening channels to the electrode surface. Evidence from attenuated total reflection FT-IR spectroscopy indicates that after the hydrolysis is essentially complete and the free volume of the film is large due to the removal of the acetate groups, the film collapses on itself.

In addition to the exchange reaction between the acetyl and hydroxyl groups, it is also possible that the polymeric chain is gradually shortened by cleavage of the ether linkages between terminal glucosidic units and the chains (229). Due to difficulty in resolving those absorption bands which are directly attributable to the inter-ring ether linkage, the extent to which this phenomenon occurs is difficult to determine.

CONCLUSION

The permselective properties of a hydrolyzed cellulose acetate film on glassy carbon have been investigated by cyclic voltammetry and correlated to molecular composition using infrared external reflection spectroscopy. The change in electrochemical permeation is correlated to the hydrolytic removal of the acetate functionalities on the polymeric skeleton, increasing the free volume of the film and its microscopic porosity. The size of these pores determines the selectivity of the film to the redox probes. For the film thickness studied, a "threshold of permeability" for the larger test species occurs at ~40 min of hydrolysis. The parameters used for film preparation and hydrolysis can be tailored to carefully control the size selective properties for films of other thicknesses, thereby facilitating or preventing mass transport to the surface for a variety of analytes.

SECTION IV. AN EX SITU EVALUATION OF THE FORMATION AND ORIENTATION OF A HOMOLOGOUS SERIES OF *n*-ALKANETHIOLS ON Au AND Ag

INTRODUCTION

Interest in the use of organosulfur materials for the fabrication of monomolecular assemblies at metal surfaces has increased in recent years (131, 219, 230-234). This is due, in part, to the relative ease by which these films can be formed, and to the variety of precursors available for constructing a monolayer with properties tailored to a particular application. These materials have a high affinity for Au and Ag and, upon exposure to a bare metal surface, will spontaneously adsorb as a nearly closest-packed array at the surface. Although the utility and performance of these films for a variety of applications has been demonstrated in the literature (6, 213, 235-237), a detailed understanding of the molecular interactions contributing to the formation and orientation of these assemblies has yet to be developed.

Monolayer films of *n*-alkanethiols on Au have been studied extensively as models for these types of interfacial systems due to their simple molecular structure, ease of availability, and the wealth of data in the literature concerning the properties of neat *n*-alkanes (238-241). These molecules adsorb at Au to form highly ordered, densely packed structures with an average chain tilt of ~35° from the surface normal, forming a partial barrier to electron and ion transport (242), and imparting the substrate with the properties of a pseudo-crystalline *n*-alkane. Adsorption kinetics for formation of the monolayer at Au are quite fast, with a nearly complete layer depositing after a few hours (230) with a metal-sulfur bond strength on the order

of ~28 kcal/mol (242). In addition, it has been demonstrated that, due to the cohesive interactions between adjacent chains, films formed from longer *n*-alkanethiols are more strongly bound than those formed from the shorter chains (243-246). Such data served as a control for the experiments performed in this laboratory on Au. In addition it provided a basis for comparison with data acquired at Ag.

There are, however, several fundamental questions concerning the molecular microstructure of these assemblies which must be resolved in order to more fully understand the nature of these types of films, and consequently, those of a more complex molecular composition. For example, what is the nature of the bond between the metal and the thiol? What is the two-dimensional periodicity of the monolayer lattice across the surface? What is the effect of conformational disorder in the chains on the packing of the monolayer? What is the effect of the roughness of the substrate on monolayer order? How do the properties of the film at Au transfer to other materials, such as Ag?

No one method of analysis can provide answers to all of the above chemical problems. Consequently, a multi-disciplinary approach was taken which concentrated on examining the molecular level processes which control the adsorption, spatial arrangement, and packing order of these materials. This chapter reports the results of a many-facetted characterization of a homologous series of *n*-alkanethiol monolayer films at Au and at Ag by IR-ERS, contact angle measurements, optical ellipsometry, scanning tunnelling microscopy,

and electrochemistry. This project was a collaborative effort among several researchers whose individual expertise is in each of the above disciplines. As a result, particular emphasis in the text is placed on the discussion concerning the examination by IR-ERS, which was this author's primary contribution to the project, and only the results and conclusions derived from the other methods will be discussed.

EXPERIMENTAL

Substrate Preparation

Two inch diameter Si wafers and 1x3 inch glass microscope slides were prepared prior to evaporation by a careful degreasing of the substrates with acetone and methanol. The substrates were then spun dry on a photo-resist spin-coater (Headway Research, Inc., Garland, TX). In cases where reclaimed substrates were used, a hydrogen peroxide/sulfuric acid bath (vide infra) was utilized prior to the degreasing step to remove any excessive organic contamination of the surface. Metal films were deposited on the substrates by resistive evaporation in a cyropumped, Edwards E360A Coating System at pressures of $<9x10^{-5}$ Pa ($7x10^{-7}$ Torr) using metals of 0.99999 purity. A 15-20 nm adhesive layer of chromium was deposited prior to a 250-300 nm layer of Au or Ag. The rate of deposition for chromium was ~0.2 nm/s, for Ag, ~2.5-3.0 nm/s, and for Au, ~0.5-1.0 nm/s. The evaporator was allowed to cool for ~45 min and back filled with dry N_2 before the samples were removed.

It is important to emphasize that these experiments were performed in the laboratory ambient or, at best, in a dry N_2 atmosphere. Consequently, impurities at the surface of these metal films due to airborne species in the laboratory are to be expected. Data from Auger electron spectroscopy showed the presence of sulfur, oxygen, chlorine, and carbon at the uncoated Ag surfaces with the predominant impurity being oxygen. At Au, the impurities are oxygen,

chlorine, and carbon. To minimize variability in the formation of the monolayer films due to the presence of the oxide layer at the metal surface, exposure to the laboratory ambient was limited to 10-15 min prior to formation of the monolayer films. No appreciable levels of organic contamination were observed by infrared spectroscopy after the formation of the monolayer films.

Monolayer preparation

Monolayer films were prepared by immersing the freshly evaporated metal films into a ~0.5 mM thiol solution in absolute ethanol for a period of ~24 h. The thiols were purified prior to use by either recrystallization from absolute ethanol or by passage through an activity 1 neutral α-alumina column. Spontaneous self-assembly of the monolayer occurs due to the high affinity of the thiol head-group for the metal, forming a densely packed structure at the surface. After emmersion, the films were rinsed with absolute ethanol and hexane to remove residual analyte and were spun dry on a photoresist spin-coater. The composition, spatial orientation, and structural integrity of these films on Au were consistent with those previously reported (230-233). There is no apparent difference in the infrared external reflection spectrum of monolayers that have been allowed to grow for only a few hours and those that were allowed to grow for 24 hours.

Infrared External Reflection Spectroscopy

Infrared external reflection spectra were obtained with a Nicolet 740 FT-IR (Nicolet Analytical Instruments, Madison, WI) using a modified variable angle reflection accessory (Harrick Scientific, Ossining, NY) set at an angle of incidence of 80° with *p*-polarized light (Cambridge Physical Sciences, U. K.). The spectrometer and sample compartment were purged with liquid N_2 boil-off. All spectra are the ratio of 1024 sample scans to 1024 background scans at 2 cm^{-1} resolution (with a single zero-filling) and Happ-Genzel apodization. Either a liquid N_2 cooled InSb or narrow band HgCdTe detector was used. All spectra are reported as $-\log(R/R_0)$ where R is the reflectivity of the sample and R_0 is the reflectivity of a "bare" Au reference substrate.

"Bare" Au reference substrates were cleaned by immersion of a Au film supported on the substrate of interest (i.e., Si or glass) in a 1:3 solution of 30% H_2O_2 and concentrated H_2SO_4 for 5-10 min followed by rinsing in deionized H_2O. The substrates were then flooded with 30% H_2O_2 and spun on a photo-resist spin-coater until near-dryness, at which time they were placed into the sampling accessory in the optical bench and allowed to dry completely in the N_2 boil-off atmosphere. The term "bare" Au does not preclude the presence of surface oxides on the Au. However, the acid/peroxide mixture, or piranha etch, is known to effectively remove all organic contamination from the Au surface. This has been verified by ratioing the IR reflection spectrum of a substrate prepared in this manner with that

of a fully deuterated thiol monolayer at Au. No reflection/absorption bands for hydrocarbon contamination at the "bare" Au were observed.

Other Instrumentation

Auger electron spectroscopy was acquired with a PHI Auger Multiprobe 600 system (Eden Prairie, MN). Advancing and receding contact angles were determined in air using a Rame-Hart Model 100-00-115 Goniometer (Mountain Lakes, NJ). The sample to sample variation in the measured angles is ±1°.

Relative thicknesses for the homologous series of the *n*-alkanethiol monolayers were determined using a Gaertner model L-116A Auto Gain Ellipsometer (Chicago, IL) at a wavelength of 632.8 nm. The optical constants for the complex refractive indices of the substrates were acquired prior to and after formation of the monolayer, and the thickness of the adsorbed layer was then determined from a two-phase, parallel layer model of the surface based on classical electromagnetic theory (238-239, 247). A value for the real refractive index of the film of 1.45 was used for direct comparison with other published results (248).

Scanning tunnelling microscopy was performed with a Nanoscope II (Digital Instruments, Inc., Santa Barbara, CA). Lateral resolution was estimated to be ±0.04 nm.

Reagents

Deionized water was obtained from a Milli-Q water purification system (Millipore Products, Bedford, MA). Absolute ethanol (Midwest Grain) and hexane (HPLC grade, Fisher Sci., Springfield, NJ) were used as received. Liquid *n*-alkanethiols ($CH_3(CH_2)_nSH$) were obtained from a variety of sources; n=1 from Alfa Products (Ward Hill, MA), n=2, 4, 6, 7, 8, and 15 from Aldrich Chemical Co. (Milwaukee, WI), n=3, 5, 9, and 11 from Eastman Kodak (Rochester, NY), and n=13 from Pflatz and Bauer, Inc. (Waterbury, CT). Chains where n=12 and 14 were synthesized in-house by C. Chung, and n=10 was a gift from Professor G. Whitesides at Harvard University. Octadecanethiol, n=17 (Aldrich), was recrystallized from ethanol. All other chemicals were reagent grade and were used as received.

EXPERIMENTAL DIFFICULTIES IN THE ACQUISITION OF HIGH QUALITY INFRARED EXTERNAL REFLECTION SPECTRA

In spite of the energy throughput, multiplex, and resolution advantages of Fourier transform IR interferometry, the acquisition of high quality reflection spectra can still pose experimental difficulties. For the specific case of monolayer films, the low absorbance of the samples also places extreme demands on sample alignment. Since most methods for obtaining reflection spectra of monolayer films require the collection of separate sample and reference files, reproducible positioning of the substrates is necessary for preventing small changes in the optical path of the reflected beam. Changes in the optical path can, for example, give rise to fringes in the ratioed spectrum because of interference phenomena at the window of the IR detector. Fringing effects are further amplified by the high refractive indices of many of the materials used for these windows (e.g., n=2.65 for CdTe, n=2.42 for ZnSe). In an effort to remove the ambiguity in substrate placement and to facilitate the acquisition of high quality spectra, special sample holders for 2 inch diameter Si wafers and for 1 x 3 inch microscope slides have been constructed. Since the principles involved are the same, this section describes only the design and performance of the Si wafer holder. A sketch and mechanical drawings for the wafer holder are shown in Figures 21 and 22.

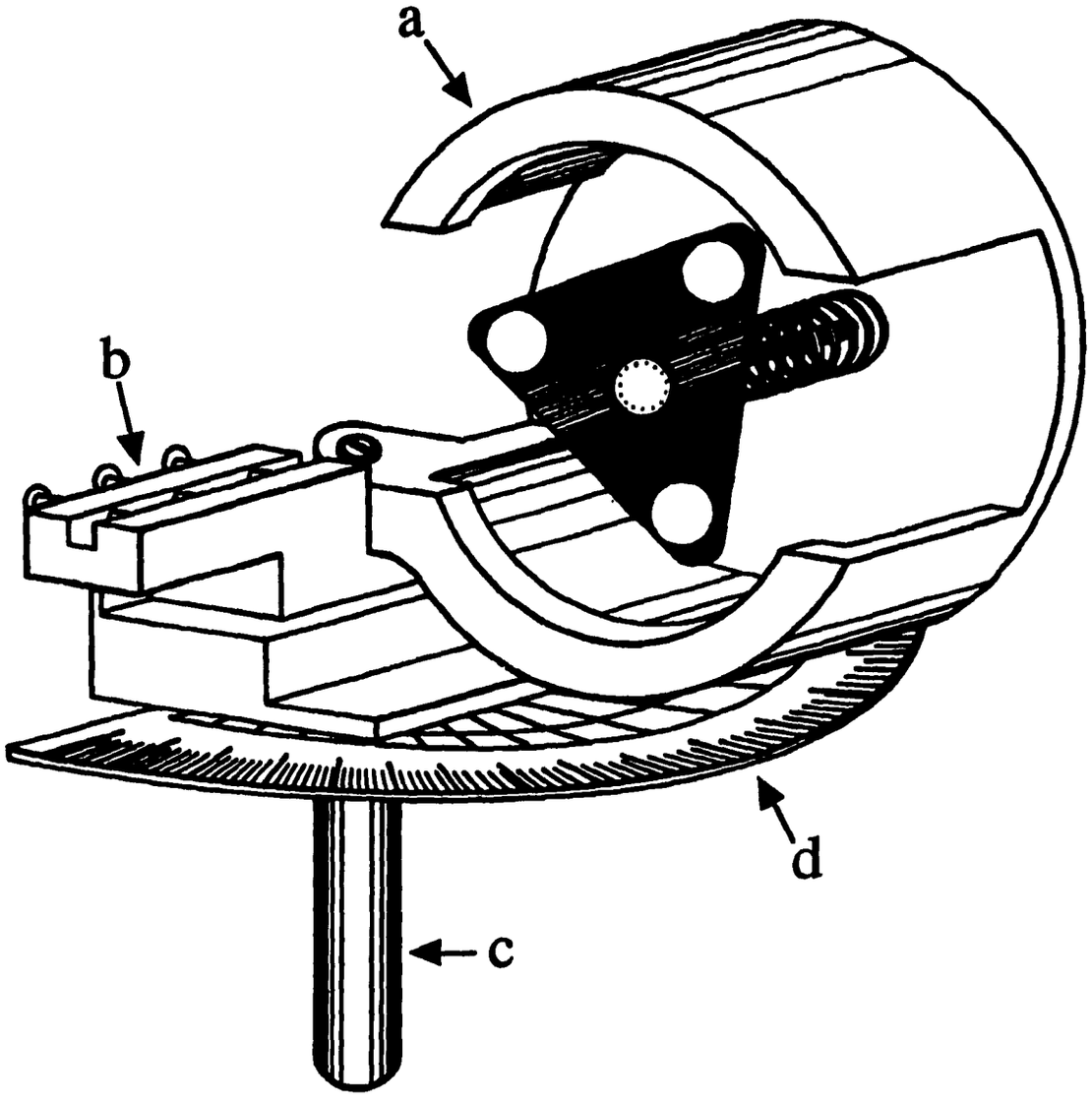

Figure 21. Substrate holder for 2 in diameter Si wafers with parts noted as follows: a) substrate holder, b) retro-mirror holder, c) centering post, d) protractor

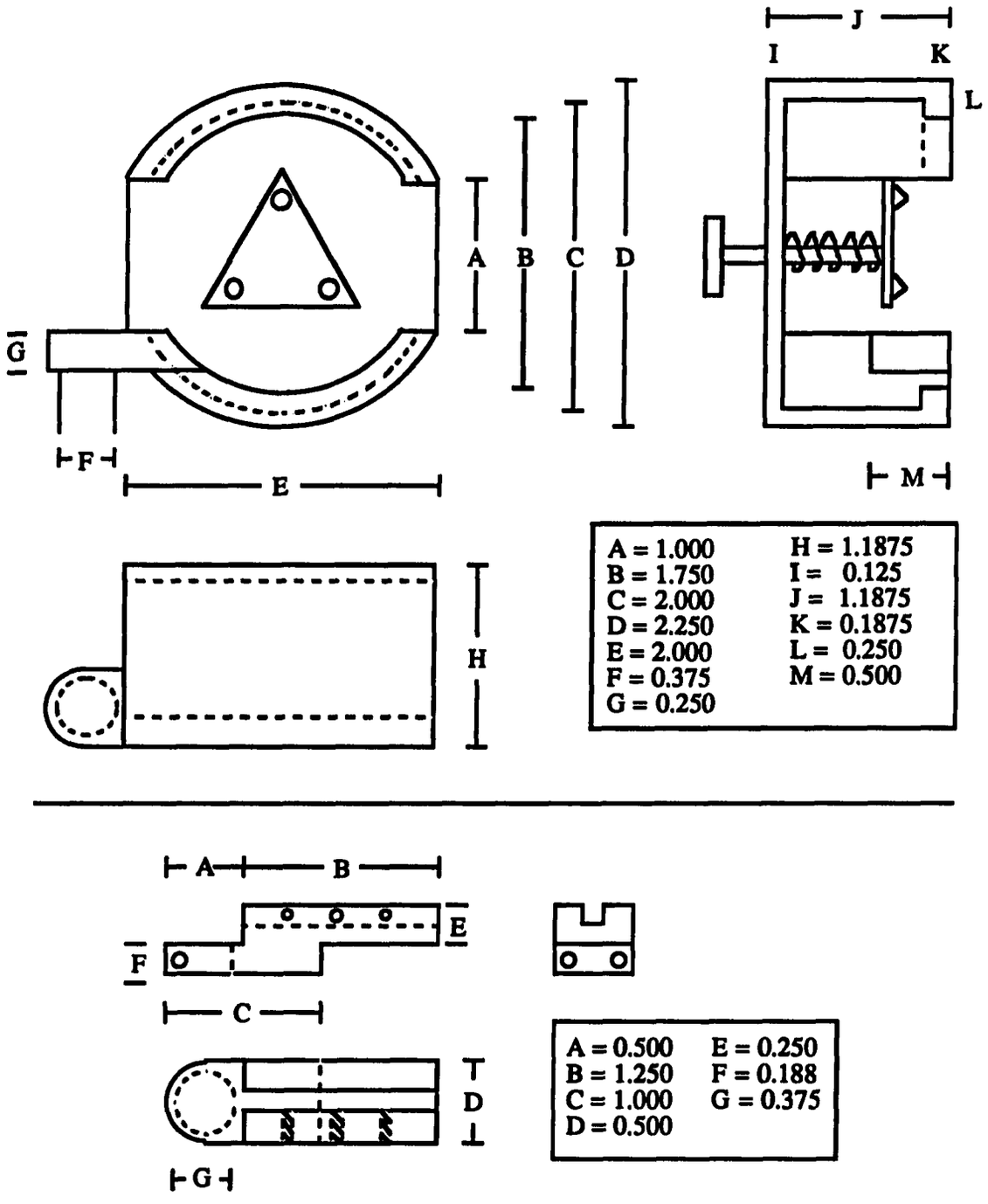

Figure 22. Mechanical drawings for the sample holder in Figure 21

Figure 23 illustrates the degradation of spectral quality caused by poor sample alignment. The spectrum is for a monomolecular assembly of *n*-octadecanethiol on Au ($CH_3(CH_2)_{17}S$/Au) referenced to bare Au at an angle of incidence of 80°. Band assignments are based on previous studies (231). The observed fringing occurs when the incident IR energies for the two single-beam spectra strike the CdTe window of the detector in slightly different locations, causing the amounts of channelling within the window to vary. The frequency of the fringing is comparable to that expected for an interference element with ~1.5 mm thickness, which is in agreement with that for the detector window (249). This fringing will not pose a problem to the acquisition of high quality monolayer spectra provided the optical path through the detector window is the same for both the reference and sample spectrum.

The sample holder in Figure 21 provides for the exacting replacement of sample and reference substrates, greatly reducing the problem of fringing. The holder was constructed for compatibility with a commercial variable angle reflection accessory (Harrick Scientific, Ossining, NY) and consists of 4 parts: 1) substrate holder, 2) retro-mirror holder, 3) centering post, and 4) protractor. Dimensional modifications may be necessary for use with other accessories.

The substrate holder was constructed from a single piece of aluminum. The top and the bottom of the Si wafer are held firmly by a lip which contacts approximately two-thirds of its circumference.

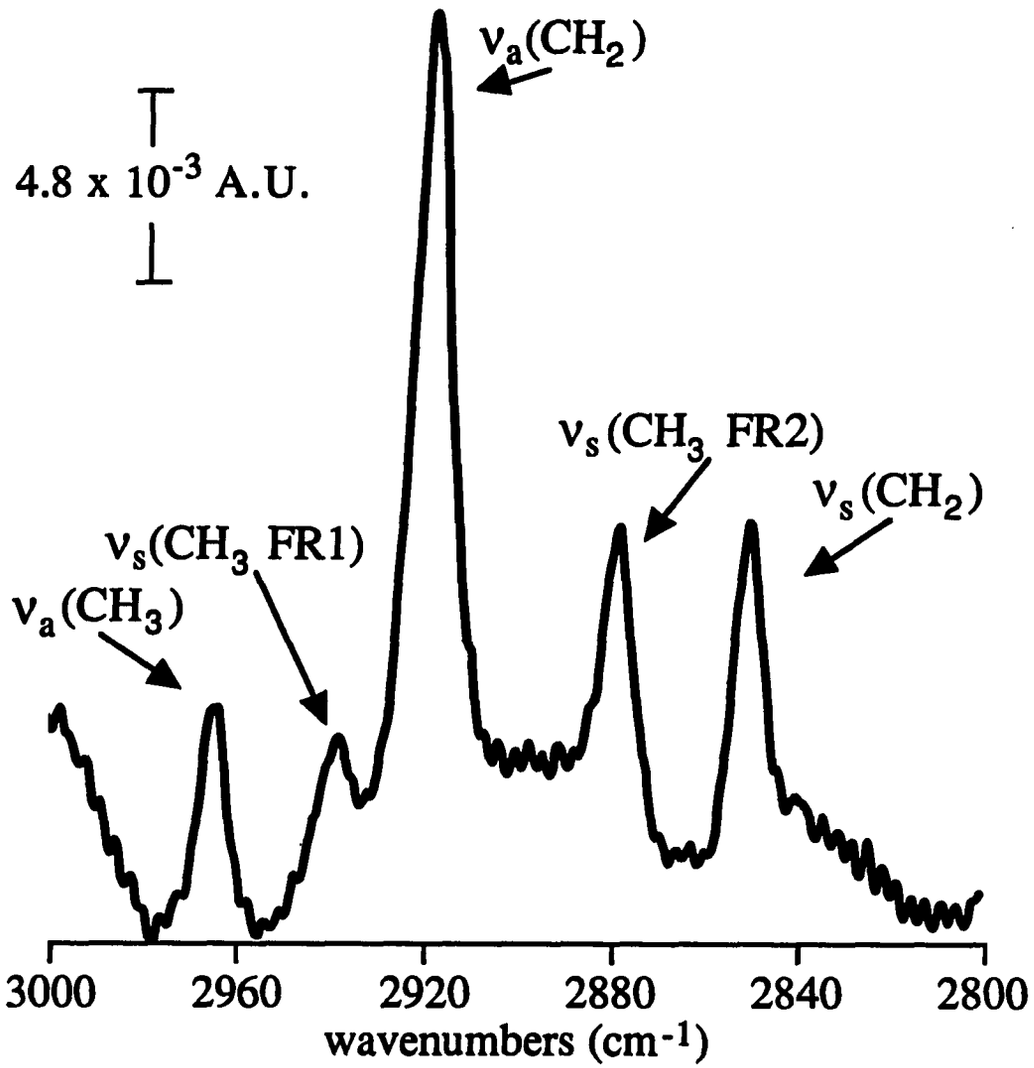

Figure 23. Infrared spectrum of *n*-octadecane thiol on Au with fringing induced by optical misalignment. Bands are as follows: 1) $\nu_a(CH_3)$, 2) $\nu_s(CH_3$, FR1), 3) $\nu_a(CH_2)$, 4) $\nu_s(CH_3$, FR2), 5) $\nu_s(CH_2)$

Reflection experiments on metallic surfaces are typically performed at grazing incidence to maximize the net electric field normal to the surface (10), therefore a portion of the lip on both sides of the holder was removed to avoid vignetting the incident beam. A spring loaded tripod presses the sample firmly in place. Care must be taken to avoid excessive pressure as Si wafers are fragile. Fringing can be induced if the applied pressure bows the sample.

The retro-mirror holder is attached to a centering post and the angle between the mirror and the sample is set to 97.5°. Set-screws lock the holder in place. A Au-coated glass slide is used as the retro-mirror and is held in place with three screws. The holder is also constructed from aluminum and the centering post from stainless steel. Careful positioning of the mirrors relative to the centering post is critical to maintain a proper optical arrangement. A protractor was mounted below the holder to facilitate an accurate determination of the angle of incidence. A spacer can be placed between the holder and the accessory to set the height of the sample in the optical path.

Figure 24 shows an IR-ERS spectrum for the same *n*-octadecanethiol monolayer at Au as obtained with this holder under the aforementioned experimental conditions. This spectrum, which is devoid of the fringing features that degraded the quality of the spectrum in Figure 23, was acquired without tedious sample alignment. The holder reduces the uncertainty of sample placement and the data collection process is greatly facilitated.

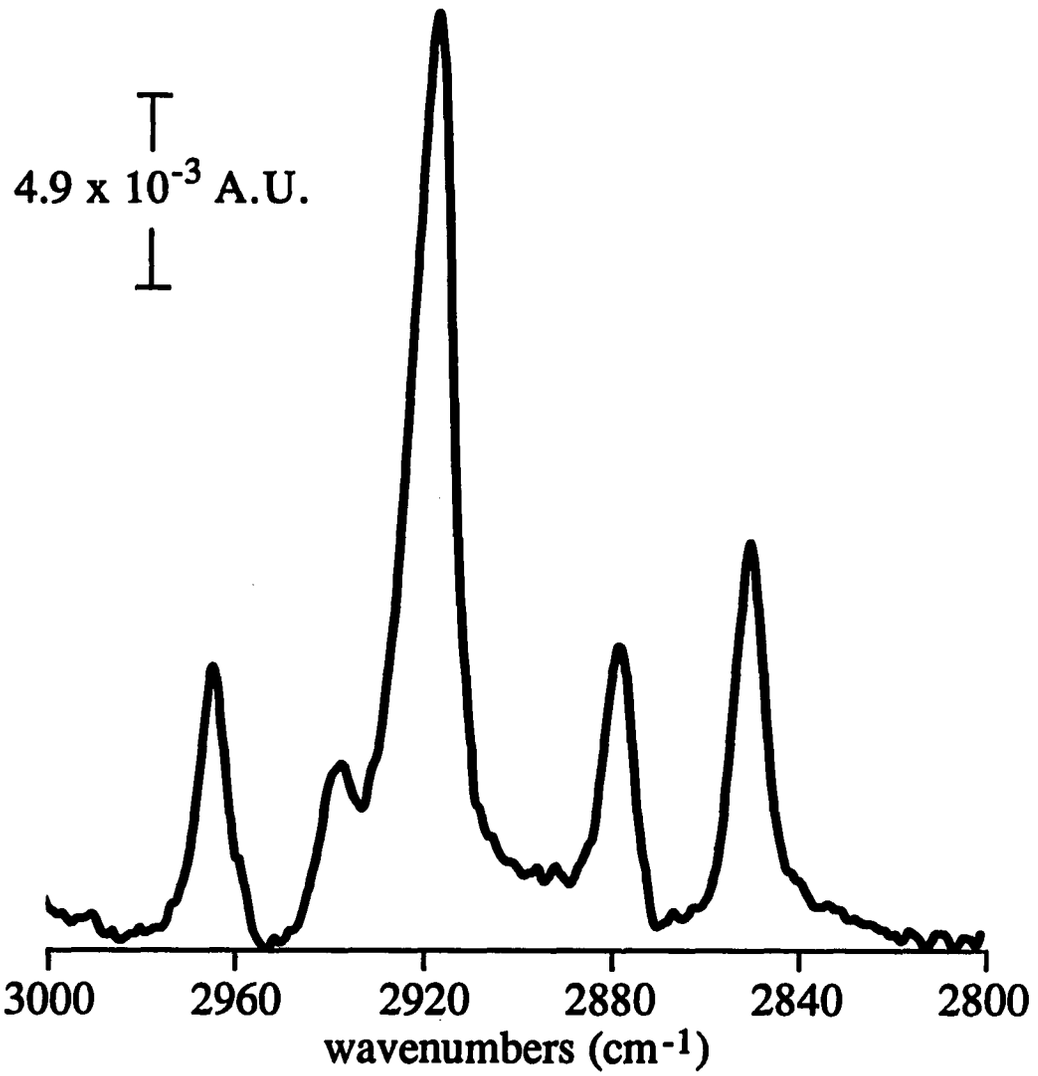

Figure 24. Infrared spectrum of *n*-octadecane thiol on Au with no fringing. Band assignments are the same as in Fig. 23

RESULTS AND DISCUSSION

Before commencing with a discussion and interpretation of the infrared external reflection spectra collected during these experiments, it is important to reiterate the infrared surface selection rule. This briefly states that only the vibrations of an adsorbate which are infrared active and which have a component of their transition dipole moment oriented along the surface normal will be excited by the incident radiation at a highly reflecting metal surface. This is due to the absence of the MSEF near the surface along the surface parallel, and an enhancement of the MSEF along the surface normal (see Section I).

Infrared External Reflection Spectroscopy

An IR-ER spectrum in the hydrocarbon stretching region (3000-2800 cm^{-1}) for a monolayer film of *n*-octadecanethiol at Au is shown in Figure 24. As has been previously discussed, monolayers of these types of materials are highly ordered and represent a pseudo-crystalline environment. For the purposes of discussion, the chains will be assumed to be in a mostly trans zig-zag conformation. Molecular dynamics calculations of Langmuir-Blodgett monolayers of Cadmium arachidate (18 methylene groups) demonstrate that only 1% of the torsional angles are gauche at 306 K (250). Further evidence for this will follow. Other evidence suggests a substantially increased amount of disorder (251). Band assignments and dipole orientations

for this monolayer spectrum as well as the peak positions and widths for three of the neat thiols are given in Table I. A pictorial description of the dipole moments is given in Figure 25. The band at 2964 cm^{-1} is due to the asymmetric in-plane methyl stretch ($\nu_a(CH_3, i.p.)$), which is oriented perpendicular to the CH_3-CH_2 axis and in the plane defined by the CH_3-CH_2-CH_2- chain. The asymmetric band shape on the low energy side is due to the presence of the asymmetric out-of-plane methyl stretch ($\nu_a(CH_3, o.p.)$), which is orthogonal to both the CH_3-CH_2 axis and $\nu_a(CH_3, i.p.)$, and which appears at 2956 cm^{-1}. The absorption band for the symmetric methyl stretch ($\nu_s(CH_3)$), oriented along the CH_3-CH_2 axis, is split due to Fermi resonance interaction with the first overtone of the asymmetric methyl bending mode ($\delta_a(CH_3)$). The effect of this resonance is the appearance of two bands with similar absorbances, each of which is a weighted combination of both absorption bands (238-239). The specific assignment of each band to either the fundamental or the overtone remains an ongoing issue in the literature, consequently, no definitive assignment will be made in this dissertation. The two $\nu_s(CH_3)$ Fermi resonance bands are noted in this work as FR1 and FR2, representing the absorption bands at 2936 cm^{-1} and 2873 cm^{-1}, respectively. The large band at 2917 cm^{-1} is due to the asymmetric methylene stretch ($\nu_a(CH_2)$) whose dipole moment is in the CH_3-CH_2-CH_2- plane and is perpendicular to the hydrocarbon chain. Finally, the band at 2849 cm^{-1} is due to the symmetric methylene stretch ($\nu_s(CH_2)$) which is orthogonal to both $\nu_a(CH_2)$ and the hydrocarbon chain. These peak positions are

Table I. Peak positions in cm^{-1} and dipole directions in the C-H stretching region for *n*-octadecanethiol monolayer at Au

Vib. Mode	Peak Positions				Direction of Dipole
	C_7SH Mono-layer	$C_{18}SH$ Mono-layer	C_6SH Neat[b] (liquid)	$C_{18}SH$ Neat[b] (solid)	
$\nu_a(CH_3$, i.p.)	2965	2964	_[c]	_[c]	⊥ to C-CH_3 bond in C-C-C plane
$\nu_a(CH_3$, o.p.)	2957	2956	2956	2955	⊥ to C-CH_3 bond, ⊥ to C-C-C plane
$\nu_s(CH_3$ FR1)[a]	2938	2936	_[c]	_[c]	∥ to C-CH_3 bond
$\nu_a(CH_2)$	2923	2918	2925	2919	⊥ to C-C-C chain plane
$\nu_s(CH_3$ FR2)[a]	2878	2877	_[c]	_[c]	∥ to C-CH_3 bond
$\nu_s(CH_2)$	2852	2849	2856	2850	∥ to C-C-C plane, bisecting H-C-H

[a]These bands are the result of Fermi resonance (FR) interactions between $\nu_s(CH_3)$ and the first overtone of $\delta_a(CH_3)$. Definitive assignment is still the subject of debate (238-239).

[b]The spectrum of C_6SH (neat) was taken with an ATR cell. The spectrum of $C_{18}SH$ (neat) was obtained using a KBr pellet.

[c]These bands were not observed in the spectra.

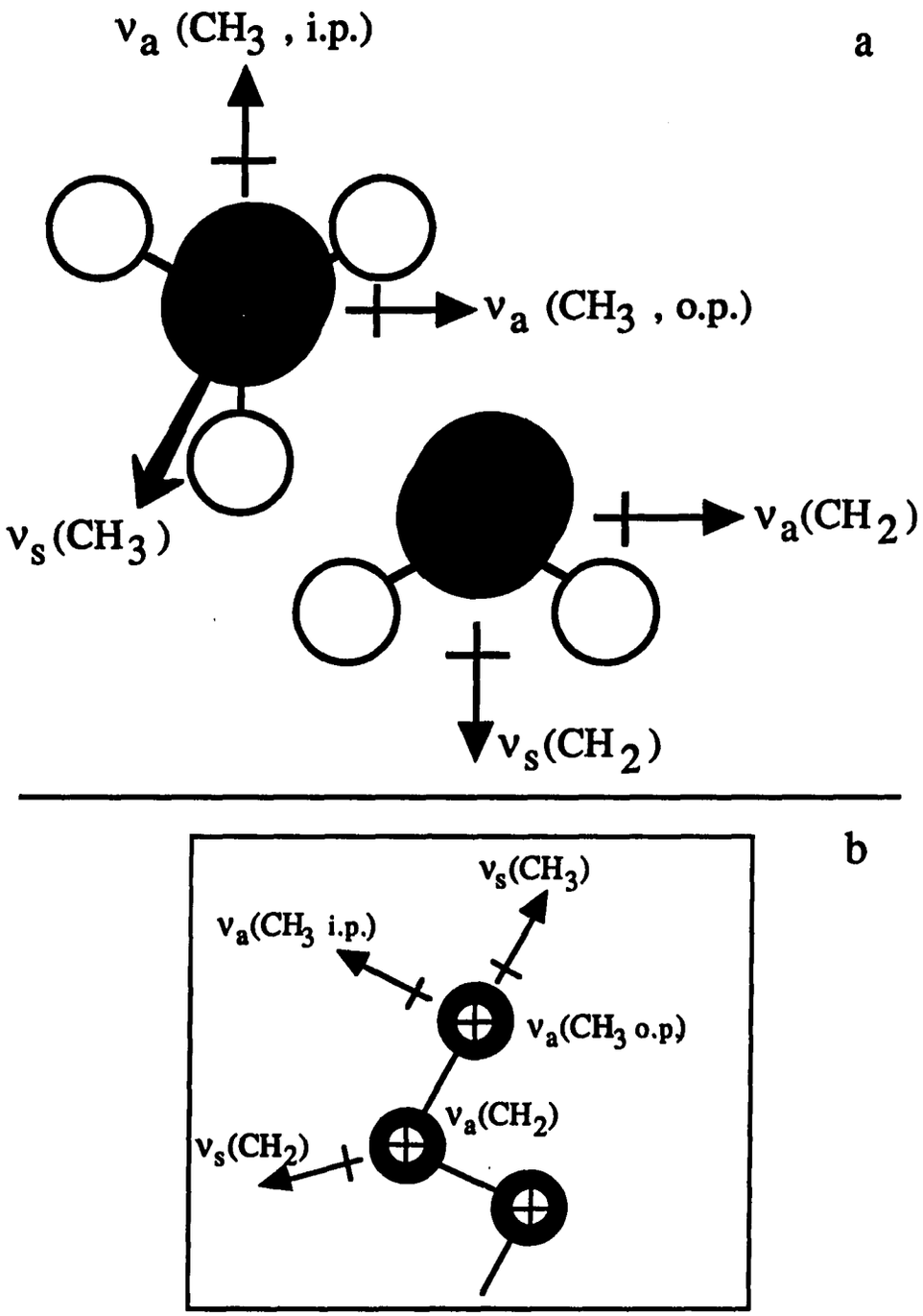

Figure 25. Two representations of the directions of the transition dipole moments for the C-H stretching modes in the *n*-alkane thiols. (a) top view looking down the C-C-C chain, (b) side view

indicative of a pseudo-crystalline environment (240), implying mostly trans hydrocarbon chains in a densely packed lattice.

Figure 26 shows the infrared external reflection spectra for the homologous series of the *n*-alkanethiols at Au. Several important observations pertaining to the average structure of the monolayer are readily observable. First, as the chain length is increased by the addition of a methylene group, the intensities of the bands corresponding to the asymmetric and symmetric methylene stretches increase accordingly in an approximately linear fashion. Second, the intensity of $\nu_a(CH_3, \text{i.p.})$ vacillates between a low value when n is odd, and a higher value when n is even. The magnitude of $\nu_s(CH_3, \text{FR2})$ also alternates between a high and low value, however, this effect is opposite that for $\nu_a(CH_3, \text{i.p.})$. The behavior of $\nu_s(CH_3, \text{FR1})$ is difficult to discern, as it overlaps strongly with $\nu_a(CH_2)$. Third, there is evidence for the presence of liquid-like character in the monolayer which is most pronounced at shorter chain lengths (vide infra). Figure 27 is a plot of the peak heights for the absorption/reflection bands in Figure 26. As noted, the predominant feature in the data is the odd-even effect in the CH_3 modes as a function of increasing chain length. The absolute intensities for the even bands and the odd bands remain approximately constant, implying that these changes are not due to a change in the CH_3 concentration at the surface, but to some other phenomenon. In addition, the intensities for the CH_2 modes increase approximately linearly as is expected with the increase in the concentration of absorbers.

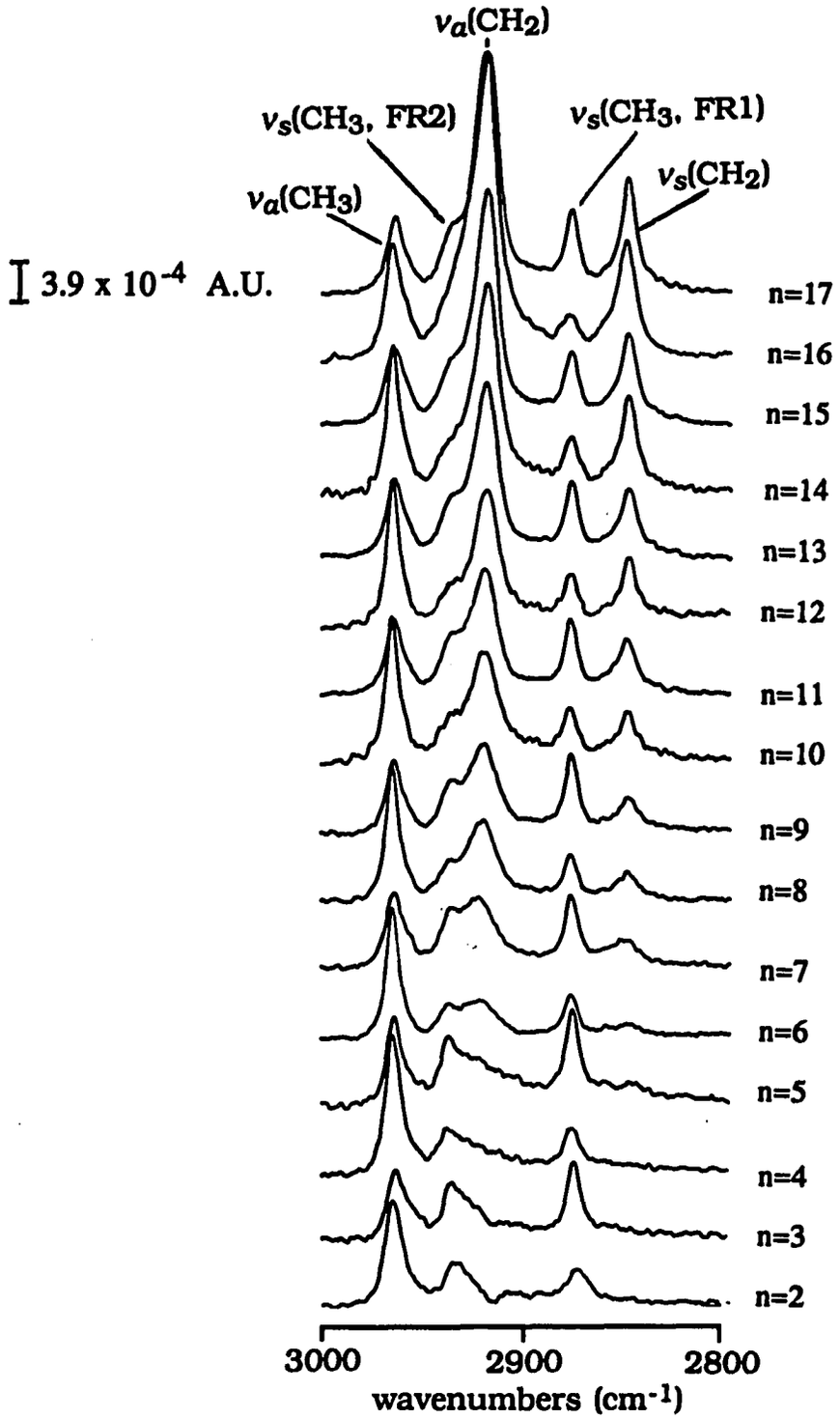

Figure 26. Infrared spectra for the homologous series of the *n*-alkanethiols at Au supported on Si wafers. *n* represents the number of methylene groups in the chain

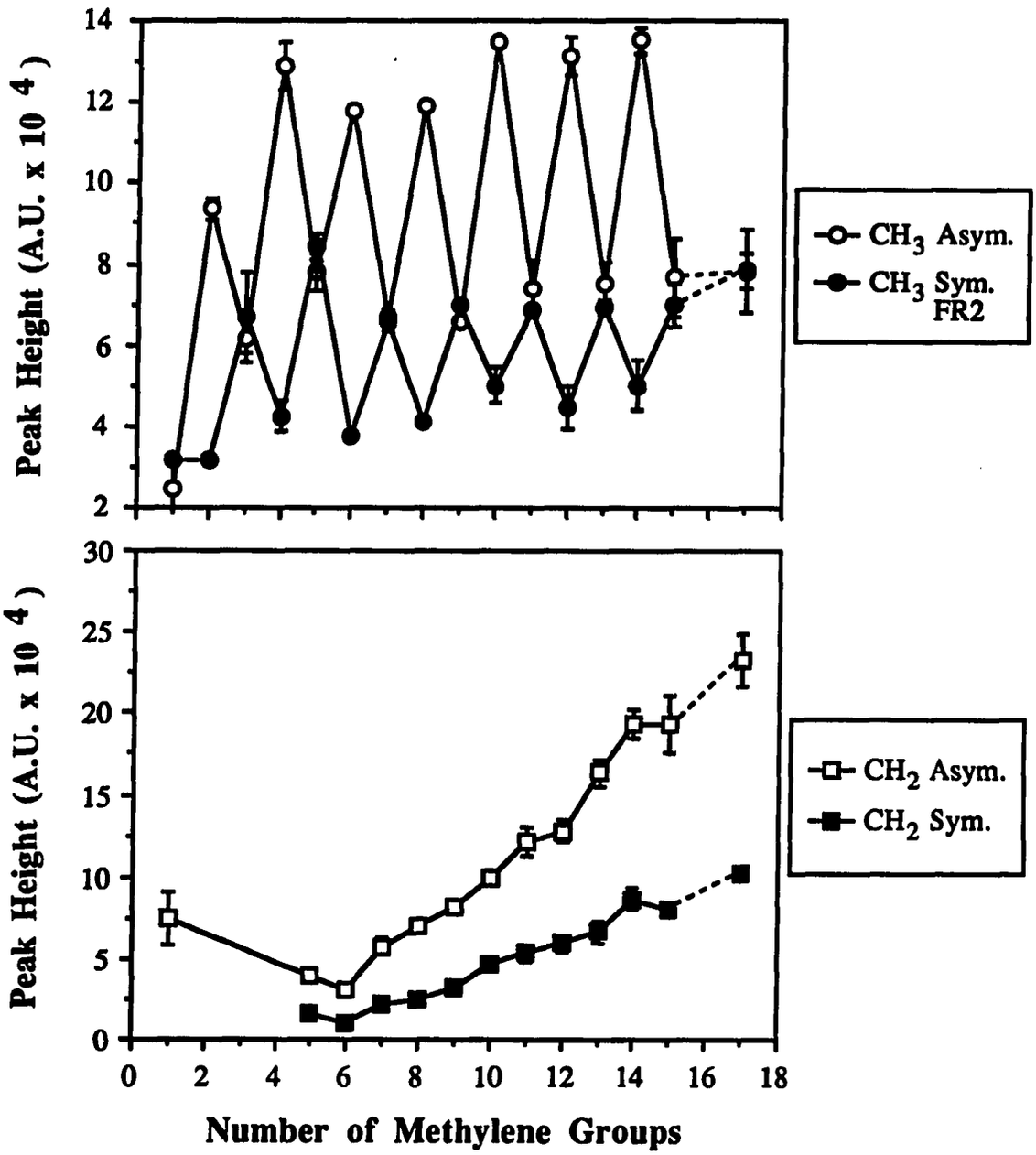

Figure 27. Infrared peak heights for the spectra in Figure 26. Error bars are the standard deviation of the measured peak heights for at least three different samples

It is advantageous to consider the methylene and methyl modes separately, and they will be discussed in that order. An examination of the peak positions and intensities for the methylene modes lends insight into the molecular orientation of the film on the surface. According to the literature (231), evidence for crystallinity in the lattice can be found in the energy of the CH_2 modes. It is observed in the monolayer spectra that, as the chains become longer, a gradual shifting of the methylene absorption bands (~6 cm^{-1}) from higher to lower energy occurs. Disorder in the monolayer due to the presence of gauche or semi-gauche kinks in the hydrocarbon chains causes the layer to have properties which are somewhat liquid-like, with absorption bands higher in energy due to the increased inter- and intramolecular forces imposed upon the vibration (248). Consequently, the energies for the CH_2 stretches resemble those for the neat liquid which appear at ~2925 and ~2856 cm^{-1}. As the chains become longer, more trans segments induce a higher proportion of crystallinity in the chains and consequently, a more stable molecular environment develops, resulting in absorption bands at lower energies. This description is supported by He diffraction data of long and short chain *n*-alkanethiols at Au (252). Decreases in the diffraction peak intensities as the chain length was decreased indicate that the monolayers become less ordered as the chain length becomes shorter, or that the long-range order of the domains decreases substantially. This is also in agreement with earlier spectroscopic and electrochemical data which suggested that more disorder occurs in

these monolayers where the chains are less than ten carbons in length (231).

The average tilt angle θ and twist angle ϕ for the adsorbed chains, as defined in Figure 28a, were calculated based on previously described methods (232-234, 253). A comparison of the measured intensities of $\nu_a(CH_2$, i.p.) and $\nu_s(CH_2$ FR2) for monolayers with $n \geq 12$ with those calculated for a hypothetical isotropic monolayer based on the KBr pellet spectrum of *n*-octadecanethiol as shown in Figure 28b leads to the determination of θ and ϕ. These calculations are based solely on experimentally determined values for the monolayer thickness and the measured optical constants of the adsorbed layer. A comparison of the peak intensities measured experimentally with those calculated for an isotropic layer of the material leads to a determination of the average tilt for the monolayer based on considerations of the infrared surface selection rule using the following equations:

$$\frac{A_e^{\nu_s}}{3A_c^{\nu_s}} = \sin^2\theta\cos^2\phi \qquad (18)$$

$$\frac{A_e^{\nu_a}}{3A_c^{\nu_a}} = \sin^2\theta\sin^2\phi \qquad (19)$$

where $A_c{}^{\nu i}$ and $A_e{}^{\nu i}$ are the absorbances for the calculated and experimental modes, with i denoting the symmetric or asymmetric modes, and θ and ϕ are defined as before. From this method, values of

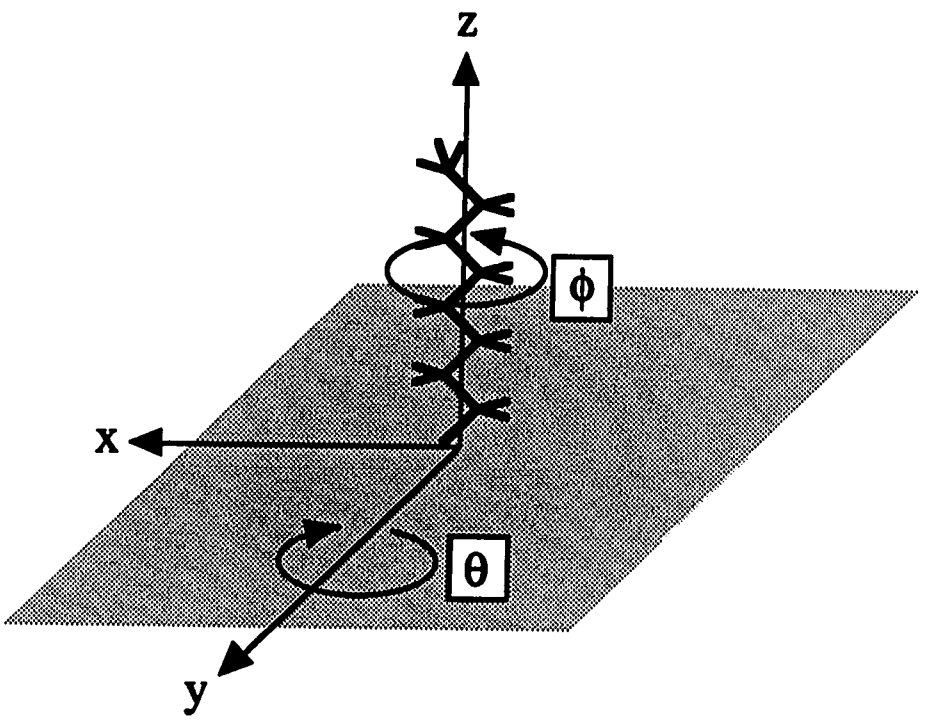

Figure 28a. Illustration of the twist (ϕ) and tilt (θ) angles used in the interpretation of the molecular orientation at the surface

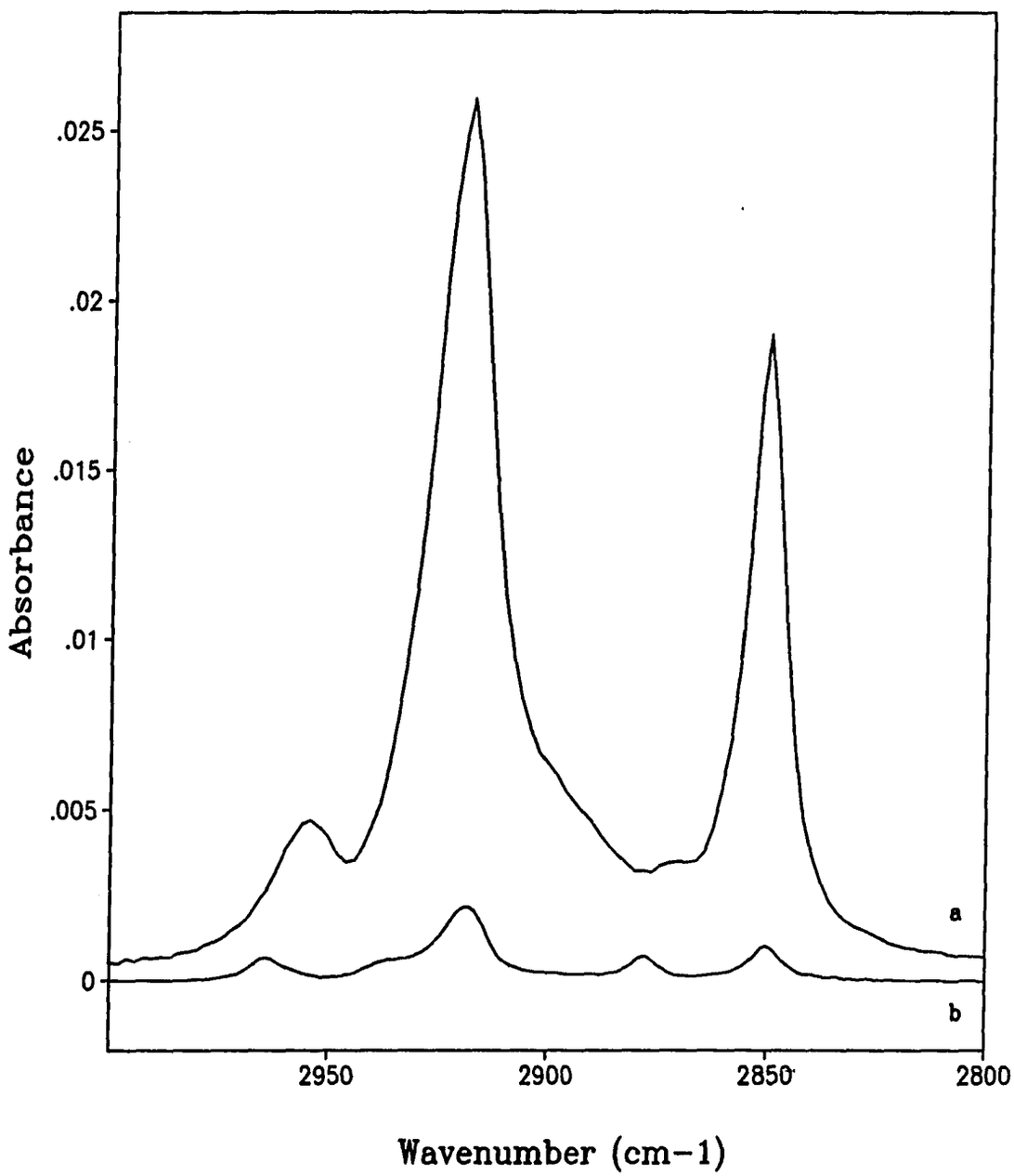

Figure 28b. Calculated (a) and experimental (b) infrared external reflection spectra of *n*-octadecanethiol at Au at 82° angle of incidence

~30° and ~50° were calculated for θ and ϕ respectively which agrees well with other published results (242). The approximately linear observed increase in peak intensity as n increases for all values of n, suggests that the chains maintain nearly the same degree of tilt relative to the surface normal regardless of chain length.

It has been shown that the monolayer chains are mostly in the trans conformation (especially at larger values of n) and retain their degree of tilt regardless of chain length. This gives rise to the odd-even effect observed in the methyl modes (Figure 27). Odd-even effects have been observed for alkanoic acids on Ag and oxidized aluminum (254), and for phenyl and benzyl mercaptans on Ag (255) as well as for alkanethiols on Au (230) using contact angle measurements, infrared spectroscopy, and surface enhanced Raman spectroscopy. Recalling the orientation of each of the dipole moments of the methyl stretches relative to the chain and to each other, it is readily apparent that the magnitude of the component of each dipole moment oriented along the surface normal will vary depending upon the orientation of the chain.

Gold films, prepared by resistive evaporation have a Au(111) exposed crystal face (256). Models based on the Van der Waals radii of the thiol atoms and the lattice constants for Au(111) suggest that the packing density for the adsorbate is 0.25 in a $(\sqrt{3} \times \sqrt{3})R30°$ configuration. The dipole moment for $\nu_s(CH_3)$ is oriented along the CH_3-CH_2 axis, which is at an angle of approximately ~30° with respect to the chain. Consequently, since the chain is known to be tilted ~35°

from the surface normal, when n is odd the dipole for this stretch is oriented nearly perpendicular to the surface and approaches a maximum interaction with the incident MSEF (see Figure 29a). If a single methylene group is added (i.e., n is even), the orientation of the chain remains essentially the same. However, the direction of the dipole moment for $\nu_s(CH_3)$ is now ~70° from the surface normal, greatly reducing the magnitude of the vibrational component in the z direction which leads to a decreased interaction with the incident MSEF and, consequently, a decreased absorption response (Figure 29b). Similarly, and as expected, $\nu_a(CH_3$ i.p.), which is orthogonal to $\nu_s(CH_3)$ and in the plane of the all trans carbon skeleton, experiences an odd-even effect dependent upon the value of n. This effect, however, is opposite that for $\nu_s(CH_3)$. The absence of any appreciable signal for $\nu_a(CH_3$ o.p.) implies that this mode, which is orthogonal to both of the previous modes, remains mostly parallel to the surface for all angles of incidence.

A discrepancy within these data that must be resolved is the strong response for $\nu_a(CH_2)$ leading to a twist angle of ~50°, yet little or no response for $\nu_a(CH_3$ o.p.). The dipole moments for these modes are oriented along the same axis in the all trans zig-zag conformation of the molecule. A slight rotation of the methyl group about the CH_3-CH_2 axis, or the addition of a small degree of conformational disorder near the chain terminus (i.e., between the last two or three CH_2 groups) would be sufficient to bring about enough of a change in the orientation of $\nu_a(CH_3$ o.p.) to keep it aligned along the surface parallel.

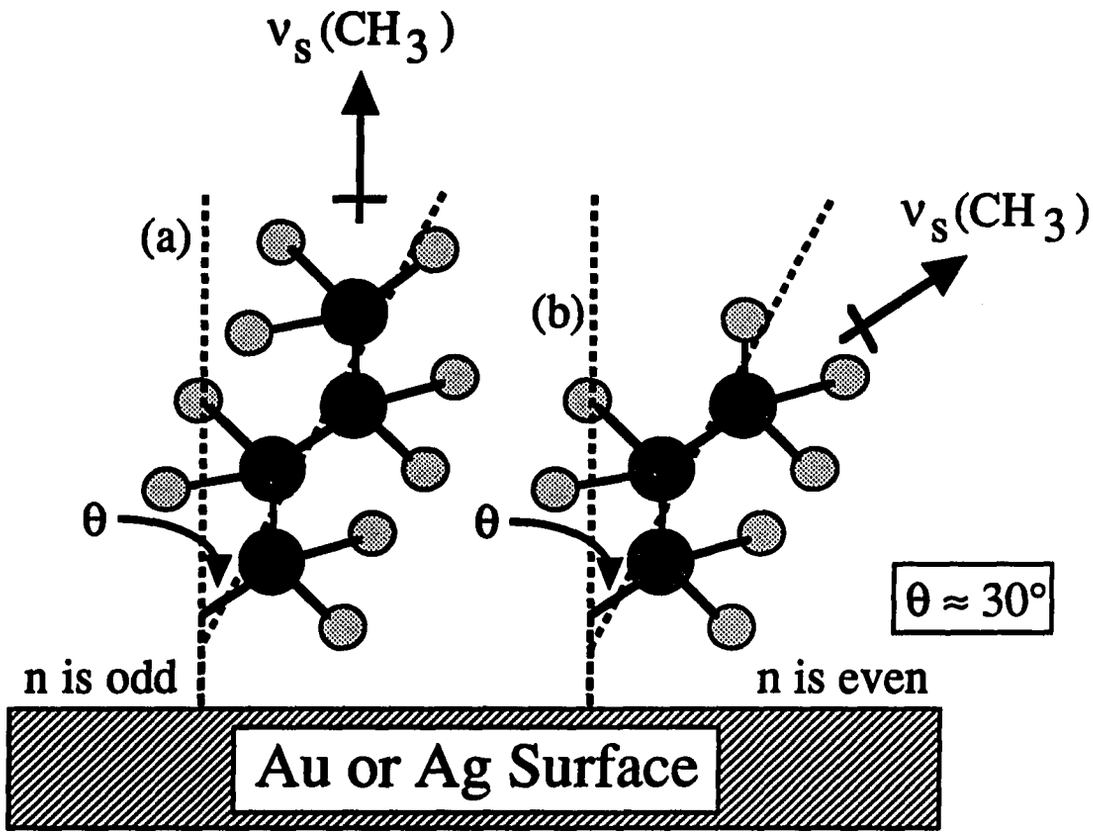

Figure 29. Pictorial representation of the origin of the odd-even effect observed in the IR data. (a) n is odd, (b) n is even

This implies a favored terminal group conformation which is in slight opposition to the favored conformation of the head group and chain.

Another discrepancy is the observation of the dramatic odd-even effect in the data which does not change dramatically even at the short chain lengths. Since the He diffraction data, electrochemical data, and the infrared spectroscopic data (231, 252) demonstrate that the monolayers are more disordered and that the hydrocarbon chains are somewhat liquid-like when the chains are short, why should the odd-even effect persist? While this question is still under investigation in this laboratory, it seems probable that the disorder in the shorter chains is not manifested as fully gauche kinking but more as some subtle disordering that maintains the orientation of the chain terminus relative to the surface normal.

The infrared external reflection spectra for the homologous series of the *n*-alkanethiols on Ag is shown in Figure 30 with the peak intensities displayed graphically in Figure 31. Band assignments are the same as those previously described. Similarities and differences between the spectra on Ag and those on Au are immediately evident. First, the intensities of $\nu_a(CH_2)$ and $\nu_s(CH_2)$ are substantially decreased. They do, however, increase monotonically with chain length, as is observed in the data at Au. Second, an odd-even effect is observed for $\nu_s(CH_3$ FR2), the periodicity of which is offset from that on Au by one methylene group. This change in absorbance is, however, not as pronounced as at Au. Again, due to overlap with $\nu_a(CH_2)$, the behavior of $\nu_s(CH_2$ FR1) is difficult to discern. Evidence

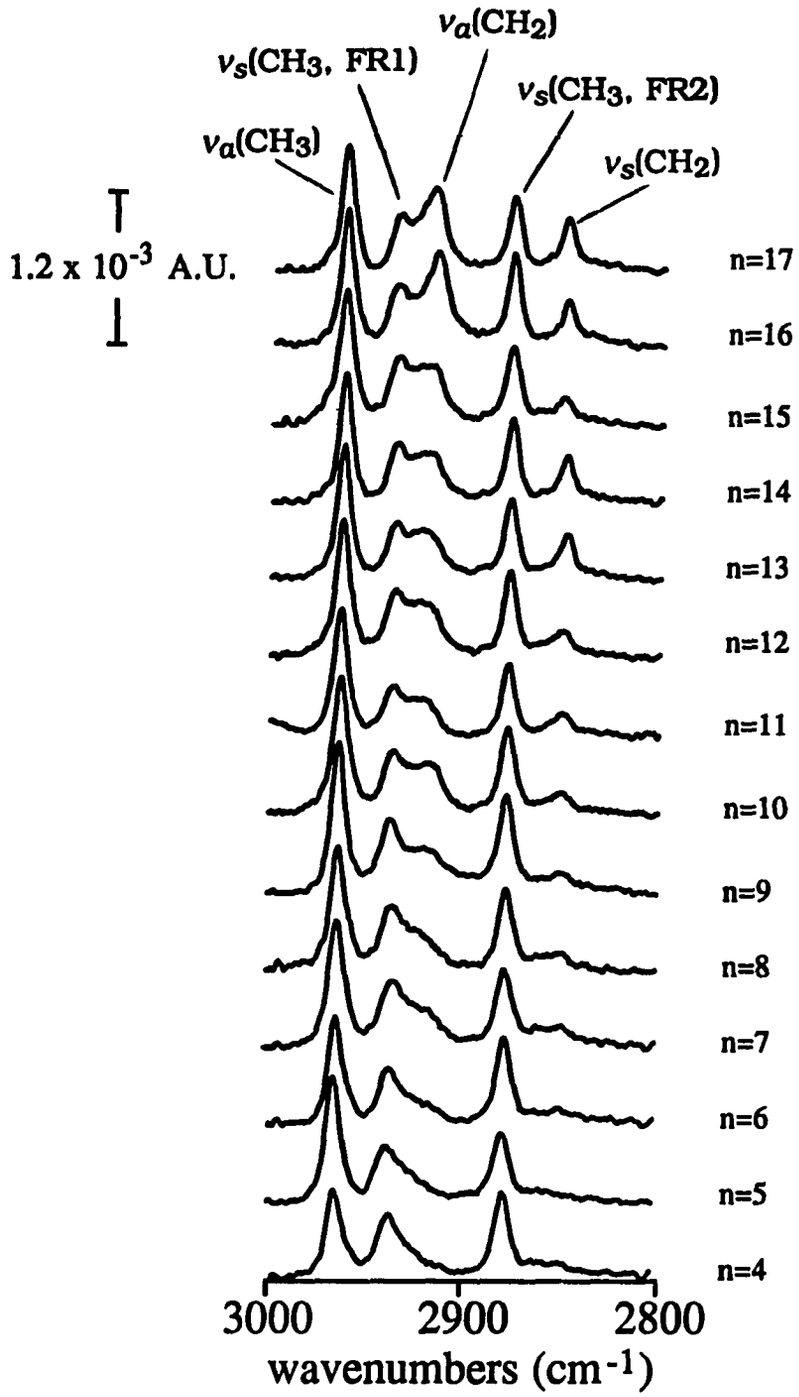

Figure 30. Infrared spectra for the homologous series of the *n*-alkanethiols at Ag supported on Si wafers. *n* represents the number of methylene groups in the chain

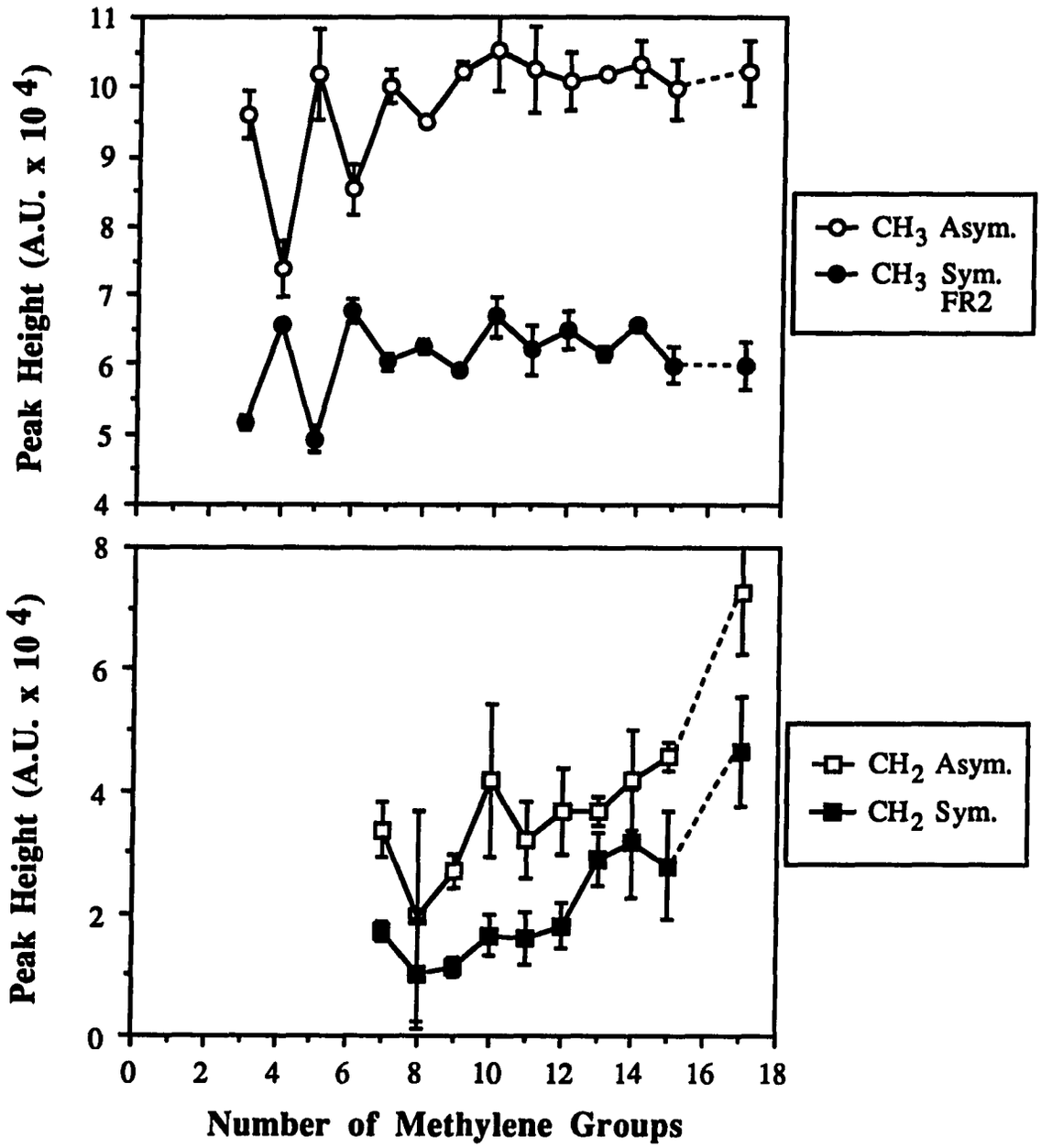

Figure 31. IR peak heights for the spectra in Figure 30. Error bars are the standard deviation of the measured peak heights for at least three different samples

for an odd-even behavior in $\nu_a(CH_3$ i.p.) as a function of chain length is not readily apparent in all of the data. This will be discussed in the following pages. Also, the odd-even effect appears to dampen as chain length increases. Third, as on Au, at shorter chain lengths, the adsorbed monolayer is somewhat "liquid-like", as evidenced by the appearance of a higher energy methylene band at about 2924 cm^{-1} (231, 252).

The decrease in relative intensity for the methylene bands, as compared to the methyl bands, is due to a decrease in the average tilt of the chains, positioning them more normal to the surface at Ag than at Au, and resulting in a decrease in the net component of the dipole moments for these modes aligned along the *z*-axis. Calculation of the average θ and ϕ for these monolayers at Ag gives values of ~14° and ~46° respectively. Evidence from underpotential Tl^+ and Pb^+ deposition on Ag performed in this laboratory indicates that the evaporated Ag films used for these experiments are a mixture of (100) and (110) surfaces, with little, if any, (111) character (257-259). Other data from scanning tunnelling microscopy indicates some (111) character, however, it is uncertain as to whether or not this may be an induced surface reconstruction due to the high current density at the scanning tip. Calculations based on Van der Waals radii for the packing densities at (110) and (100) surfaces and allowing the all trans chains to tilt until they come in contact with their nearest neighbor indicate that, for a (110) surface, the predicted chain tilt would be ~42° while that for a (100) surface would be ~0°. Since

infrared external reflection spectroscopy probes a macroscopic area of the film, and since the average orientation of the adsorbate differs so dramatically on the various crystal faces, if the surface were composed of some combination of (100) and either (110) or (111) crystal faces, then it would be expected that the tilt angle for the sampled region would be a weighted average of the actual tilts on the individual crystallites.

The odd-even effect observed in $\nu_s(CH_3$ FR2) indicates that, on Ag as well as Au, the chain orientation is independent of chain length. However, the absence of an odd-even effect for $\nu_a(CH_3$ i.p.) in some of the data indicates that the orientation of the chain terminus may be more strongly dependent on the local monolayer environment for Ag than it is on Au. When observed, the odd-even effect for this mode is opposite that of $\nu_s(CH_3)$ as is expected based on the orthogonality of the dipole moments. The source of this inconsistency is still under investigation. It is expected that, for chains with ~0° of tilt, there will be no odd-even effect, since the orientation of the dipole relative to the surface normal would not change with n. Therefore, the observed odd-even effect must arise from those crystal faces where the chains pack at angles other than 0°.

Ulman and Tillman have shown (260) that the energetically favored conformation for these chains, calculated by considering only the two-body terms (van der Waals and electrostatics) and the intermolecular terms, is where the methylene modes are interlocked in an all-trans arrangement, and that this occurs when the tilt and

twist angles are 34° and 55°, respectively. The model assumes that the chains are in an all trans configuration (250) and are unable to distort to accommodate perturbations in nearest neighbor chains. The model also assumes an atomically smooth surface, thereby eliminating the effects due to substrate defects. Steric hindrances induced by the lattice constants of the (100) crystal face force the chains to pack with 0° tilt, while at the (110) surface they pack at ~42°. Since the energetically favored conformation is 34°, this suggests that some free volume is present between the chains which would allow for some rotation around the C-C bonds and possibly a change in orientation of the methyl group with respect to the surface normal. This may explain the observation of liquid-like components in the infrared as well as the decreasing odd-even effect in the methyl modes.

The presence of a high energy shoulder on $\nu_a(CH_2)$ for the spectra at Ag suggests that the monolayers contain some liquid-like as well as crystalline character. Curvefitting analysis was performed on the data using a subroutine of Spectra Calc (Galactic Industries Corp., Nashua, NH) assuming the presence of a liquid-like component and that this band would appear as a single peak and not as several peaks. Representative spectra are shown in Figure 32. Data for the entire spectral series show a varying amount of liquid-like character for each chain length. These data suggest a higher percentage of liquid-like character in the monolayers at Ag than at Au. Due to the relatively low signal-to-noise ratio and the assumptions made, conclusions based on curvefitting analysis can only suggest the presence of some amount

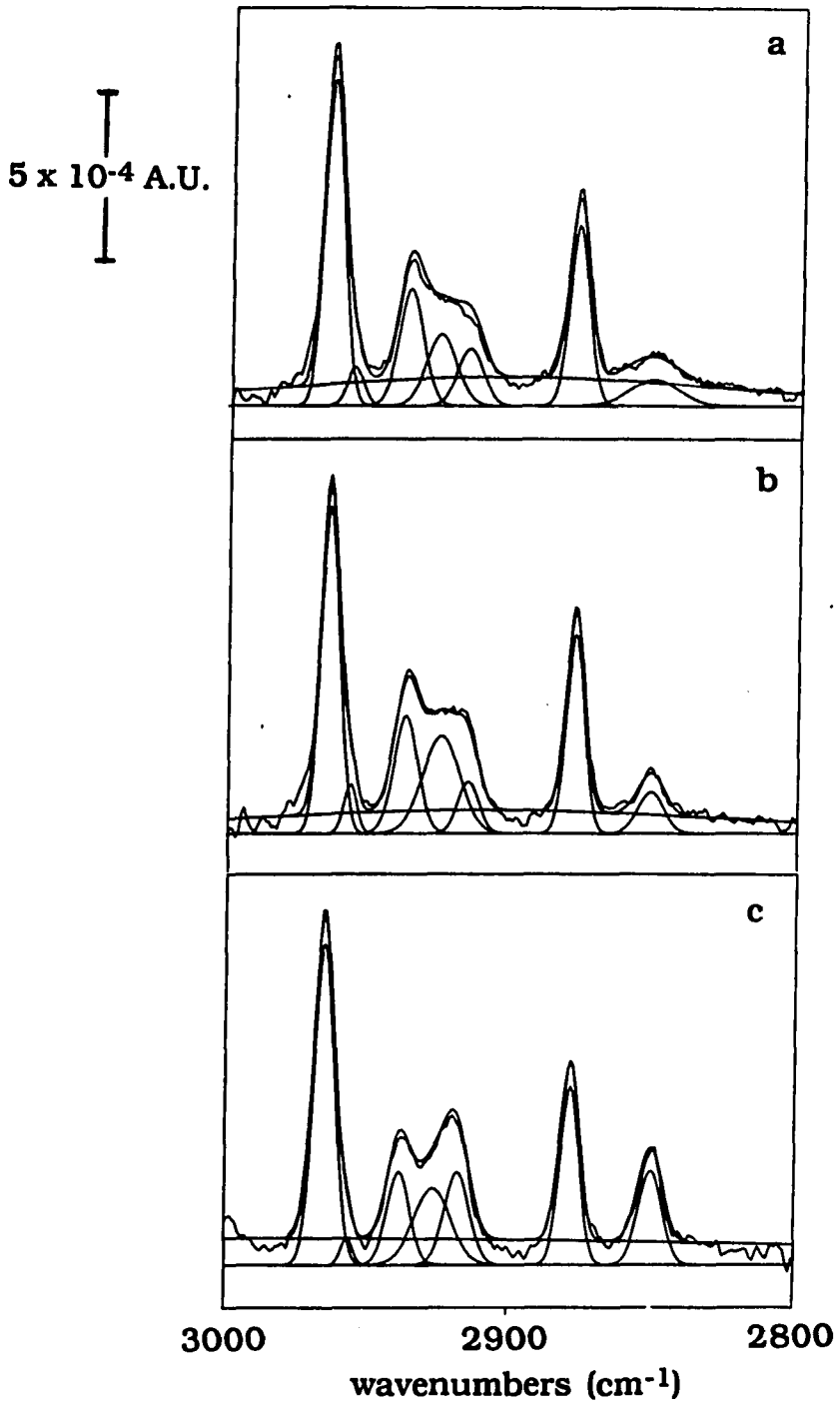

Figure 32. Examples of curvefitting to detect the presence of the liquid-like CH_2 band at 2925 cm^{-1} for $CH_3(CH_2)_nSH$ at Ag on Si where (a) n=9, (b) n=12, (c) n=15. Other band assignments are as in Figure 30

of liquid-like character in the monolayers, but cannot be considered as absolute evidence.

The C-S (600-700 cm^{-1}), S-H (2550-2600 cm^{-1}), and C-H (1150-1500 cm^{-1}) regions of the infrared spectrum were also examined, however, no evidence for these modes was found. The absence of these features may be due to the inherently weak cross-sections for the modes or due to the mode being orientated along the surface parallel. For S-H, the lack of response may simply be due to a cleavage of the bond during adsorption. This cleavage is supported by surface enhanced Raman data (255, 261-262).

Ellipsometry

Ellipsometry was performed to probe the average thickness of the monolayers as a function of *n* on both Au and Ag. The thickness data in Figure 33 show a linear increase for the homologous series of the *n*-alkanethiols as *n* is increased. The slope of 1.2-1.3 Å per $-CH_2-$ group indicates that the chains are extended (as based on molecular modelling) in a mostly trans zig-zag conformation. A decrease in the slope would be observed if a large proportion of gauche kinks were present in the film, as they are more compact than the trans bonds. It is important to note that these measurements assume the refractive index of the monolayer to be 1.45 and assume that the optical constants of the metal film do not change due to the adsorption of the thiol monolayer, or that any change that does occur does not vary with chain length. Consequently, the ellipsometric data reported for the

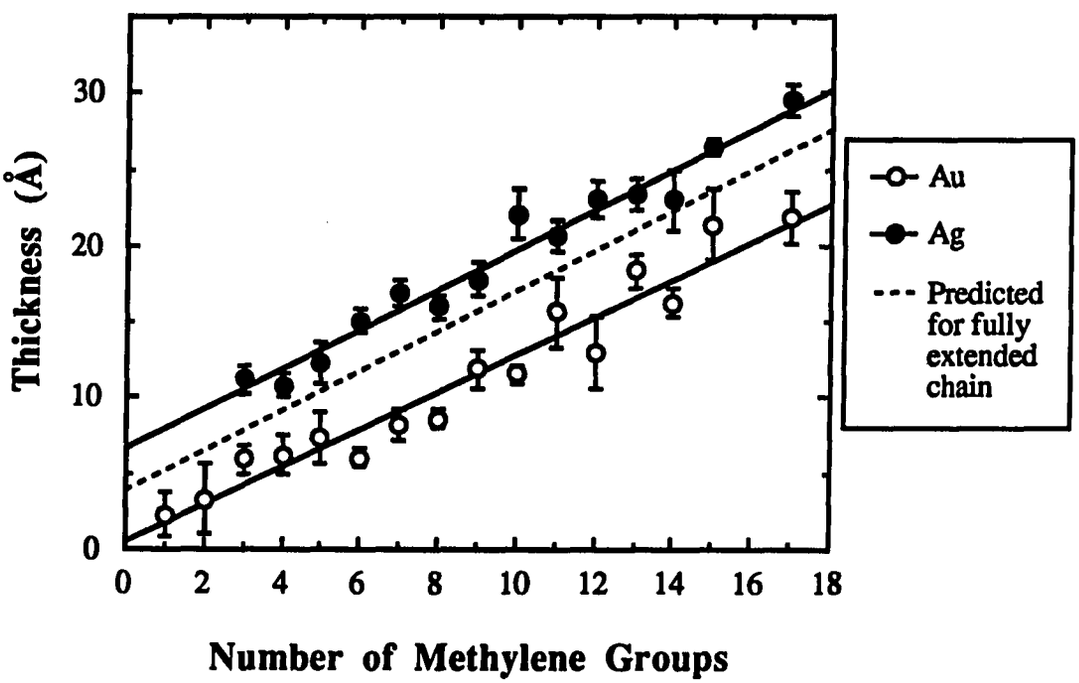

Figure 33. Ellipsometric thicknesses for the homologous series of *n*-alkanethiols at Au and Ag supported on Si. Dashed line represents the thickness predicted from molecular modelling

homologous series demonstrate that the thickness of the monolayer becomes longer, relative to the previous chains, as n is increased at an interval approximating the length of a methylene group. Conclusions pertaining to the absolute thicknesses of the monolayers are tentative at best. The observed trend does, however, lend support to the above conclusions pertaining to a mostly trans zig-zag structure. The effect of a changing real refractive index has been shown in this lab to have a minimal effect on the measured thickness.

Contact Angle

Contact angle measurements with water and hexadecane as contacting liquids were performed to evaluate the character of the chain terminus. Contact angles are dependent on the free energy of the exposed surface, with high free energy surfaces causing the droplet to spread across the substrate, resulting in a lower contact angle. Methyl groups have an intrinsically lower surface free energy than do methylene groups (230, 263). Consequently, a surface which is predominantly "methyl-like" in character will have a higher contact angle than a mostly "methylene-like" surface.

The contact angle data are shown in Figure 34 and represent the mean of at least six measurements on each of several substrates with an error of ±1°. While the effect is manifested as a change of only a few degrees, the observed odd-even effect is greater than the error in the measurements and corroborates the conclusions from the infrared. As expected, based on the lower average tilt angle and the indication

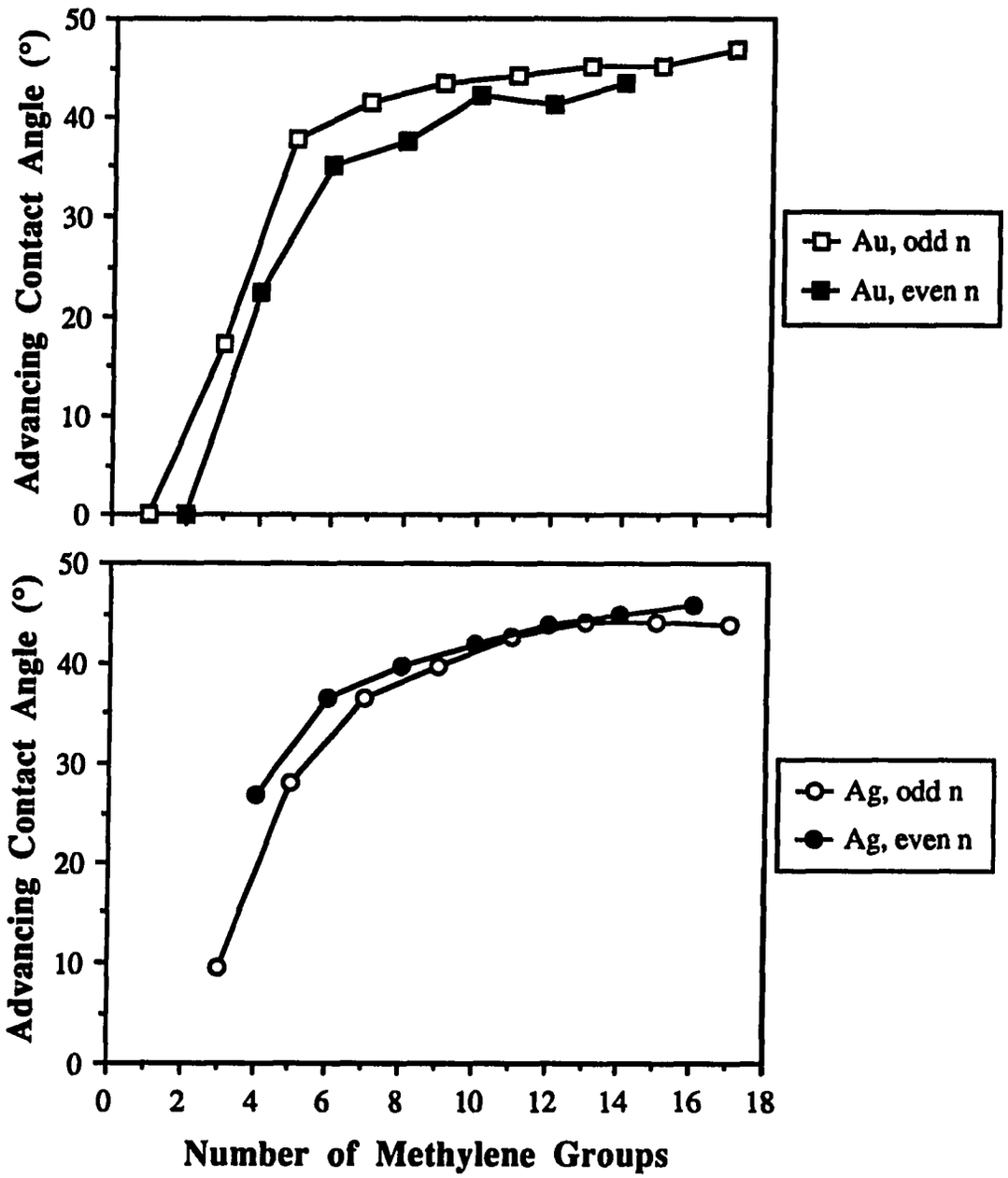

Figure 34. Advancing contact angles with hexadecane for the homologous series of the *n*-alkanethiols at Au and Ag supported on Si

from the infrared of a greater amount of disorder near the chain terminus for Ag, the odd-even effect in the contact angles is more poorly defined (i.e., less separation between odd and even contact angle values).

Orientational Conclusions from other Techniques

The conclusions concerning the orientation of the *n*-alkanethiols on Au and Ag, drawn from the infrared external reflection data and contact angle data, indicate that the chain terminus, with respect to the surface, vacillates between $\nu_s(CH_3)$ being oriented mostly along the surface normal and substantially off of the surface normal depending on the number of methylene groups in the chain and the metal at which the monolayer is adhered. The data show that when *n* is odd, $\nu_s(CH_3)$ is oriented normal to the surface on Au and away from the normal on Ag as shown in Figure 29, and that the reverse holds when *n* is even.

It is known from the literature that monolayers of *n*-alkanethiols are attached to Au surfaces through the thiol head-group, with the hydrocarbon chain protruding away from the surface with some angle of tilt from the normal (230-231, 234). This probably occurs as a thiolate on both Au and Ag, since there is no evidence from the infrared or from surface enhanced Raman (at Ag) for the S-H stretch (261-262, 264). The methylene chain is predominantly in the trans conformation leading to a well ordered, crystalline-like packing at the surface. This agrees with calculations based on interaction energies

between adjacent chains for these materials on Au (260). The predominant differences between the chain orientations on the two substrates are in the magnitude of the tilts and the direction of the odd-even effect. This points to differing modes of attachment for the thiols (or thiolates) on the two metals. Experiments performed in this laboratory have shown that monolayers which were self-assembled from solutions prepared from the thiols and from the thiolates formed equally well with no discernible differences. For the Au substrates, the mode of attachment is likely via the loss of the thiolic hydrogen and the subsequent formation of a mostly covalent Au thiolate at the surface (Figure 35). This type of bond would provide a chain tilt of ~40° which is in good agreement with the 35° tilt angle calculated from the infrared data. This would also facilitate the chains orienting themselves in such a manner as to interlock the hydrogens of the methylene modes, thereby arranging in a lowest energy configuration.

In order for the chains to tilt the opposite direction on Ag, providing for the opposite odd-even effect that is observed, the mode of attachment for the thiol is likely more ionic in nature, forming a Ag-S-C bond angle of ~180° (266). As has been shown, at (110) and (111) surfaces, the spacing between nearest neighbors is sufficient to allow the chains to tilt to ~35° from the surface normal. However, for Ag(100), the packing density is such that the chains would be forced to maintain an orientation normal to the surface (Figure 36). Further investigation into the mode of attachment is underway in this laboratory.

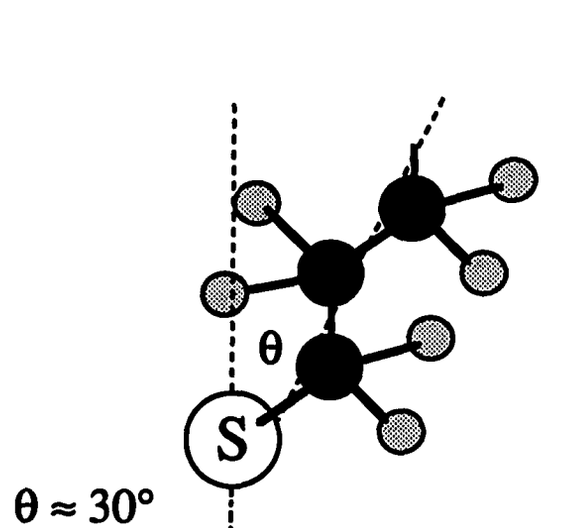

Figure 35. Pictorial depiction of the average chain tilt at Au

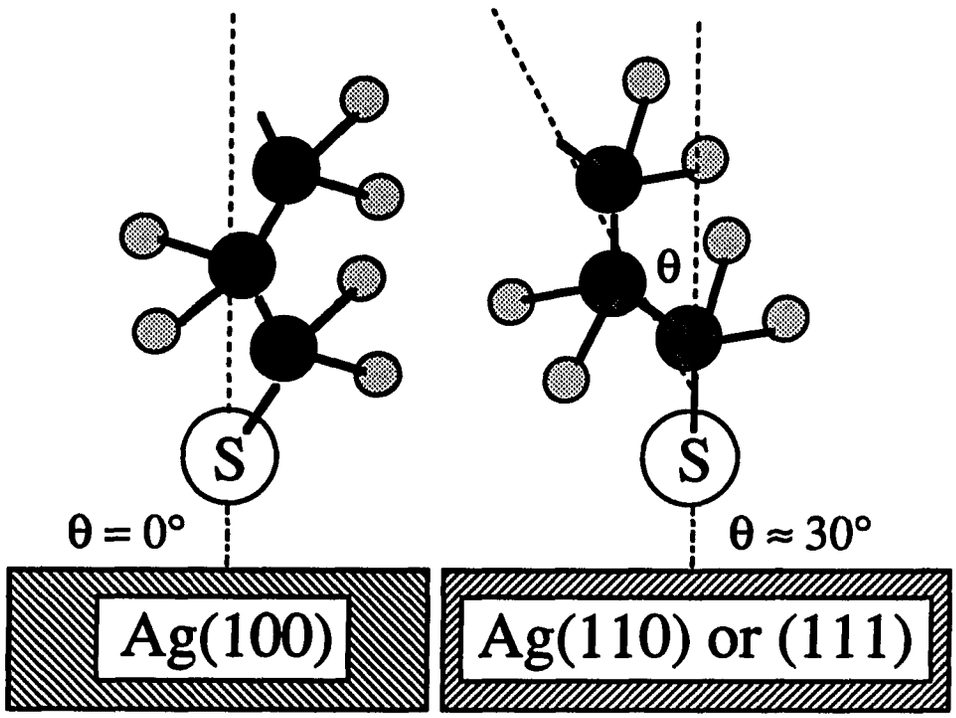

Figure 36. Pictorial depiction of the average chain tilts at the two crystal faces at Ag

Effect of Substrate Roughness

The previous discussion indicates that the predominant effect on the packing of alkanethiols at Au and Ag is the interaction between the metal and the thiol (or thiolate) head-group. It follows then, that the surface morphology will play a significant role in the integrity of the monolayer. To investigate this effect, infrared reflection spectra for the *n*-alkanethiol series at Au and Ag supported on glass microscope slides were acquired and the results compared to those supported at Si wafers (Figure 37a-b). The effect on the data is that the reproducibility of the peak intensities, positions, and shapes is substantially decreased, implying a greater amount of disorder in the monolayers. It follows, if the majority of defect sites in the monolayers are assumed to occur at the grain boundaries, that a rougher surface would induce more defects in the layer, and the spectra would be less reproducible.

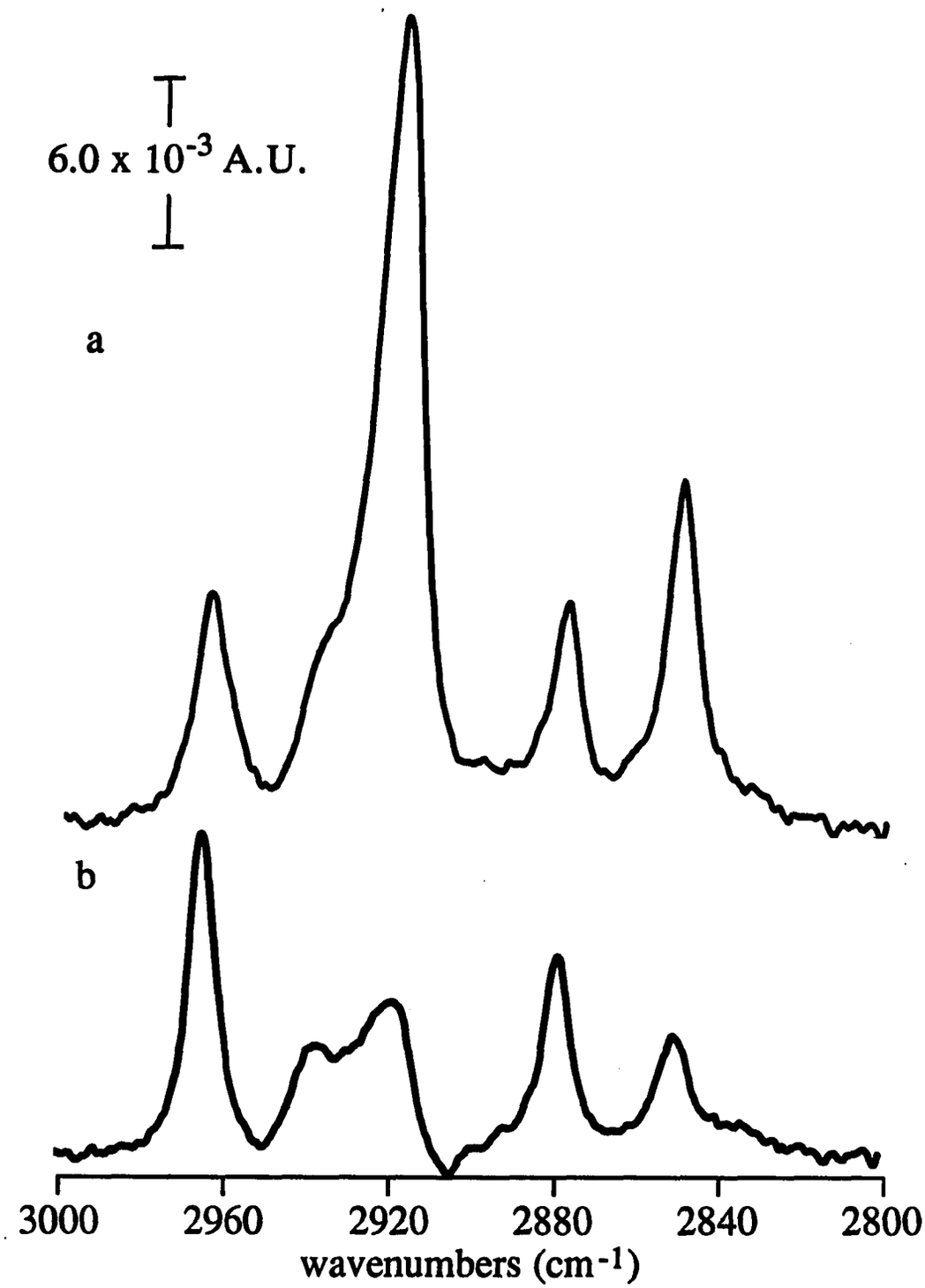

Figure 37. IR spectra of *n*-octadecanethiol at (a) Au and (b) Ag supported on a glass microscope slide

CONCLUSION

Self-assembled monolayers of *n*-alkanethiols at Au and Ag form ordered structures in a mostly trans zig-zag conformation, with the chains oriented at some angle θ from the surface normal. Since this angle is essentially independent of chain length, the absorption/reflection bands for the methyl stretching modes exhibit an odd-even effect. Further, due to the mode of attachment to the surface, the orientation of the monolayer at Au is opposite that at Ag, as evidenced by the phase of the odd-even effects at the two metals. At Au, which is predominantly (111), the monolayers have an average tilt of ~35° due to the spacing between the Au atoms, while at Ag the average tilt is ~14°. The decrease in tilt at Ag relative to Au is due to the presence of the (100) crystal face which, due to its lattice spacing, facilitates the packing of the monolayer with 0° tilt. The remainder of the Ag surface may be composed of (110) and/or (111) crystallites, or some higher order face, whose lattice spacing would lead to a tilt of 30-40°. The average tilt measured is then a composite of the monolayers at all the crystal faces and is less at Ag than at Au.

This project utilized a multi-technique approach to explore the composition of these layers, and each suggested that the monolayers have a specific molecular orientation which is dependent on the head group interactions at the metal surface. The mode of attachment for the thiols at the metal surface is most likely as a covalently attached thiolate (264) with bond angles at Ag and Au of ~180° and ~140°,

respectively. Work will continue in this laboratory and others to discern the nature of these bonds and to better understand the mechanism of attachment.

SECTION V. AN IN SITU EVALUATION OF THE EFFECT OF A VARIETY OF SOLVENTS ON MONOLAYER ORIENTATION ON Au AND Ag WITHOUT THE NECESSITY OF MODULATION METHODS

INTRODUCTION

The previous section presented a molecular description of the self-assembled *n*-alkanethiols at both Au and Ag. It was demonstrated that these materials form in a predominantly closest-packed arrangement at the surface with a mostly trans zig-zag conformation. The angle at which the chains tilt is dependent on the exposed crystal face of the metal. This angle, coupled with the trans conformation leads to an odd-even effect in the character of the chain terminus. This is manifested in the contact angles and infrared external reflection spectra of the monolayers. The observation that this odd-even effect is offset by one methylene group for the monolayers at Au relative to Ag leads to the conclusion that, while the layers adhere to the metals via a thiolate, the mode of attachment of the chains to the surface is different at the two surfaces. This differing mode of attachment causes the initial metal-sulfur-carbon bond angle to be ~110° at Au and ~180° at Ag.

As was demonstrated in the literature review section, the acquisition of in situ infrared external reflection spectra of thin films in the presence of highly absorbing aqueous and organic solvents has, prior to this research, required the application of a modulation technique to observe the adsorbed species at the surface. Potential modulation only allows the observation of those vibrational modes which are altered by the presence of the applied electric field. Polarization modulation, due to the anisotropy of the *s*- and *p*-

polarized components of the MSEF of the incident radiation, only works well in those spectral regions where the solvent does not absorb. As part of the ongoing efforts in this laboratory to understand the chemical and physical properties of monolayer films at a variety of surfaces and under various environmental conditions, the primary goal of this research was to study the effects of a variety of solvents on the integrity and orientation of an *n*-alkanethiol monolayer without the necessity for modulation methodologies. To achieve this goal, the technology to acquire the infrared external reflection spectra of *any* adsorbed monolayer film in situ directly was developed and is outlined below.

When a new technique is being developed, it is wise to choose a test probe that has been well characterized in order to better understand the effects of the new system. Consequently, for reasons discussed above and in previous sections, *n*-octadecanethiol was selected as the test molecule to examine in situ. This section reports the first in situ infrared external reflection spectra for an *n*-alkanethiol monolayers at Au and Ag in the presence of a variety of solvents without the need for potential or polarization modulation. Descriptions provided by such measurements promise to expand the understanding of the fundamental intermolecular forces that control the chemical and physical properties of these interfaces. Further, this technique has far-reaching applicability to a variety of other interfacial systems with varying properties.

EXPERIMENTAL

Over the course of this project, data were successfully acquired utilizing two similar, yet distinctly different in situ cells. Consequently, a description of each follows along with a discussion regarding the strengths and weaknesses of each.

Figure 38 shows schematically the early working version of the in situ cell. The cell interior (solution reservoir) was constructed from a solid piece of Teflon® to ensure chemical inertness and to facillitate sealing. The Teflon® interior was encased by an aluminum housing to provide structural rigidity. The front plate of the cell was also made of these materials and was held tightly in place by several screws. Sandwiched within the front plate was a 32 mm diameter x 3 mm thick CaF_2 window. A Kalrez o-ring (DuPont) provided a chemically inert seal around the window. A slotted 300 nm Au spacer was resistively evaporated on the surface of the CaF_2 to maintain a constant solution thickness. Two Au mirrors were positioned at either side of the cell window to bring the incident infrared beam into the cell at a pre-determined angle of incidence and then to collect the reflected beam and return it to the detector. A high-precision micrometer, with a Kel-F tripod plunger at the end, was inserted into the back of the cell to provide for careful positioning of the sample substrate against the optical window.

Au films (~200 nm thickness) were deposited onto highly polished (l/10 wave) 25-mm diameter pyrex substrates after

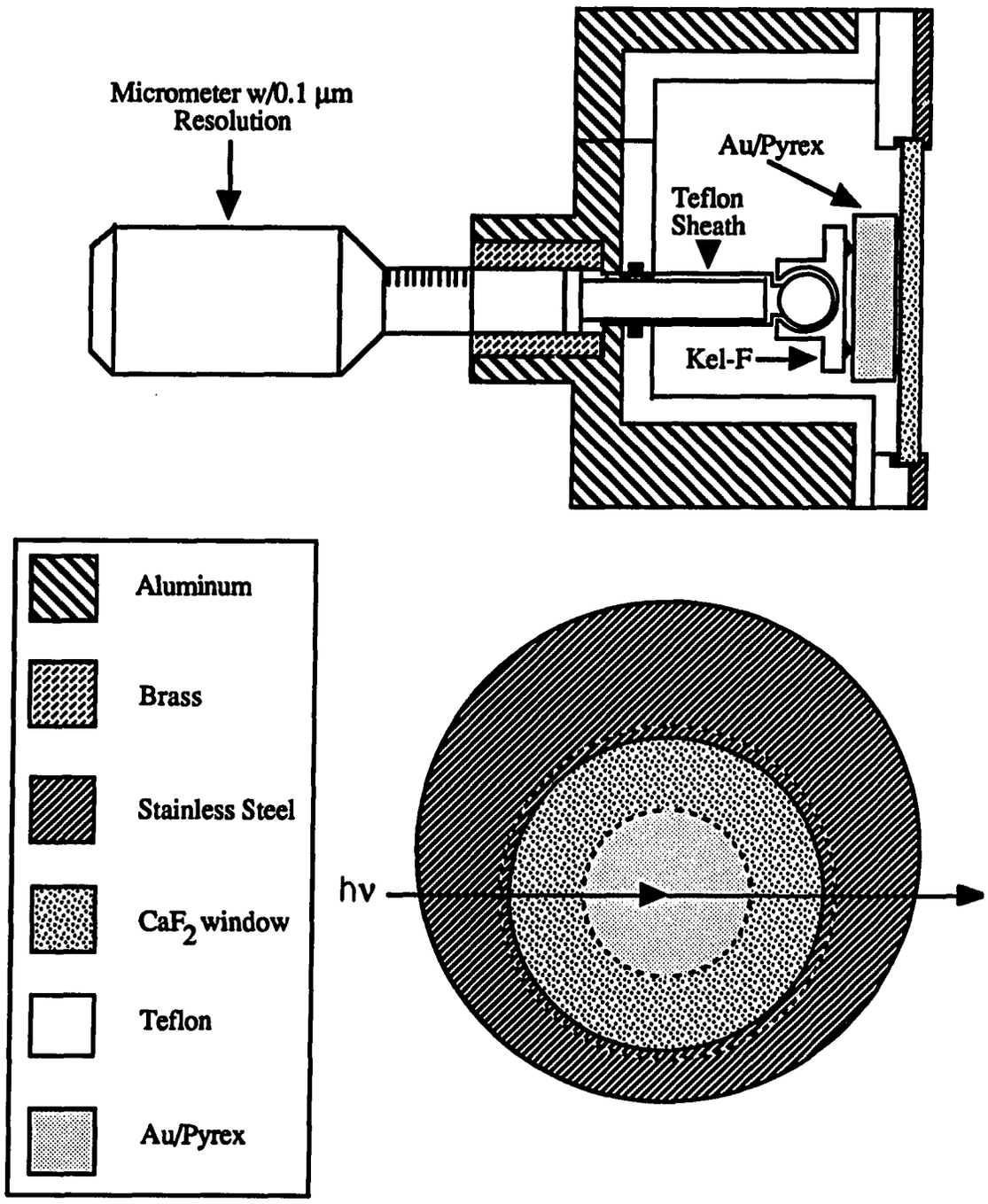

Figure 38. First generation in situ IR external reflection spectroscopy cell

deposition of a thin (~30 nm) adhesive layer of Cr. Monolayer films of *n*-octadecane thiol were then self-assembled from ethanol following the procedure described in Section IV. The composition, spatial orientation, and structural integrity of these films were consistent with those previously reported, as confirmed by optical ellipsometry, contact angle measurements, and ex situ (dry N_2 atmosphere) infrared external reflection spectroscopy. Reference substrates were also prepared as in Section IV.

Spectra were acquired sequentially. The micrometer was used to position the bare substrate tightly against the Au spacers. After the background spectrum was collected, the substrate was then removed and the monolayer coated substrate was inserted into the cell. The micrometer was adjusted to push the sample against the spacers so as to match the solution layer thickness of the reference spectrum (matched interactively through the FTIR software), thereby nullifying the contributions of the solvent to the ratioed spectrum.

Although important data were acquired with this cell (vide infra), there were several significant problems that hindered consistently successful data collection. The most prominent problem was that the substrates could only be pushed forward toward the cell window with the micrometer and could not be retracted. Consequently, if the null point was overshot while positioning the sample, the substrate had to be pulled away from the window and the alignment procedure repeated. With solution layer thicknesses on the order of nanometers, this presented a formidable problem. Also, since

a tripod was used to apply pressure on the substrate, slight differences in solution layer uniformity made exact repositioning exceedingly difficult.

The use of an optical flat limited the angle of incidence that could be attained at the substrate surface. From a practical standpoint, the best that could be achieved was ~40° at the solvent/metal interface due to the refractive indices of the solvent. (It is important to recall from Section I that the refractive indices of the solvents change dramatically across the solvent absorption bands, further complicating the acquisition and interpretation of the data.) Since the magnitude of the MSEF at the surface is dependent on the angle of incidence and is maximized at near grazing angles, this greatly hinders the sensitivity of the technique to the surface moieties.

A problem that occurred with this cell dealt with the evaporated Au spacer on the CaF_2 window. The evaporator in this laboratory did not have the capability to clean the substrates while under vacuum by electron-beam methods. Consequently, the adhesion between the CaF_2 and the Cr underlayer was poor and the spacers pealed loose after only a few uses. This led to irreproducibility in solution layer thickness from sample to sample.

In an effort to create consistency and reproducibility in spectral acquisition, the second in situ cell was designed. This was an improvement on the EMIRS cell developed by Pons (see Section II) and is shown in Figure 39. The body was constructed from a Kel-F rod (3M, St. Paul, MN) which had been hollowed out to allow passage of a

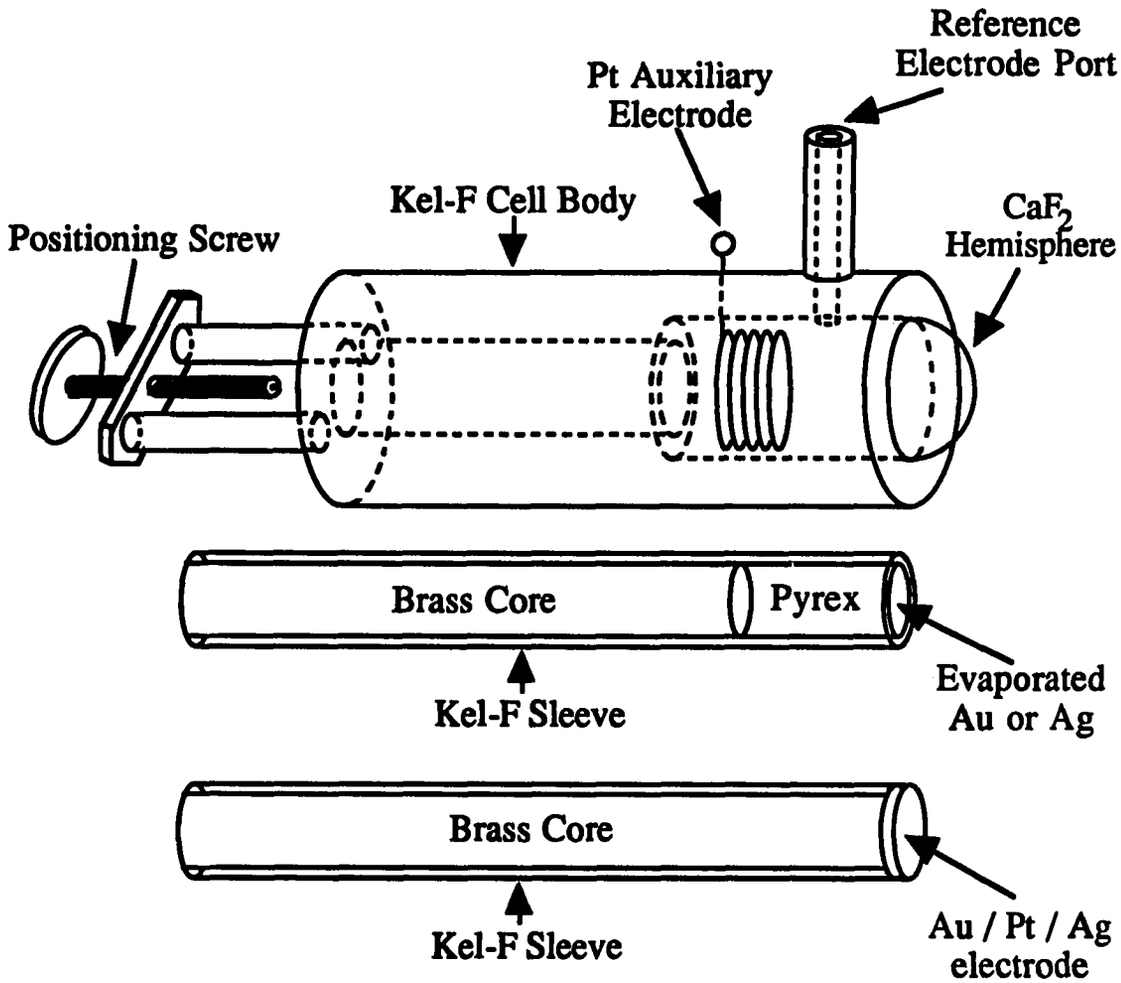

Figure 39. Second generation in situ IR external reflection spectroscopy cell

Kel-F plunger. Near the front of the cell was a reservoir for solvent (~5-7 ml). The cell was constructed such that it could be used for potential modulation as well. Therefore a Pt auxiliary electrode was installed and a port was positioned at the top of the cell for a Ag/AgCl electrode to be placed. The material Kel-F® is a rigid fluoropolymer which has sufficient mechanical strength to stand alone without the need for a metal jacket. A 25 mm diameter CaF_2 hemisphere was held in place via a clamp at the front of the cell which did not vignette the incident beam. A Kalrez® O-ring maintained a seal between the cell body and the hemisphere. Gold mirrors were again used to direct the infrared beam into and out of the cell.

A 25 mm long by 7 mm diameter Pyrex plug was inserted into the end of a Kel-F sheathed brass plunger and polished smooth with 600 grit sandpaper followed by 1μm alumina until a mirror-like finish was obtained. The metal of interest was then resistively evaporated onto the polished surface as before; again with a Cr adhesive layer. Monolayers were formed by self-assembly. A positioning screw was used to move and maintain the position of the substrate surface within the cell. Plungers were also constructed to provide electrical contact with the metallic surface. Au and Pt disks (2.5 mm thick) were soldered directly onto the brass core and then polished smooth by mechanical methods.

Due to swelling of the Kel-F upon heating, the use of Piranha etch for cleaning the reference substrates was not possible. Swelling of the Kel-F allowed the Piranha etch to be siphoned between it and

the pyrex plug, allowing contact with the brass and leading to corrosion of the plunger interior. This caused the diameter of the plunger to increase, rendering it useless. Consequently, a perdeutero-alkanethiol monolayer was self-assembled at a fresh Au surface and used as the reference. This technique was used by others in this laboratory and its validity as a reference was confirmed by ratioing the perdeutero monolayer to a freshly cleaned, bare Au substrate. No infrared peaks were observed in the hydrocarbon stretching region.

The procedure for acquiring spectra was the same as with the previous cell design. The solution layer attainable with this new cell design is ~0.1-0.5 μm as calculated from the observed fringing at the interface between the window and the metal substrate. This thinner layer, coupled with the increased control of the position of the substrate with respect to the window, allowed for a more precise nullification of the solvent absorption bands. While the monolayer absorption bands which fall immediately under a solvent band are still obscured, those which occur near or on the shoulder of these solvent bands are detectable. Further, since the solvent layer thickness is quite small (i.e., ~100 nm), the solvent absorption bands do not obscure as much of the spectral region, and a larger optical window is available. This cell provided for the routine acquisition of monolayer spectra in a variety of solvents (vide infra) with performance far superior to the previous cell design.

Spectra are again presented as $-\log(R/R_0)$. To facilitate in situ data acquisition in the hydrocarbon stretching region, deuterium-

labeled solvents were used, providing a spectral window devoid of vibrational features in the C-H stretching region of the monolayer. Spectra taken in H_2O were also obtained. Spectral subtraction to remove components due to solvent impurities was utilized. There were no observable differences in the ex situ infrared reflection spectrum of the monolayer before and after acquisition of an in situ spectrum. The absolute absorbances of the in situ bands are less than those ex situ due to a necessarily lower angle of incidence at the liquid-solid interface which decreases the net MSEF at the surface. All spectra were taken at 2 cm^{-1} or 4 cm^{-1} resolution prior to Happ-Genzel apodization with 1024 or 2048 scans on both coated and reference substrates.

An example of the reproducibility of this cell for sample placement is shown in Figure 40. This illustrates the ability of the cell coupled with the interactive subtraction capabilities of the instrument for effectively nullifying the absorption bands due to the solvent. A reference spectrum of the solvent was acquired using the cell set at the conditions of the experiment for two different solution layer thicknesses. An unratioed spectrum of *n*-octadecanethiol at Au was acquired in deuterated acetonitrile (Cambridge Isotope, 98% purity). The sample plunger was then withdrawn from the cell and repositioned so as to closely match the spectral intensity of the previous spectrum. The ratio of these two spectra contained a small artifact due to impurities in the solvent which could be removed effectively by spectral subtraction. A nominally flat baseline in the

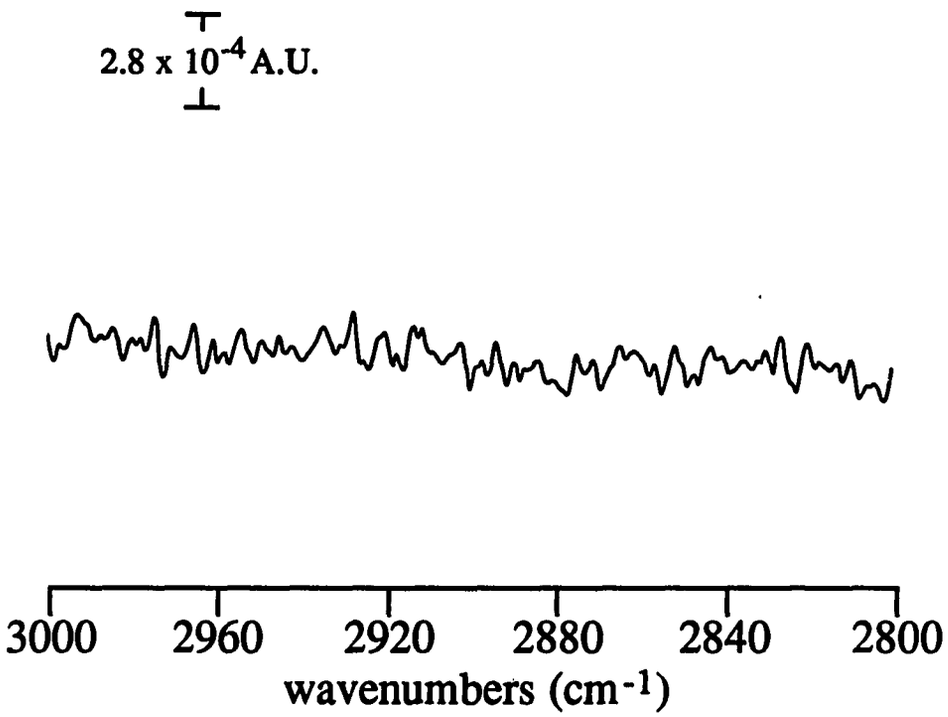

Figure 40. IR spectrum demonstrating the effective removal of all artifacts due to the solvent for *n*-octadecanethiol at Au vs. itself after repositioning in acetonitrile-d_6

region of interest remained, as shown in the figure. For good success, the residual contribution of the solvent to the spectrum must be minimal. It is also extremely important to note that no artifacts due to the thiol monolayer are present as a result of the slight difference in substrate position. Consequently, band-shapes observed in the spectrum can be attributed with confidence to the monolayer.

RESULTS AND DISCUSSION

Monolayers at Au

It was shown in Section IV that *n*-alkanethiol monolayers have an average orientation at a Au(111) surface of ~35° relative to the surface normal. Figure 41a shows the ex situ spectrum of the monolayer at Au in the C-H stretching region taken at ~80° angle of incidence. Band assignments, peak positions, and estimated widths are given in Table II along with the refractive indices and dielectric constants of the solvents. The band assignments and interpretations of peak positions were discussed in Section IV. Figures 41b-e are the in situ infrared external reflection spectra for the same monolayer in contact with the liquids D_2O, CD_3OD, and CCl_4, respectively, taken with the first version of the in situ cell. The peak positions, widths, and relative intensities of several of these bands differ markedly from those in the ex situ spectrum, providing insights for a qualitative description of the interactions between solvent and monolayer. For the methyl modes, both components of the $\nu_s(CH_3, FR)$ couplet are shifted to slightly lower energies. Differences in the position, width, and intensity of $\nu_s(CH_3, FR1)$ are masked by overlap with $\nu_a(CH_2)$. The magnitudes of the shifts of $\nu_s(CH_3, FR2)$ are relatively independent of the dielectric constants, and hence, the polarities of the solvents. Such an observation points to polarization interactions as the dominant contributor to the observed shifts, and is consistent with a recent examination of the C-H stretching modes of *n*-octane in

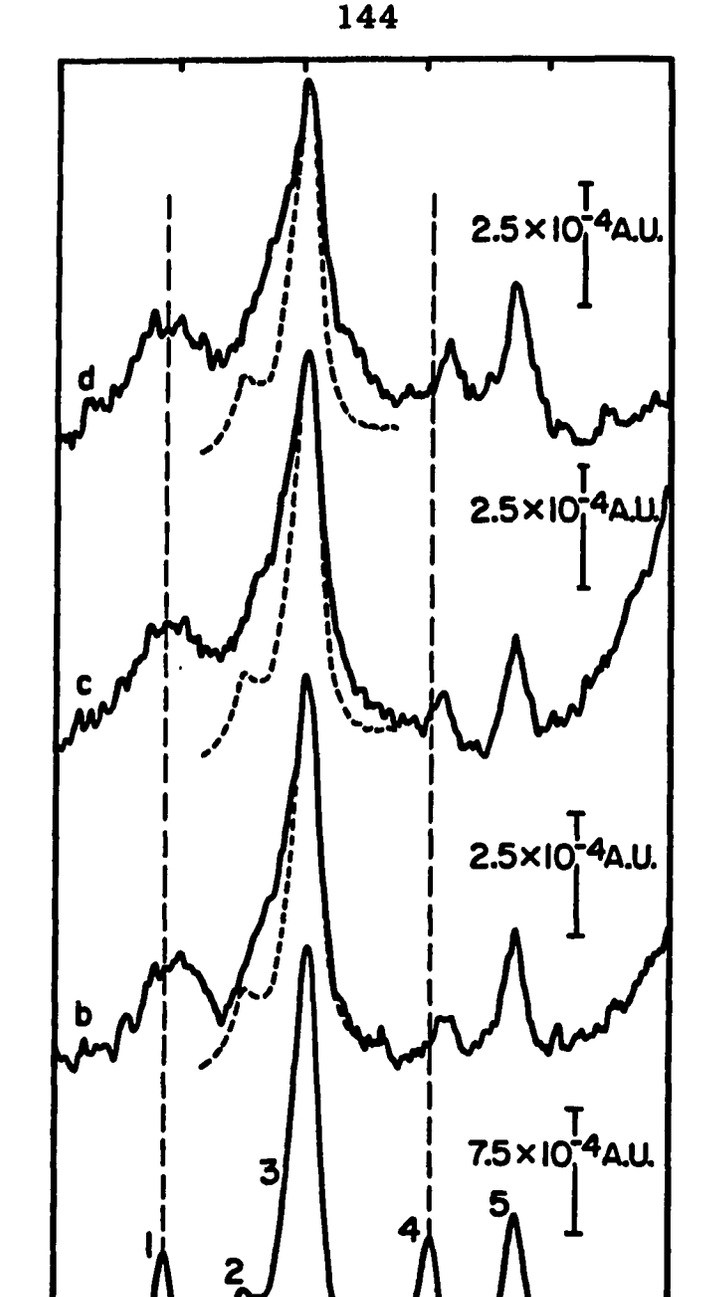

Figure 41. IR external reflection spectra of *n*-octadecanethiol at Au taken with the cell in Figure 38: (a) ex situ, (b) in D_2O, (c) in CD_3OD, and (d) in CCl_4. Peak positions are as in Figure 26. The dashed line in b-d is the ex situ band shape for the corresponding peaks

Table II. Peak positions, widths, and solvent properties for the C-H stretching modes of *n*-octadecanethiol ex situ and in situ for the first generation in situ cell

	Peak Position (band width) in cm^{-1}			
Vib. Mode	ex situ	D_2O	CD_3OD	CCl_4
$\nu_a(CH_3)$[a]	2964(7)	2961(20)	2962(18)	2962(19)
$\nu_s(CH_3$ FR1)[b]	2936		2932	
$\nu_a(CH_2)$	2918	2918	2918	2918
$\nu_s(CH_3$ FR2)[b]	2877(7)	2872(10)	2873(10)	2871(10)
$\nu_s(CH_2)$	2849(8)	2850(8)	2850(9)	2849(9)
n_D 25°[c]		1.333	1.327	1.457
ε 25°[c]		78.304	32.66	2.238

[a] This absorption band is represents both the in-plane mode at 2964 cm^{-1} and the out-of-plane mode at 2956 cm^{-1}.

[b] These bands are the result of Fermi resonance (FR) interactions between $\nu_s(CH_3)$ and the first overtone of $\delta_a(CH_3)$. Definitive assignment is still the subject of debate (238-239).

[c] Values are from reference 265 and are for the hydrogenated analogs of the solvents.

solvents with comparable polarizability and dipolar properties (267). A shift to lower energies is also suggested for $\nu_a(CH_3)$, but cannot be separated from a contribution of the out-of-plane $\nu_a(CH_3)$ at the present signal-to-noise level (vide infra).

A description of the solvent-monolayer interactions that cause the observed increase in the width of $\nu_a(CH_3)$ is somewhat complicated. Because of an almost three-fold increase in the width of the band assigned in the ex situ spectrum to the in-plane $\nu_a(CH_3)$, it is concluded that solvent-monolayer interactions induce a change in the average orientation of the methyl group with respect to the surface normal. This change may either be a partial rotation of the methyl group about the CH_2-CH_3 bond or a more subtle disordering of the chain terminus relative to the stable conformation of the ex situ monolayer. These changes are confined to the region near the chain terminus, as there is little evidence for an extensive perturbation of the chain conformation in the methylene modes. Based on considerations of the infrared surface selection rule, a reorientation of the methyl group would increase the interaction of the transition moment of the out-of-plane $\nu_a(CH_3)$ with the surface electric field, and the overlap would give the appearance of a broadened in-plane $\nu_a(CH_3)$. The increase in the width of this mode may also be induced by small differences in the local solvent environment near the chain terminus, resulting in inhomogeneous broadening. However, the contribution to such a broadening mechanism is probably minimal,

since there is little evidence for any appreciable increase in the width of the low energy $\nu_s(CH_3, FR)$.

The increase in the width of $\nu_a(CH_2)$ provides further evidence for a solvent-induced perturbation of the surface structure. The asymmetry on the high energy side of the band, as previously noted, results primarily from a shift of the high energy component of the $\nu_s(CH_3, FR)$ couplet to lower energies. Although speculative with the present signal-to-noise ratio, the broadening observed on the low energy side of the band with CD_3OD and CCl_4 as contacting solvents in some of the data also suggests a perturbation of the methylene chain near the chain terminus. Such a broadening is caused by a decrease in the interchain coupling of the methylene bending modes (238, 240, 241). These modes are strongly coupled in the crystalline phase, resulting in a broad, weakly absorbing secondary maximum due to Fermi resonance between $\nu_s(CH_2)$ and overtones of the methylene bending modes. An increase in chain disorder decreases the frequency spread of the overtone bands, narrowing and increasing the intensity of the secondary maximum. The narrowing of this secondary maximum with CD_3OD and CCl_4 correlates qualitatively with the polarity of the solvent in the in situ spectra, pointing to an increase in the perturbation of the chain packing with decreasing solvent polarity. Similarly, we attribute the lack of observed broadening with D_2O to both the densely packed arrangement and the hydrophobicity of the chains (262). It is important to note that this effect is not observed in all the data, and is likely due to differences in the substrate

morphology rather than to solvent induced perturbations. As was discussed in the previous section, inconsistencies in the character of the monolayer, due to the roughness of the substrate and subtle differences in the evaporation of the metals, leads to spectra with some variation in peak shape and position. Efforts are underway in this laboratory to attain more exacting control of the substrate morphology prior to monolayer formation.

Figure 42 shows the infrared spectrum of the monolayer on the Au coated plunger taken ex situ at ~55° angle of incidence, closely approximating the conditions of the in situ measurements. Calculations of the average tilt and twist of the monolayer are 36° and 52°, respectively. The band-shapes of this spectrum closely resemble those on Au coated microscope slides. This is not surprising, since these pyrex substrates are rougher than those used for the early version of the cell. This is because the end of the plunger was polished only with 1μm alumina prior to the deposition of the metal. A finer grade of polishing compound was not used, since visible pitting of the pyrex was observed. The observation that this spectrum closely matches the spectra taken in situ with the first version of the cell lends support to the argument that the substrate morphology plays a dominant role in the character of the monolayer. It is also important to note that the peak width of $\nu_a(CH_3)$ is less than that for the in situ spectra, supporting the conclusions about the effect of solvent on the chain terminus.

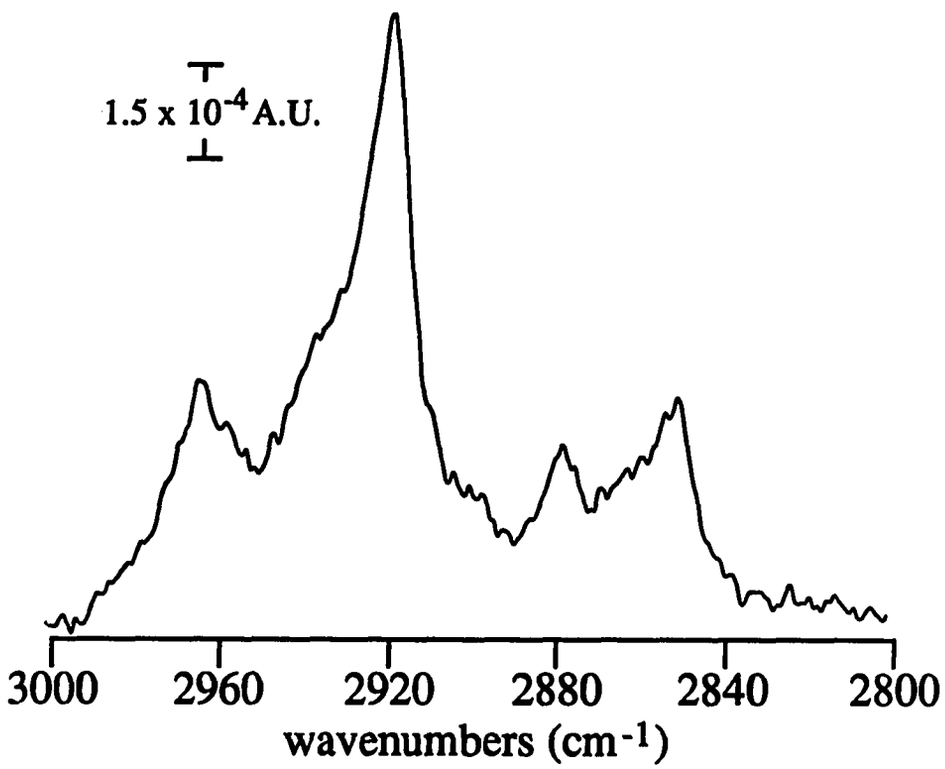

Figure 42. Ex situ IR spectrum of *n*-octadecanethiol at Au on pyrex plunger at 55° angle of incidence

Spectra acquired with the second in situ cell in a variety of solvents whose properties are listed in Table II are shown in Figure 43a-f. As observed in the earlier spectra, the positions and intensities of the methylene bands remain essentially unchanged in the presence of the solvents. The methyl bands are perturbed substantially. Again a broadening of $\nu_a(CH_3)$ is observed for all solvents and $\nu_s(CH_3$ FR2) is shifted to lower energy. No apparent broadening on the low energy side of $\nu_a(CH_2)$ has been observed in spectra acquired with this cell. Calculations of tilt and twist based on comparisons of the asymmetric and symmetric peak height ratios for the thiol monolayers in a variety of solvents with that ex situ shows that the average tilt and twist vary by ±3° and ±5° from sample to sample. This is within the expected variation of the monolayer due to sample preparation and suggests little if any solvent effects on the orientation of the monolayer chains.

Among all of the in situ spectra obtained, the greatest variability in these data arises in the character of $\nu_a(CH_3)$. This band varies substantially in absorbance, width, and peak center from monolayer to monolayer. This is due to differences in monolayer formation due to changes in the morphology of the substrates. At Si wafers and glass slides, the characteristics of this band ex situ remained approximately constant, as would be expected since these substrates are manufactured to provide uniformity. Slight changes in the roughness of the pyrex substrates for this cell would lead to different percentages of defects at the surface, effecting both the formation of the metal overlayer and the integrity of the monolayer film.

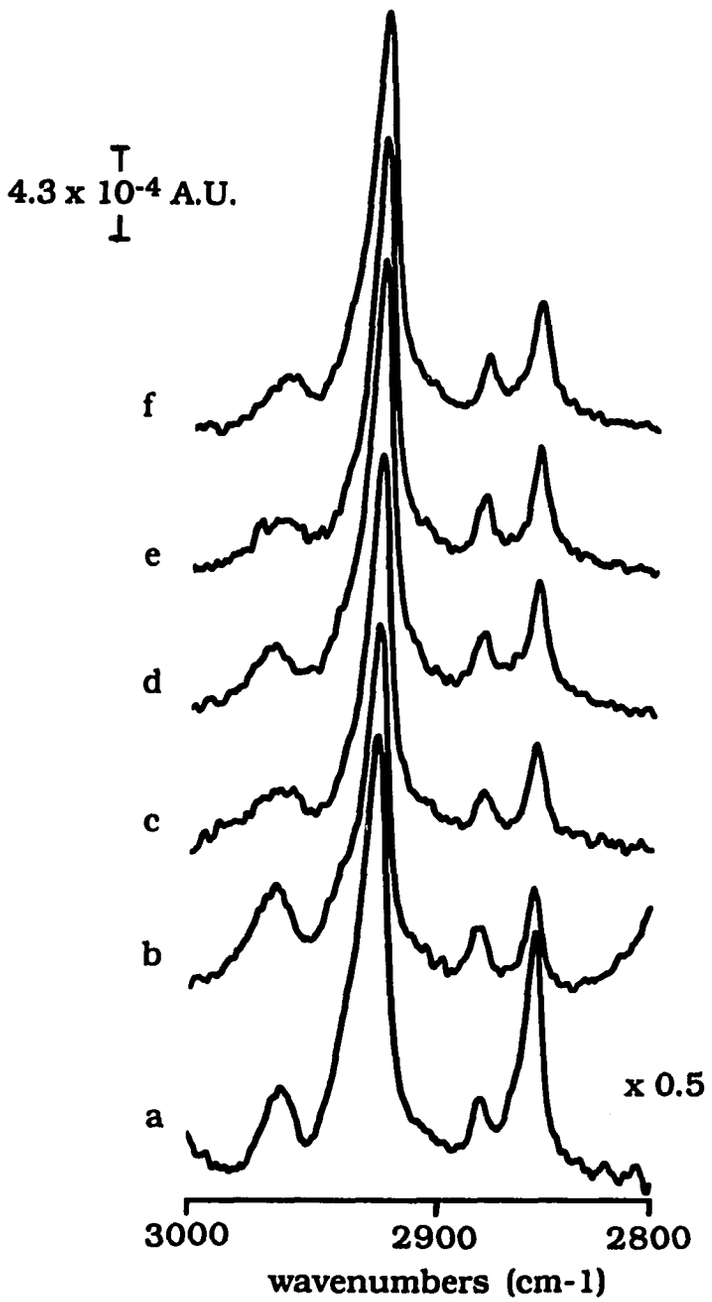

Figure 43. Infrared in situ external reflection spectra of *n*-octadecanethiol at Au taken with the cell in Figure 39: (a) in H_2O, (b) in D_2O, (c) in *d*-DMSO, (d) in *d*-acetonitrile, (e) in *d*-acetone, (f) in CCl_4

An interesting and puzzelling phenomena was observed in one of the spectra. An in situ spectrum was obtained in D_2O and is shown in Figure 44a. The substrate was removed from the cell and then reinserted so as to acquire another spectrum in the same solvent. The resulting spectrum (Figure 44b) showed essentially no absorbance for $\nu_a(CH_3)$. The substrate was re-immersed in the thiol solution overnight and the spectrum taken again. The band was still absent. The spectrum of the monolayer on the plunger was then acquired ex situ to see if the band was present. This spectrum is shown in Figure 44c. As is evident, the observed effect was induced by the solvent and did not permanently alter the monolayer. The likely cause of this phenomenon is that the perturbation of the chain terminus due to the presence of the solvent, coupled with the conformational effects induced by the substrate morphology, leads to an orientation for the methyl functional group such that both the in-plane and out-of-plane $\nu_a(CH_3)$ modes are parallel to the surface, thereby making those modes infrared inactive. It is uncertain as to why this is observed only occasionally and why the expected spectrum was attainable initially. This model is, however, consistent with that proposed in the preceding paragraphs since some perturbation of the chain terminus has been shown to occur upon contact with solvent. It can be concluded that the observed effects on the methyl group are dependent on polarization interactions with the solvent, as well as the orientation of the monolayer dictated by the surface morphology.

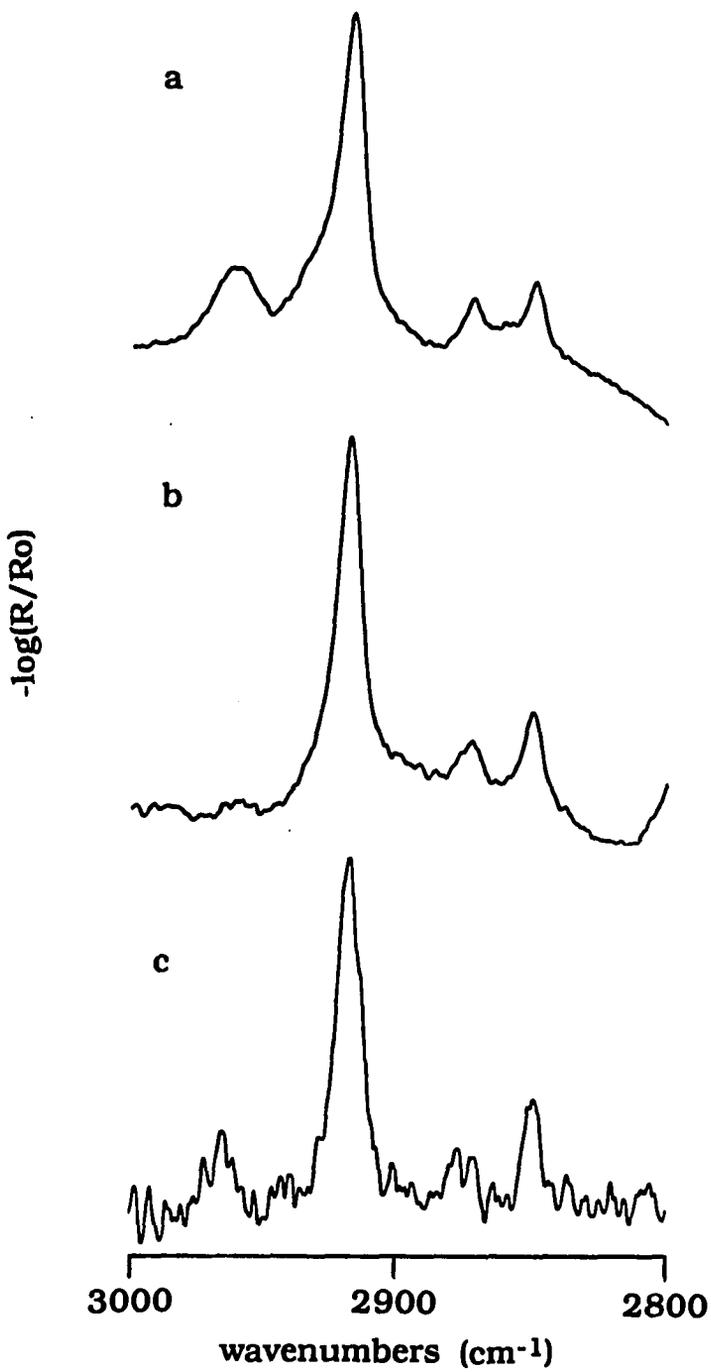

Figure 44. Infrared spectra of *n*-octadecanethiol at Au in D_2O. (a) first immersion in D_2O, (b) second immersion in D_2O, (c) ex situ after immersion

Monolayers at Ag

It was concluded in Section IV that *n*-alkanethiol monolayers have an average orientation at Ag of ~14° relative to the surface normal. This effect was attributed to the polycrystalline nature of the exposed crystal face of the substrate, with a (100) surface dictating a 0° chain tilt and (110) and (111) surfaces having tilts of ~35°. At Ag, the surface was concluded to be a composite of (100) and one or more other crystal faces, resulting in the observed tilt. It follows that if the chains are forced by the lattice constants of the substrate to pack closer together at the (100) surface, then the monolayer should be, on average, more impervious to the effects of solvent. Information obtained in situ in a variety of solvents can probe this effect and provide insight into the molecular arrangement of the terminus.

Figure 45 shows the ex situ spectrum of *n*-octadecanethiol at Ag on a glass microscope slide acquired at a 52° angle of incidence with the techniques previously described. This angle closely approximates that at the surface in the in situ cell. It is important to note that this spectrum shows decreased absorbances for all of the methyl modes relative to the methylene modes as compared to other ex situ spectra at Ag acquired previously. Tilt and twist angles for this monolayer are calculated to be 14° and 47°, respectively which agrees quite well with those calculated for the ex situ data. Since monolayer and substrate preparation procedures had not changed, the noticeable changes in the spectrum may have been due to slight changes in the purity of the Ag used in the evaporation, subtle differences in evaporation rates

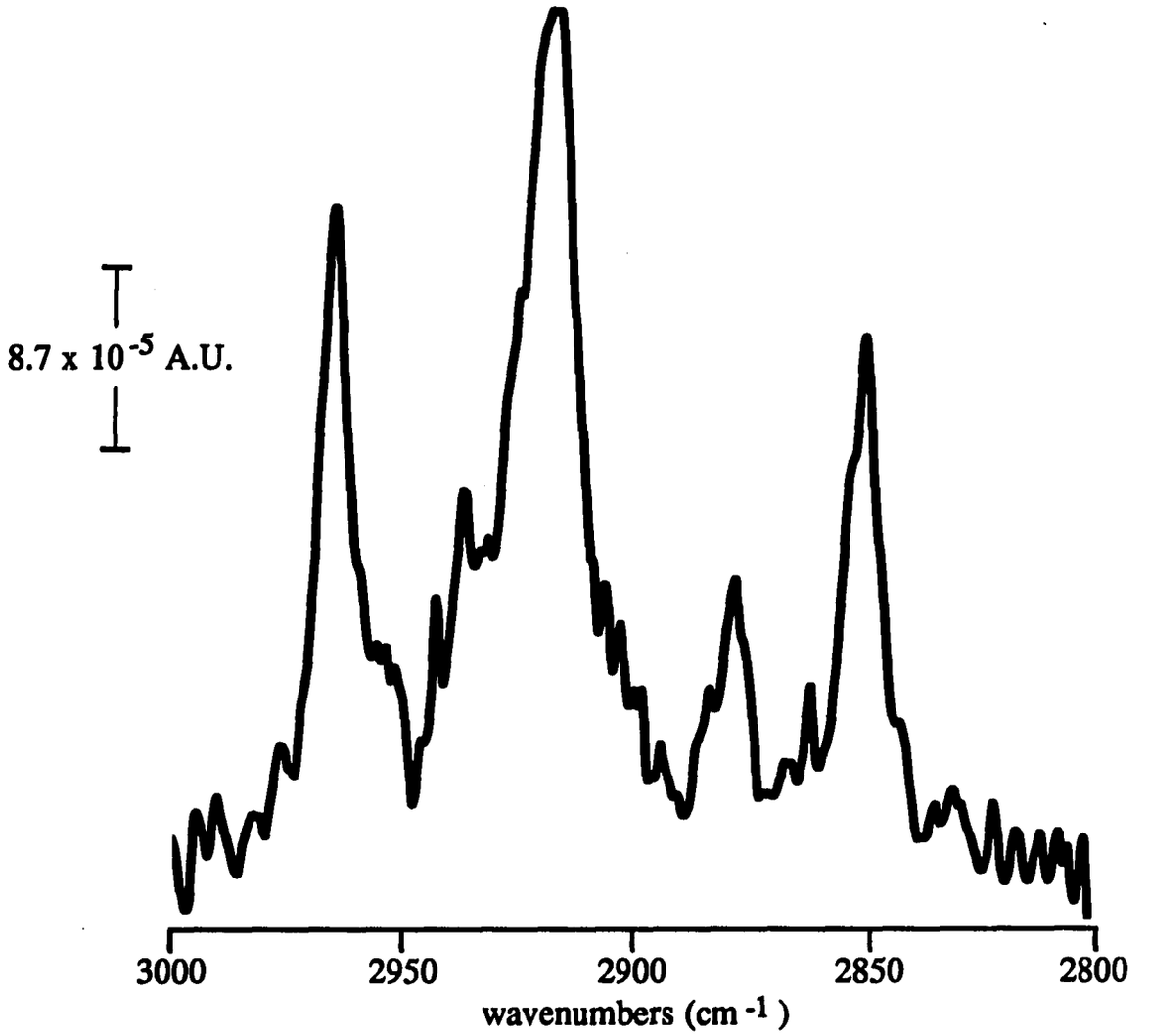

Figure 45. Infrared reflection spectrum of *n*-octadecanethiol at a Ag coated glass slide at 52° angle of incidence, closely approximating the angle of incidence for the in situ cell

giving rise to a varying crystallography of the surface, or to differences in the "smoothness" of the particular batch of microscope slides used. The thiol had been recently purified by recrystallization from methanol prior to use. Since all the Ag substrates on the pyrex plungers were prepared from the same lot of Ag and within a 2-3 week period, this ex situ spectrum serves as a reference state for the structure of the monolayer prior to immersion in the various solvents.

The spectrum in Figure 45 has peak positions and widths consistent with a pseudo-closest packed monolayer. These values are shown in Table III. The most significant difference between this spectrum and the spectra at Au or Ag on Si is the prominent appearance of $\nu_a(CH_3$ o.p.) at 2953 cm^{-1}. The band is significantly more pronounced in this spectrum, indicating regions at this surface with significant differences in packing relative to those acquired previously at the Si or glass substrates examined earlier. Calculations (discussed in Section III) demonstrate that this monolayer has an average tilt of ~14° with a twist of ~47°, consistent with the model previously discussed. It will be important to the following discussion to mention that $\nu_s(CH_2)$ has a peak intensity approximately 62% of $\nu_a(CH_2)$. Also, since molecular orientation is dependent on the surface morphology of the substrate, peak intensities do vary somewhat from sample to sample.

Figure 46a-e shows representative spectra for *n*-octadecanethiol at Ag on pyrex taken in situ in D_2O, dimethylsulfoxide-d_6, acetonitrile-d_3, acetone-d_6, and CCl_4. Physical constants for the solvents are

Table III. Peak positions, widths, and solvent properties for the C-H stretching modes of *n*-octadecanethiol ex situ and in situ for the second version in situ cell

		Peak Position (band width), cm^{-1} and [Peak Height] (x 10^4 A.U.)							
	Vib. Mode	ex situ		H_2O		D_2O		DMSO-	
A_u	$\nu_a(CH_3)$[a]	2964(10)	[8.3]	2958(16)	[7.3]	2961(18)	[2.3]	2961(26)	
	$\nu_s(CH_3$ FR1)[b]	_[c]		_[c]		_[c]		_[c]	
	$\nu_a(CH_2)$	2919(13)	[29.2]	2918(11)	[38.4]	2918(10)	[13.6]	2918(10)	[
	$\nu_s(CH_3$ FR2)[b]	2878(10)	[8.1]	2872(10)	[6.6]	2872	[3.8]	2872(12)	
	$\nu_s(CH_2)$	2851(9)	[12.5]	2850(10)	[21.2]	2849(12)	[5.1]	2849(10)	
A_g	$\nu_a(CH_3)$	2965(8.5)	[3.2]			2961(20)	[5.9]	2960(22)	
	$\nu_s(CH_3$ FR1)[b]	2936				_[c]		2931	
	$\nu_a(CH_2)$	2917(14)	[4.3]	_[d]		2917(10)	[15.5]	2917(15)	
	$\nu_s(CH_3$ FR2)[b]	2877(9)	[1.6]			2873(10)	[2.6]	2872(10)	
	$\nu_s(CH_2)$	2849(10)	[2.7]			2849(9)	[10.3]	2849(12)	
	$n_D^{25°}$ [e]			1.333		1.333		1.478	
	$\varepsilon^{25°}$ [e]			78.304		78.304		46.45	

[a] This absorption band represents both the in-plane mode at 2964 cm^{-1} and the out-of-plane mode at 2956 cm^{-1}.

[b] These bands are the result of Fermi resonance (FR) interactions between $\nu_s(CH_3)$ and the first overtone of $\delta_a(CH_3)$. Definitive assignment is still the subject of debate (238-239).

[c] Overlap of this absorption band with $\nu_a(CH_2)$ prevents its measurement.

[d] Data were not collected in this solvent.

[e] Values are from reference 265 and are for the hydrogenated analogs of the solvents.

for the C-H
and in situ

[1] and

D_2O		DMSO-d_6		CD_3CN		Acetone-d_6		CCl_4	
)61(18)	[2.3]	2961(26)	[2.7]	2964(20)	[2.8]	2962(22)	[2.2]	2959(20)	[2.3]
_[c]		_[c]		_[c]		_[c]		_[c]	
)18(10)	[13.6]	2918(10)	[17.8]	2918(10)	[20.2]	2918(10)	[19.3]	2918(10)	[18.7]
372	[3.8]	2872(12)	[2.5]	2873(12)	[3.4]	2874(10)	[3.3]	2872(11)	[3.2]
349(12)	[5.1]	2849(10)	[4.6]	2850(10)	[5.7]	2850(10)	[5.5]	2850(11)	[5.5]
)61(20)	[5.9]	2960(22)	[2.7]	2963(23)	[2.5]	2962(24)	[3.4]	2962(19)	[2.6]
_[c]		2931	[3.4]	2932(21)	[3.1]	2931	[3.8]	2930	[2.9]
)17(10)	[15.5]	2917(15)	[4.5]	2917(16)	[4.7]	2916(12)	[8.3]	2916(11)	[7.0]
373(10)	[2.6]	2872(10)	[3.2]	2873(11)	[3.2]	2874(14)	[2.9]	2873(10)	[2.4]
349(9)	[10.3]	2849(12)	[2.6]	2850(9)	[2.7]	2849(10)	[5.3]	2850(8.5)	[4.5]
1.333		1.478		1.342		1.356		1.457	
78.304		46.45		35.94		20.56		2.238	

lane mode at

onance (FR)
of $\delta_a(CH_3)$.
39).
prevents its

hydrogenated

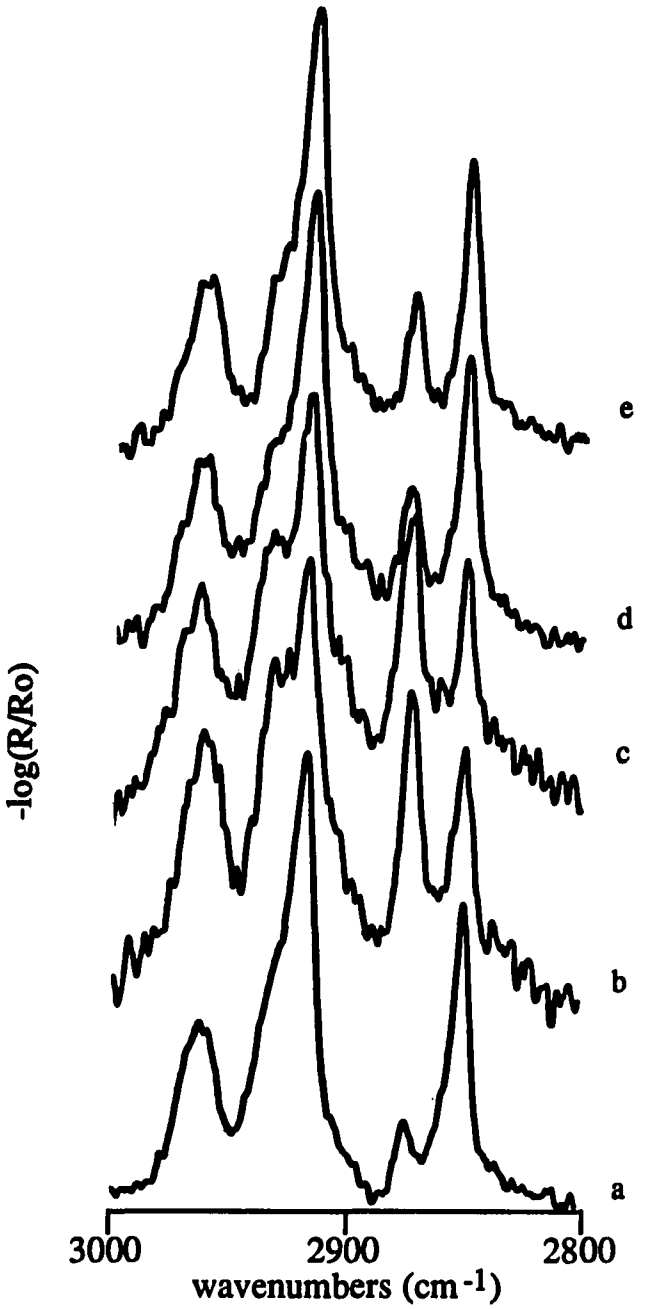

Figure 46. Infrared in situ external reflection spectra of *n*-octadecanethiol at Ag taken with the cell in Figure 39: (a) in D_2O, (b) in *d*-DMSO, (c) in *d*-acetonitrile, (d) in *d*-acetone, (e) in CCl_4

shown in Table II. It is evident that the presence of solvent has little, if any, effect on the character of the methylene modes. Peak positions for both $\nu_a(CH_2)$ and $\nu_s(CH_2)$ remain unchanged relative to the ex situ spectrum and are indicative of a mostly crystalline environment. The peak intensities for these bands remain proportional, with $\nu_s(CH_2)$ maintaining 55-65% of $\nu_a(CH_2)$, arising from differences in tilt and twist for the monolayers of ±1° and ±2° respectively. This decrease in variability for the methylene intensities at Ag as compared to Au may be due to more rigidly oriented chains that are less susceptible to the effects of the solvents, consequently maintaining the original conformation regardless of the contacting medium. Differences due to substrate morphology cannot, however, be ruled out at this juncture. In addition, no appreciable changes in peak width or position are observed. This suggests that permeation of the solvent into the monolayer is limited to the chain terminus, with the majority of the monolayer remaining tightly packed.

The effect of the various solvents on the methyl modes for the Ag substrates is comparable to that at the Au substrates. Substantial broadening (2.5 - 3 times) of $\nu_a(CH_3)$ along with a shift to lower energy of 3-5 cm^{-1} indicates a conformational disordering of the methyl group when in contact with solvent. Referring to the ex situ spectrum in Figure 45, the increase in intensity of the out-of-plane mode, if it becomes approximately the same magnitude as the in-plane mode, would give a net bandshape that is substantially broadened and centered between the two bands at ~2960 cm^{-1}. This effect is readily

observed in the data. With the current level of noise in the spectra, it is difficult to determine the extent that both the in-plane and out-of-plane modes are shifted, if at all. It may be that the effect of the solvent on the asymmetric modes is different from that on the symmetric modes, giving rise to different amounts of shifting. Again, some broadening due to the inhomogeneity of the solvent overlayer may occur, however, the absence of significant changes in the peak width of $\nu_s(CH_3$ FR2) suggests that this effect is again minimal. Shifting to lower energies by 3-5 cm^{-1} for $\nu_s(CH_3$ FR1) and $\nu_s(CH_3$ FR2) is again observed.

Evidence from Section IV demonstrated that a discrepancy exists between the observed orientation of the methylene chains in the monolayers and the orientation of the methyl groups at the chain terminus. This indicates that, while the methylene chain has a preferred packing, with a tilt and twist dependent upon the substrate composition and morphology, the methyl mode has a different preferred orientation requiring a perturbation of the chain at the terminus when exposed to air. This conformation is aligned with the out-of-plane $\nu_a(CH_3)$ dipole along the surface parallel, making it inactive to the infrared. The data in Section V show that, when in the presence of solvent, the methyl terminus rearranges to take on a new preferred orientation, thereby activating this mode. As improvements are made in the preparation of the substrates and monolayers, as well as in the sensitivity of the in situ technique, more quantitative data will surely be attainable to better define this phenomena.

Conclusion

It has been shown that in situ infrared external reflection spectroscopy provides a unique opportunity for gaining insight into the structural perturbations induced in long chain alkanethiol monolayer films by an overlying solvent. These perturbations are mostly confined to the region near the chain terminus, since there are no observable changes in the position or width of $\nu_s(CH_2)$. Such a conclusion is supported by the crystalline-like packing of the alkyl chains. The relative intensities of the methylene bands do suggest that the chains at Au are perturbed to a slightly greater extent than they are at Ag, however. Studies with deuterium-labeled segments of the alkyl chains to define the extent of solvent penetration and the subsequent structural perturbations are in progress by other researchers in this laboratory. Correlations between the penetration of the contacting solvent and its molecular size and shape are also underway.

CONCLUSIONS AND FUTURE DIRECTIONS

Polymer, monolayer, and sub-monolayer films of a variety of chemical species at differing types of surfaces have proven to be of great value both commercially and scientifically. Fundamental to the development of new materials and methodologies to better utilize the interfacial properties of these types of systems is an understanding of the basic chemical and physical phenomena which occur at the molecular level. Due to the complexity of these types of molecular systems, no single technique is sufficient to elucidate fully a complete description of the properties of the materials. Consequently, a multi-disciplinary approach to the investigation of these interfaces was initiated in this laboratory, and the primary emphasis of this researcher dealt with the examination of thin organic films at glassy carbon and noble metals by infrared external reflection spectroscopy. Central to this project has been the goal of developing the requisite methodologies to probe the molecular environment of the air/solid and liquid/solid interface in "real-world" conditions (i.e., in the laboratory environment or in the presence of condensed solvent).

The permselective properties of a hydrolyzed cellulose acetate film at a glassy carbon electrode were investigated. Data from electrochemistry and IR-ERS led to the conclusion that these films undergo some type of pre-conditioning (most likely an absorption of H_2O leading to a swelling of the film), followed by replacement of the acetate groups with hydroxide groups. An understanding of the optical

phenomena contributing to the band distortions in the spectra, caused by the decreased reflectivity of the surface, was necessary to interpret the observed band-shapes.

The acquisition of high quality IR-ERS spectra of monolayer films at metallic surfaces requires exact repositioning of the substrate in the optical beam. The development of the means to easily and reproducibly obtain high quality monolayer spectra facillitated the multi-disciplinary characterization of the *n*-alkanethiols at Au and Ag. The information obtained from these spectra led to the discovery of the opposite odd-even for these monolayers at Ag relative to Au, and provided information regarding the relative tilts of the monolayers at the two metals. Without spectra of this quality, this odd-even effect would most likely have been obscured by the higher degree of uncertainty in the measurements.

Transfering the technology of IR-ERS to the acquisition of monolayer spectra in the presence of aqueous and organic solvents without the necessity of modulation techniques posed the most formidable challenge of this entire research project. Due to the exceptionally strong infrared absorbances of most solvents, acquiring these spectra by direct means requires the use of methodologies which allow for both solution layer thicknesses on the order of hundreds of nanometers and control of this thickness on the order of tens of nanometers. Section V detailed the experiments and presented the first examples of this new technique. This initial data shows that the closely packed monolayers of *n*-octadecanethiol are

perturbed by the solvents at the chain terminus, leading to band-widths that are more broad and shifted to lower energies. Some evidence exists and was presented indicating that the ω-methylene group is perturbed in some cases by the solvent also. Of more far-reaching implications, however, is the fact that spectra of any type of adsorbate, not just those that are electroactive, can now be investigated directly in situ without the need for potential or polarization modulation.

It has become evident throughout the course of this work that the greatest single obstacle that must be overcome before more detailed information can be acquired, is the control of the morphology of the substrates and the metal overlayer that is deposited on them. The use of atomically smooth mica as the support material instead of Si wafers or glass slides may serve to provide the long range order and consistency necessary to eliminate some of the variability from sample to sample. This will be experimentally difficult, however, the increased control of the morphology will make the effort worthwhile. It will also be necessary to establish greater control of the evaporation parameters for the metal overlayers to maintain uniform proportions of the various exposed crystal faces, especially when Ag films are studied.

Work continues in this laboratory to further the methodologies of these techniques and to explore more intricate chemical moieties at a variety of surfaces. Experiments are currently underway to examine different types of cellulosic polymer films at glassy carbon,

comparing changes in the chemical structure with the permselectivity of the material. Investigations into the effects of surface composition on the character of multilayer, monolayer and mixed-monolayer films at Au, Ag, Cu, and other metals is also in progress. Once better reproducibility of the substrates has been achieved, more definitive conclusions concerning the monolayer integrity will be attainable. This information can then be used as a standard by which to compare the results from the in situ cell. Also, there are still many unanswered questions concerning the relatively simple n-alkanethiol monolayers at Au and Ag. For example, how much disorder is actually present in the film, how is it manifested (i.e., fully gauche or semi-gauche, near the head-group or terminus, etc.) and what is the cause of this disorder? Why is the out-of-plane methyl stretch so elusive (i.e., why is it always parallel to the surface?)? What is the mode of attachment of these molecules to the metal surfaces? As with most scientific endeavors, the answer to one question usually leads to several other questions.

Mechanical improvements in the in situ cell and spectrometer will increase the signal-to-noise of the cell, thereby providing for the definitive attribution of band shapes and positions to solvent induced phenomena. The use of deuterium-labeled *n*-alkanethiols will serve to isolate particular absorption bands in the spectrum, removing ambiguity from the analysis. For example, the use of $CH_3(CD_2)_nSH$ to remove the contribution of the methylene bands from the C-H stretching region will not only allow a detailed study of the effects of the various solvents on the chain terminus, but will provide

information concerning the nature of the Fermi resonance interactions that occur. Studies with $CD_3(CH_2)_n(CD_2)_mSH$, provided sufficient sensitivity has been achieved to adequately detect a single or very few methylene modes, will lend insight into the permeation of the solvent into the monolayer and its effects on the methylene modes.

Preliminary efforts to explore the effects of solvent on more reactive monolayer materials were significantly hampered by the current signal-to-noise ratio for the experiment. Once adequate detection is available, materials such as $HOOC(CH_2)_nSH$, will provide a plethora of information concerning the behavior of such bound species in situ upon exposure to varying pH, allowing for comparison with the species in solution. In situ spectra of cyclodextrinthiols at the surface will allow for the determination of the nature of the cyclodextrin cavity and the requirements for molecular incorporation. Essential to such measurements is a firm control of the substrate morphology. Without it, these data will remain untainable.

It has been shown that infrared external reflection spectroscopy is a powerful tool for determining the molecular identity and structural composition of organic materials at reflecting surfaces. Information gleaned from these techniques, coupled with those from other disciplines, aids in developing a fuller understanding of the chemical and physical interactions occurring at interfaces. With ever-improving developments in data acquisition, the chemical subtleties now hidden in these systems will become more and more attainable.

ACKNOWLEDGEMENTS

The author gratefully acknowledges Dr. Marc Porter for his guidance, patience, and tolerance during the past four years of study. Discussions with the other members of this group have been invaluable throughout each of these research projects, and their contributions are greatly appreciated. This research was funded primarily by Ames Laboratory - USDOE and Iowa State University under contract No. W-7405-eng-82.

REFERENCES

1. Wu, S. Polymer Interfaces and Adhesion New York: Marcel Dekker, **1982**.
2. Roberts, G. *Adv. Phys.* **1985**, *34*, 475.
3. Bowden, F.; Tabor, D. The Friction and Lubrication of Solids London: Oxford Press, **1968**, and references therein.
4. Baier, R.; Meyer, A.; Natiella, J.; Natiella, R.; Carter, J. *J. Biomed. Mat. Res.* **1984**, *18*, 337.
5. Gristina, A. *Science* **1987**, *237*, 1588.
6. Swalen, J. D.; Allara, D. L.; Andrade, J. B.; Chandross, E. A.; Garoff, S.; Isrealachvili, J.; McCarthy, T. J.; Murray, R.; Pease, R. F.; Rabolt, J. F.; Wynne, K. J.; Yu, H. *Langmuir* **1987**, *3*, 932.
7. Hubbard, A. T. *Chem. Rev.* **1988**, *88*, 633.
8. Bellier, J.; Lecoeur, J.; Rousseau, A. *J. Electroanal. Chem.* **1986**, *200*, 55.
9. Peukert, M.; Ibach, H. *Surf. Sci.* **1984**, *136*, 319.
10. Greenler, R. G. *J. Chem. Phys.* **1966**, *44*, 310.
11. Greenler, R. G. *J. Chem. Phys.* **1969**, *50*, 1963.
12. Francis, S. A.; Ellison, A. H. *J. Opt. Soc. Am.* **1959**, *49*, 131.
13. Foley, J. K.; Pons, B. S. *Anal. Chem.* **1985**, *57*, 945A.
14. Pons, S.; Foley, J. K.; Russell, J.; Severson, M. In *Modern Aspects of Electrochemistry* eds. Bochris, J. O'M.; Conway, B. E.; White, R. E., **1986**, *17*, 223.
15. Ashley, K.; Pons, B. S. *Chem. Rev.* **1988**, *88*, 673.

16. Korzeniewski, C.; Pons, S. *Prog. Analyt. Spectrosc.* **1987**, *10*, 1.

17. Beden, B.; Lamy, C. In Spectroelectrochemistry: Theory and Practice. ed. Gale, R. J., New York: Plenum Press, **1988**, 189.

18. Weast, R. C.; Astle, M. J. CRC Handbook of Chemistry and Physics. 61st ed., Cleveland, OH: Chemical Rubber Co., **1980-1981**.

19. Hansen, W. N., *J. Opt. Soc. Am.* **1968**, *58(3)*, 380.

20. Hansen, W. N. "Internal Reflection Spectroscopy in Electrochemistry" in Vol. 9 of Advances in Electrochemistry and Electrochemical Engineering, New York: John Wiley and Sons, **1973**.

21. Palik, E. D. Handbook of Optical Constants of Solids Orlando, FL: Academic Press, **1985**.

22. Pearce, H. A.; Sheppard, N. *Surf. Sci.* **1976**, *59*, 205.

23. Porter, M. D.; Bright, T. B.; Allara, D. L.; Kuwana, T. *Anal. Chem.* **1986**, *58(12)*, 2461.

24. Allara, D. L.; Baca, A.; Pryde, C. A. *Macromolecules* **1978**, *11*, 1215.

25. Yang, X. Q.; Inagaki, T.; Chen, J.; Skotheim, T. A. *Mol. Cryst. Liq. Cryst.* **1988 (Volume date 1987)**, *160*, 261.

26. Allara, D. L.; Pryde, C. A. *Org. Coat. Plast. Chem.* **1978**, *38*, 638.

27. Webb, J. D.; Schissel, P.; Czanderna, A. W.; Smith, D. M.; Chughtai, A. R. *Energy Res. Abstr.* **1982**, *7(21)*, Abstr. No. 56613.

28. Beck, F.; Braun, P.; Oberst, M. *Ber. Bunsen-Ges. Phys. Chem.* **1987**, *91(9)*, 967.

29. Hatta, A.; Matsumoto, H.; Suetaka, W. *Chem. Lett.* **1983**, *(7)*, 1077.

30. Watanabe, A.; Tanaka, M.; Tanak, J. *Bull. Chem. Soc. Jpn.* **1981**, *54(8)*, 2278.

31. Xue, G.; Ding, J.; Wu, P.; Ji, G. *J. Electroanal. Chem.* **1989**, *270(1-2)*, 163.

32. Osawa, M.; Nakane, T.; Ito, K.; Suetaka, W. *J. Electroanal. Chem.* **1989**, *270(1-2)*, 459.

33. Karpowicz, R. J. *Rev. Sci. Instrum.* **1990**, *61(1, Pt. 1)*, 188.

34. Doblhofer, K.; Cappadonia, M. *Colloids Surf.* **1989**, *41(1-2)*, 211.

35. Niwa, K.; Doblhofer, K. *Electrochim. Acta* **1986**, *31(5)*, 549.

36. Tada, H.; Yano, Y.; Fujino, K.; Kawahara, H. *J. Polym. Sci., Part A: Polym. Chem.* **1987**, *25(7)*, 1745.

37. Hussla, I.; Philpott, M. R. *J. Electron Spectrosc. Relat. Phenom.* **1986**, *39*, 255.

38. Grunze, M.; Unertl, W. N.; Gnanarajan, S.; French, J. *Gov. Rep. Announce. Index (U. S.)* **1988**, *88(20)*, Abstr. No. 850,903.

39. Yang, X. Q.; Chen, J.; Hale, P. D.; Inagaki, T.; Skotheim, T. A.; DenBoer, M. L. *Synth. Met.* **1989**, *28(1-2)*, C329.

40. Wu, C. R.; Liedberg, B. *J. Polym. Sci., Part B: Polym. Phys.* **1988**, *26(5)*, 1127.

41. Eng, F. P.; Ishida, H. *Polym. Mater. Sci. Eng.* **1985**, *53*, 725.

42. Boerio, F. J.; Gosselin, C. A. *Adv. Chem. Ser.* **1983**, *203(Polym. Charact.)*, 541.

43. Webb, J. D.; Jorgensen, G.; Schissel, P.; Czanderna, A. W.; Chughtai, A. R.; Smith, D. M. *ACS Symp. Ser.* **1983**, *220(Polym. Sol. Energy Util.)*, 143.

44. Allara, D. L. *Pap. Meet. - Am. Chem. Soc., Div. Org. Coat. Plast. Chem.* **1976**, *36(1)*, 399.

45. Webb, J. D.; Czanderna, A. W. *Macromolecules* **1986**, *19(11)*, 2810.

46. Sergides, C. A.; Chughtai, A. R.; Smith, D. M.; Schissel, P. *Macromolecules* **1986**, *19(5)*, 1448.

47. Durcova, O.; Rzyman, T.; Samuhelova, Z.; Benovic, B. *Polym. Degrad. Stab.* **1985**, *13(3)*, 201.

48. Sergides, C. A.; Chughtai, A. R.; Smith, D. M. *Appl. Spectrosc.* **1985**, *39(4)*, 735.

49. Webb, J. D. *Energy Res. Abstr.* **1985**, *10(2)*, Abstr. No. 2169.

50. Webb, J. D. *Energy Res. Abstr.* **1985**, *10(2)*, Abstr. No. 2168.

51. Webb, J. D.; Schissel, P.; Thomas, T. M.; Pitts, J. R.; Czanderna, A. W. *Sol. Energy Mater.* **1984**, *11(3)*, 163.

52. Webb, J. D.; Schissel, P.; Thomas, T. M.; Pitts, J. R.; Czanderna, A. W. *Proc. SPIE - Int. Soc. Opt. Eng.* **1983**, *428(Opt. Mater. Process Technol. Energy Effic. Sol. Appl.)*, 112.

53. Webb, J. D.; Schissel, P.; Czanderna, A. W.; Smith, D. M.; Chughtai, A. R. *Proc. - Electrochem. Soc.* **1983**, *83-1(Proc.*

Symp. Corros. Batteries Fuel Cells Corros. Sol. Energy Syst.), 202.

54. Teramae, N.; Tanaka, S. *Mikrochim. Acta* **1988 (Volume date 1987)**, *2(1-6)*, 159.
55. Webb, J. D.; Czanderna, A. W.; Pitts, J. R. *J. Vac. Sci. Technol., A* **1988**, *6(3, Pt. 1)*, 997.
56. Webb, J. D.; Czanderna, A. W.; Pitts, J. R. *J. Polym. Sci., Part A: Polym. Chem.* **1987**, *25(12)*, 3395.
57. Briggs, L. M.; Bauer, D. R.; Carter III, R. O. *Ind. Eng. Chem. Res.* **1987**, *26(4)*, 667.
58. Vettegren, V. I.; Tshmel, A. E. *Eur. Polym. J.* **1976**, *12(12)*, 853.
59. Fiala, V.; Sotolova, O.; Trbusek, V.; Vrbova, M.; Vasku, A.; Urbanek, P.; Vasku, J.; Lukas, J.; Houska, M.; Tyrackova, V. *Biomaterials* **1987**, *8(4)*, 259.
60. White, D. C. *Toxic. Assess.* **1986**, *1(3)*, 315.
61. Stolz, H. J.; Wendel H.; Otto, A.; Pintschovius, L.; Kahlert, H. *Phys. Status Solidi B* **1976**, *78(1)*, 277.
62. Bright, A. A.; Cohen, M. J.; Garito, A. F.; Heeger, A. J.; Mikulski, C. M.; Russo, P. J.; MacDiarmid, A. G. *Phys. Rev. Lett.* **1975**, *34(4)*, 206.
63. Stolz, H. J.; Otto, A.; Pintschovius, L. *Proc. Int. Conf. Light Scattering Solids, 3rd, Meeting Date* **1975**, 737-741. Eds. Balkanski, M.; Leite, R. C. C. Porto, S. P. S. New York: Wiley.

64. Lu, J.; Bewick, A. *J. Electroanal. Chem. Interfacial Electrochem.* **1989**, *270(1-2)*, 225.

65. Malik, I. J.; Trenary, M. *Surf. Sci.* **1989**, *214(1-2)*, L237.

66. Boecker, D.; Wicke, E. *Springer Ser. Synergetics* **1985**, *29(Temporal Order)*, 75.

67. Boecker, D.; Wicke, E. *Ber. Bunsen-Ges. Phys. Chem.* **1985**, *89(6)*, 629.

68. Hoffmann, F. M.; Paul, J. *J. Chem. Phys.* **1987**, *87(3)*, 1857.

69. Tompkins, H. G.; Greenler, R. G. *Surf. Sci.* **1971**, *28(1)*, 194.

70. King, S. T. *Appl. Spectrosc.* **1980**, *34(6)*, 632.

71. Edwards, J. F.; Schrader, G. L. *Appl. Spectrosc.* **1981**, *35(6)*, 559.

72. Kiss, J. T.; Gonzalez, R. D. *Ind. Eng. Chem. Prod. Res. Dev.* **1985**, *24(2)*, 216.

73. Arakawa, H.; Fukushima, T.; Ichikawa, M. *Appl. Spectrosc.* **1986**, *40(6)*, 884.

74. Fukushima, T.; Arakawa, H.; Ichikawa, M. *J. Phys. Chem.* **1985**, *89(21)*, 4440.

75. Saymeh, R. A.; Gonzalez, R. D. *J. Phys. Chem.* **1986**, *90(4)*, 622.

76. Kiss, J. T.; Gonzalez, R. D. *J. Phys. Chem.* **1984**, *88(5)*, 892.

77. Kiss, J. T.; Gonzalez, R. D. *J. Phys. Chem.* **1984**, *88(5)*, 898.

78. Arakawa, H.; Fukushima, T.; Ichikawa, M.; Takeuchi, K.; Matsuzaki, T.; Sugi, Y. *Chem. Lett.* **1985**, *(1)*, 23.

79. Fukushima, T.; Fujimoto, K.; Tominaga, H. *Appl. Catal.* **1985**, *14(1-3)*, 95.

80. Haaland, D. M.; Williams, F. L. *Proc. SPIE - Int. Soc. Opt. Eng.* **1981**, *289(Int. Conf. Fourier Transform Infrared Spectrosc.)*, 3.

81. King, D. L. *J. Catal.* **1980**, *61(1)*, 77.

82. Dalla Betta, R. A.; Shelef, M. *J. Catal.* **1977**, *48(1-3)*, 111.

83. Gun, J.; Iscovici, R.; Sagiv, J. *J. Colloid Interface Sci.* **1984**, *101(1)*, 201.

84. Mumby, S. J.; Rabolt, J. F.; Swalen, J. D. *Thin Solid Films* **1985**, *133*, 161.

85. Umemura, J.; Kamata, T.; Kawai, T.; Takenaka, T. *J. Phys. Chem.* **1990**, *94(1)*, 62.

86. Popovitz-Biro, R.; Hung, D. J.; Shavit, E.; Lahav, M.; Leiserowitz, L. *Thin Solid Films* **1989**, *178*, 203.

87. Kamata, T.; Umemura, J.; Takenaka, T.; Takehara, K.; Isomura, K.; Taniguchi, H. *Thin Solid Films* **1989**, *178*, 427.

88. Kawai, T.; Umemura, J.; Takenaka, T. *Langmuir* **1990**, *6(3)*, 672.

89. Schlotter, N. E.; Porter, M. D.; Bright, T. B.; Allara, D. L. *Chem. Phys. Lett.* **1986**, *132(1)*, 93.

90. Golden, W. G.; Saperstein, D. D.; Severson, M.W.; Overend, J. *J. Phys. Chem.* **1984**, *88(3)*, 574.

91. Golden, W. G.; Dunn, D. S.; Overend, J. *J. Catal.* **1981**, *71(2)*, 395.

92. Waldman, D. A.; Kolb, B. U.; McCarthy, T. J.; Hsu, S. L. *Polym. Mater. Sci. Eng.* **1988**, *59*, 326.

93. Buffeteau, T.; Desbat, B.; Turlet, J.-M. *Mikrochim. Acta* **1988(Volume Date, 1987)**, *2(1-6)*, 23.

94. Sekiguchi, A.; Wadayama, T.; Suetaka, W. *Anal. Sci.* **1985**, *1(5)*, 403.

95. Saperstein, D. D.; Golden, W. G.; *ACS Symp. Ser.* **1985**, *288(Catal. Charact. Sci.)*, 435.

96. Golden, W. G. *Polym. Prepr. (Am. Chem. Soc., Div. Polym. Chem.)* **1984**, *25(2)*, 158.

97. Golden, W. G.; Kunimatsu, K.; Seki, H. *J. Phys. Chem.* **1984**, *88(7)*, 1275.

98. Golden, W. G.; Saperstein, D. D. *J. Electron Spectrosc. Relat. Phenom.* **1983**, *30*, 43.

99. Dowrey, A. E.; Marcott, C. *Appl. Spectrosc.* **1982**, *36(4)*, 414.

100. Wadayama, T.; Suetaka, W.; Sekiguchi, A. *Jpn. J. Appl. Phys., Part 1* **1988**, *27(4)*, 501.

101. Wadayama, T.; Hanata, Y.; Suetaka, W. *Surf. Sci.* **1985**, *158(1-3)*, 579.

102. Wadayama, T.; Wada, M.; Suetaka, W. *Appl. Surf. Sci.* **1986**, *25(1-2)*, 231.

103. Miura, H.; Gonzalez, R. D. *J. Phys. E.* **1982**, *15(3)*, 373.

104. Mahos, K.; Nakamura, R.; Niiyama, H. *Sekiyu Gakkaishi* **1988**, *31(6)*, 485.

105. Saussey, J.; Lavalley, J. C. *J. Mol. Catal.* **1989**, *50(3)*, 343.

106. Wenig, R. W.; Schrader, G. L. *J. Phys. Chem.* **1987**, *91(22)*, 5674.

107. Do, N. T.; Baerns, M. *Appl. Catal.* **1988**, *45(1)*, 9.

108. Kou, Y.; Yin, Y.; Luo, Y.; Fu, H. *J. Mol. Sci. (Int. Ed.)* **1986**, *4(2)*, 177.

109. Xiaoding, X.; Mol, J. C.; Boelhouwer, C. *J. Chem. Soc., Faraday Trans.* **1986**, *82(9)*, 2707.

110. Groeneveld, C.; Wittgen, P. P. M. M.; Swinnen, H. P. M.; Wernsen, A.; Schuit, G. C. A. *J. Catal.* **1983**, *83(2)*, 346.

111. Delobel, R.; Le Bras, M.; Traisnel, M.; Leroy, J.-M. 1982,*Vib. Surf., [Proc. Int. Conf.], 2nd Meeting Date 1980*, **1982**, 315, Eds. Caudano, R.; Gilles, J.-M.; Lucas, A. A., New Youk: Plenum.

112. Blackmond, D. G.; Goodwin, J. G. Jr.; Lester, J. E. *J. Catat.* **1982**, *78(1)*, 34.

113. Whyman, R. *J. Organometal. Chem.* **1974**, *66(1)*, C23.

114. Ehlers, D. H.; Spitzer, A.; Lueth, H. *Surf. Sci.* **1985**, *160(1)*, 57.

115. Olsthoorn, A. A.; Moulijn, J. A. *J. Mol. Catal.* **1980**, *8(1-3)*, 147.

116. Obara, T.; Yamada, M.; Amano, A. *Chem. Lett.* **1986**, *(12)*, 2003.

117. Szilagyi, T.; Koranyi, T. I.; Paal, Z.; Tilgner, J. *Catal. Lett.* **1989**, *2(5)*, 287.

118. Mielczarski, J. A.; Yoon, R. H. *J. Colloid Interface Sci.* **1989**, *131(2)*, 423.

119. Allara, D. L.; Nuzzo, R. G. *Polym. Prepr. (Am. Chem. Soc., Div. Polym. Chem.)* **1984**, *25(2)*, 185.

120. Liedberg, B.; Carlsson, C.; Lundstroem, I. *J. Colloid Interface Sci.* **1987**, *120(1)*, 64.

121. Mielczarski, J.; Leppinen, J. *Surf. Sci.* **1987**, *187(2-3)*, 526.

122. Liedberg, B.; Lundstroem, I.; Wu, C. R.; Salaneck, W. R. *J. Colloid Interface Sci.* **1985**, *108(1)*, 123.

123. Hayden, B. E.; Prince, K.; Woodruff, D. P.; Bradshaw, A. M. *Surf. Sci.* **1983**, *133(2-3)*, 589.

124. Monti, D. M.; Cant, N. W.; Trimm, D. L.; Wainwright, M. S. *J. Catal.* **1986**, *100(1)*, 17.

125. Bouwman, R.; Freriks, I. L. C. *Appl. Surf. Sci.* **1980**, *4(1)*, 21.

126. Golden, W. G.; Snyder, C. D.; Smith, B. *J. Phys. Chem.* **1982**, *86(24)*, 4675.

127. Bradshaw, A. M. *Appl. Surf. Sci.* **1982**, *11-12(1-3)*, 712.

128. Marcott, C. *Proc. SPIE - Int. Soc. Opt. Eng.* **1981**, *289(Int. Conf. Fourier Transform Infrared Spectrosc.)*, 121.

129. Allara, D. L. *ACS Symp. Ser.* **1980**, *137(Vib. Spectrosc. Adsorbed Species)*, 37.

130. Allara, D. L.; Swalen, J. D. *J. Phys. Chem.* **1982**, *86(14)*, 2700.

131. Nuzzo, R. G.; Allara, D. L. *J. Am. Chem. Soc.* **1983**, *105(13)*, 4481.

132. Allara, D. L.; Hebard, A. F.; Padden, F. J.; Nuzzo, R. G.; Falcone, D. R. *J. Vac. Sci. Technol. A.* **1983**, *1(2, Pt. 1)*, 376.

133. Allara, D. L.; Nuzzo, R. G. *Langmuir* **1985**, *1(1)*, 52.

134. Finklea, H. O.; Melendez, J. A. *Spectroscopy (Springfield, Oreg.)* **1986**, *1(4)*, 47.

135. King, S. T.; Strojny, E. J. *J. Catat.* **1982**, *76(2)*, 274.

136. Riffe, D. M.; Sievers, A. J. *Surf. Sci.* **1989**, *210(3)*, L215.

137. Brueesch, P.; Koetz, R.; Neff, H.; Pietronero, L. *Phys. Rev. B: Condens. Matter* **1984**, *29(8)*, 4691.

138. Koller, K. B.; Schmidt, W. A.; Butler, J. E. *J. Appl. Phys.* **1988**, *64(9)*, 4704.

139. Foley, J. K.; Pons, S., *Langmuir* **1985**, *1*, 697.

140. Bewick, A.; Pons, S., "Infrared Spectroscopy of the Electrode-Electrolyte Solution Interface" in Advances in Infrared and Raman Spectroscopy, Vol 12, Eds. Clark, R. J. H.; Hester, R. E., New York: Wiley, **1985**.

141. Roe, D. K.; Sass, J. K.; Bethune, D. S.; Luntz, A. C. *J. Electroanal. Chem.* **1987**, *216*, 293.

142. Pons, S. *J. Electroanal. Chem.* **1983**, *150*, 495.

143. Lavialle, F.; Adams, R. G.; Levin, I. W. *Biochemistry* **1982**, *21*, 2305.

144. Pons, S.; Khoo, S. B.; Bewick, A.; Datta, M.; Smith, J. J.; Hinman, A. S.; Zachmann, G. *J. Phys. Chem.* **1984**, *88*, 3575.

145. Leung, L.-W. H.; Wieckowski, A.; Weaver, M. J. *J. Phys. Chem.* **1988**, *92(24)*, 6985.

146. Pons, S.; Davidson, T.; and Bewick, A. *J. Electroanal. Chem.* **1984**, *63*, 1960.

147. Habib, M. A.; Bockris, J. O'M. *J. Electrochem. Soc.* **1985**, *132*, 108.

148. Bewick, A.; Kunimatsu, K.; Pons, B. S.; Russell, J. W. *J. Electroanal. Chem.*, **1984**, *160*, 47.

149. Seki, H.; Kunimatsu, K.; Golden, W. G. *Appl. Spectrosc.* **1985**, *39*, 437.

150. Golden, W. G. In Fourier Transform Infrared Spectroscopy, Ed. Ferraro, J. R.; Basile, L. J., Vol. 4. New York: Academic Press, **1985**.

151. Yaniger, S. I.; Vidrine, D. W. *Appl. Spectrosc.* **1986**, *40*, 174.

152. Daschbach, J.; Heisler, D.; Pons, B. S. *Appl. Spectrosc.* **1986**, *40*, 489.

153. Li, J.; Daschbach, J.; Smith, J. J.; Morse, M. D.; Pons, S. *J. Electroanal. Chem.* 209 387.

154. Kemp, J. C. Polarized Light and its Interaction with Modulating Devices, a Methodology Review Hillsboro, OR: HINDS International, Inc., **1987**.

155. Biegler, T.; Koch, D. F. A. *J. Electrochem. Soc.* **1967**, *114*, 904.

156. Kamath, V. N.; Lal, H. *J. Electroanal. Chem.* **1968**, *19*, 137.

157. Kazarinov, V. E.; Tisyachnaya, Y. G.; Andreev, V. N. *Elektrokhimiya* **1972**, *8*, 396.

158. Breiter, M. W. *J. Electroanal. Chem.* **1967**, *15*, 221.

159. Wieckowski, A.; Sobkowski, J. *J. Electroanal. Chem.* **1975**, *63*, 365.

160. Beden, B.; Bewick, A.; Lamy, C. *J. Electroanal. Chem.* **1983**, *148*, 147.

161. Kunimatsu, K. *J. Electroanal. Chem.* **1983**, *145*, 219.

162. Kunimatsu, K.; Kita, H. *J. Electroanal. Chem.* **1987**, *218*, 155.

163. Albert, M. R.; Yates, J. T., Jr. The Surface Scientist's Guide to Organometallic Chemistry, Washington, D. C.: ACS Books, **1987**.

164. Pons, S.; Bewick, A. *Langmuir* **1985**, *1*, 141.

165. Beden, B.; Hahn, F.; Leger, J.-M.; Lamy, C.; Lopes, M. I. dos Santos *J. Electroanal. Chem. Interfacial Electrochem.* **1989**, *258(2)*, 463.

166. Perez, J. M.; Beden, B.; Hahn, F.; Aldaz, A.; Lamy, C. *J. Electroanal. Chem.* **1989**, *262(1-2)*, 251.

167. Islam, M. S.; Kunimatsu, K. *J. Bangladesh Acad. Sci.* **1989**, *13(2)*, 165.

168. Hahn, F.; Beden, B.; Lamy, C. *J. Electroanal. Chem.* **1986**, *204(1-2)*, 315.

169. Self, V. A.; Sermon, P. A. *J. Phys.: Condens. Matter* **1989**, *1(Suppl. B)*, SB221.

170. Korzeniewski, C.; McKenna, W.; Pons, S. *J. Electroanal. Chem.* **1987**, *235(1-2)*, 361.

171. Korzeniewski, C.; Pons, S. *J. Vac. Sci. Technol., B* **1985**, *3(5)*, 1421.

172. Holze, R. *J. Electroanal. Chem.* **1988**, *246(2)*, 449.

173. Blackwood, D. J.; Pons, S. *J. Electroanal. Chem.* **1988**, *247(1-2)*, 277.

174. Iwasita, T.; Vielstich, W. *J. Electroanal. Chem.* **1988**, *250(2)*, 451.

175. Holze, R.; Vielstich, W. *Electrochim. Acta* **1988**, *33(11)*, 1629.

176. Beden, B.; Bewick, A. *Electrochim. Acta* **1988**, *33(11)*, 1695.

177. Blackwood, D.; Korzeniewski, C.; McKenna, W.; Li, J.; Pons, S. *ACS Symp. Ser.* **1988**, *378(Electrochem. Surf. Sci.: Mol. Phenom. Electrode Surf.)*, 338.

178. Kunimatsu, K.; Samant, M. G.; Seki, H. *J. Electroanal. Chem. Interfacial Electrochem.* **1989**, *258(1)*, 163.

179. Blackwood, D.; Korzeniewski, C.; McKenna, W.; Li, J.; Pons, S. *Gov. Rep. Announce. Index (U. S.)* **1989**, *89(5)*, Abstr. No. 910,748.

180. Blackwood, D.; Pons, S. *Gov. Rep. Announce. Index (U. S.)* **1989**, *89(9)*, Abstr. No. 921,305.

181. Ashley, K.; Lazaga, M.; Samant, M. G.; Seki, H.; Philpott, M. R. *Surf. Sci.* **1989**, *219(3)*, L590.

182. Kunimatsu, K.; Samant, M. G.; Seki, H. *J. Electroanal. Chem.* **1989**, *272(1-2)*, 185.

183. Kunimatsu, K.; Shimazu, K.; Kita, H. *J. Electroanal. Chem.* **1988**, *256(2)*, 371.

184. Kunimatsu, K.; Lezna, R. O.; Enyo, M. *J. Electroanal. Chem.* **1989**, *258(1)*, 115.

185. Ozanam, F.; Chazalviel, J. N. *J. Electroanal. Chem.* **1989**, *269(2)*, 251.

186. Christensen, P. A.; Hamnett, A.; Weeks, S. A. *J. Electroanal. Chem.* **1988**, *250(1)*, 127.

187. Koreniewski, C.; McKenna, W.; Pons, S. *Gov. Rep. Announce. Index (U. S.)* **1989**, *89(5)*, Abstr. No. 910,728.

188. Bewick, A. *Proc. - Electrochem. Soc.* **1984**, *84-12(Chem. Phys. Electrocatal.)*, 301.

189. Solomun, T. *J. Electroanal. Chem.* **1986**, *199(2)*, 443.

190. Solomun, T. *Ber. Bunsen-Ges. Phys. Chem.* **1986**, *90(6)*, 556.

191. Solomun, T. *Surf. Sci.* **1986**, *176(3)*, 593.

192. Hahn, F.; Beden, B.; Kadirgan, F.; Lamy, C. *J. Electroanal. Chem.* **1987**, *216(1-2)*, 169.

193. Daroux, M. L.; Yeager, E. B.; Kalaji, M.; Cuong, N. H.; Bewick, A. *Makromol. Chem., Macromol. Symp.* **1987**, *8*, 127.

194. Beden, B.; Morin, M. C.; Hahn, F.; Lamy, C. *J. Electroanal. Chem.* **1987**, *229(1-2)*, 353.

195. Hahn, F.; Floner, D.; Beden, B.; Lamy, C. *Electrochim. Acta* **1987**, *32(11)*, 1631.

196. Lezna, R. O.; Kunimatsu, K.; Ohtsuka, T.; Sato, N. *J. Electrochem. Soc.* **1987**, *134(12)*, 3090.

197. Blackwood, D. J.; Pons, S. *J. Electroanal. Chem.* **1988**, *244(1-2)*, 301.

198. Bockris, J. O.; Yang, B. *J. Electroanal. Chem.* **1988**, *252(1)*, 209.

199. Kunimatsu, K. *J. Electroanal. Chem.* **1982**, *140(1)*, 205.

200. Kunimatsu, K. *J. Electron Spectrosc. Relat. Phenom.* **1983**, *30*, 215.

201. Kunimatsu, K. *J. Phys. Chem.* **1984**, *88(11)*, 2195.

202. Furuya, N.; Motoo, S.; Kunimatsu, K. *J. Electroanal. Chem.* **1988**, *239(1-2)*, 347.

203. Kunimatsu, K.; Seki, H.; Golden, W. G.; Gordon, J. G., II; Philpott, M. R. *Langmuir* **1988**, *4(2)*, 337.

204. Kunimatsu, K.; Seki, H.; Golden, W. G.; Gordon, J. G. *Gov. Rep. Announce. Index (U. S.)* **1988**, *88(12)*, Abstr. No. 830,008.

205. Guillaume, F.; Griffin, G. L. *Langmuir* **1989**, *5(3)*, 783.

206. Wragg, J. L.; White, H. W.; Sutcu, L. F. *Gov. Rep. Announce. Index (U. S.)* **1989**, *(7)*, Abstr. No. 915,343.

207. Lau, A.; Miller, L. *J. Am. Chem. Soc.* **1983**, *105*, 5271.

208. Sittampalam, G.; Wilson, G. *Anal. Chem.* **1983**, *55*, 1608.

209. Wang, J.; Hutchins, L. *Anal. Chem.* **1985**, *57*, 1536.

210. Ikeda, T.; Schmehl, R.; Denisevich, P.; Willman, K.; Murray, R. *J. Am. Chem. Soc.* **1982**, *104*, 2683.

211. Ohnuki, Y.; Matsuda, H.; Ohsaka, T.; Oyama, N. *J. Electroanal. Chem.* **1984**, *158*, 55.

212. Murray, R. in Electroanalytical Chemistry; Ed. Bard, A. J., New York: Dekker, **1984**; Vol. 13.

213. Notoya, T.; Poling, G. W. *Corrosion* **1979**, *35*, 193.

214. Guadalupe, A.; Abruna, H. *Anal. Chem.* **1985**, *57*, 142.

215. Cotton, C.; Smith, K.; Merrill, E.; Farrell, P. *J. Biomed. Mater. Res.* **1971**, *5*, 459.

216. Loeb, S.; Sourirajan, S. *Adv. Chem. Ser.* **1963**, *38*, 117.

217. Jones, T. P.; Porter, M. D. *Anal. Chem.* **1988**, *60*, 404.

218. Chau, L.-K.; Porter, M.D. *in press.*

219. Li, T. T. T.; Weaver, M. J.; *J. Am. Chem. Soc.* **1984**, *106*, 6107.

220. Rubinson, K.; Baker, P. *Proc. R. Soc. London, Ser. B*, **1979**, *205*, 323.

221. Pauling, L. The Nature of the Chemical Bond, Ithaca, New York: Cornell University Press, **1960**.

222. Soriaga, M.; Hubbard, A. *J. Am. Chem. Soc.* **1982**, *104*, 2735.

223. Tipson, R.; Parker, F. in The Carbohydrate, Eds. Pigman, W., Horton, D. New York: Academic Press, **1980**.

224. Toprak, C.; Agar, J.; Falk, M. *J. Chem. Soc. Faraday Trans. I*, **1979** *75*, 803.

225. Nelson, M.; O'Conner, R. *J. Appl. Polym. Sci.* **1964**, *8*, 1325.

226. Silverstein, R. M.; Bassler, G. C.; Morrill, T.C. Spectrometric Identification of Organic Compounds, 4th ed., New York: John Wiley & Sons, **1981**.

227. Atalla, R. in Preservation of Paper and Textile of Historic and Artistic Value, Ed. Williams, J., Washington, D.C.: American Chemical Society Symposium Series, **1981**.

228. Espenson, J. H. Chemical Kinetics and Reaction Mechanisms, New York: McGraw-Hill, **1981**.

229. Ward, K.; Seib, P. in The Carbohydrates, Eds. Pigman, W.; Horton, D., New York: Academic Press, **1970**, Vol *IIA*.

230. Bain, C. D.; Troughton, Y. T. T.; Evall, J.; Whitesides, G. M.; Nuzzo, R. G. *J. Am. Chem. Soc.* **1989**, *111*, 321.

231. Porter, M. D.; Bright, T. B.; Allara, D. L.; Chidsey, C. E. D. *J. Am. Chem. Soc.* **1987**, *109*, 3559.

232. Nuzzo, R. G.; DuBois, L. H.; Allara, D. L. *J. Am. Chem. Soc.* **1990**, *112*, 558.

233. Nuzzo, R. G.; Korenic, E. M.; DuBois, L. H. *in press.*

234. Sabatani, E.; Rubinstein, I.; Maoz, R.; Sagiv, J. *J. Electroanal. Chem.* **1987**, *219*, 365.

235. Somorjai, G. A. Chemistry in Two Dimensions: Surfaces, Ithaca, New York: Cornell University Press, **1981**.

236. Zisman, W. A. in Friction and Wear, Ed. Davies, R., New York: Elsevier, **1959**.

237. Kaelble, D. H. Physical Chemistry of Adhesion New York: Wiley-Interscience, **1971**.

238. Snyder, R. G.; Hsu, S. L.; Krimm, S. *Spectrochim. Acta, Part A* **1978**, *34*, 395.

239. Hill, I. R.; Levin, I. W. *J. Chem. Phys.* **1979**, *70*, 842.

240. Snyder, R. G.; Strauss, H. L.; Ellinger, C. A. *J. Phys. Chem.* **1982**, *86*, 5145.

241. MacPhail, R. A.; Strauss, H. L.; Snyder, H. L.; Ellinger, C. A. *J. Phys. Chem.* **1984**, *88*, 334.

242. Nuzzo, R. G.; Zegarski, B. G.; DuBois, L. H. *J. Am. Chem. Soc.* **1987**, *109*, 733.

243. Langmuir, I. *J. Chem. Phys.* **1933**, *1*, 756.

244. Epstein, H. T. *J. Phys. Colloid Chem.* **1950**, *54*, 1053.

245. Safran, S. A.; Robbins, M. O.; Garoff, S. *Phys. Rev. A* **1986**, *33*, 2186.

246. Finklea, H. O.; Avery, S.; Lynch, M.; Furtsch, T. *Langmuir* **1987**, *3*, 409.

247. Heavens, O. S. Optical Properties of Thin Solid Films, New York: Dover, **1965**.

248. Silverstein, R. M.; Bassler, G. C.; Morrill, T. C.; Spectrometric Identification of Organic Compounds, 4th ed., New York: John Wiley and Sons, **1981**.

249. Private communication, Nicolet Inst. Corp., Madison, WI.

250. Cardini, G.; Bareman, J. P.; Klein, M. L. *Chem. Phys. Lett.* **1988**, *145(6)*, 493.

251. Hautman, J.; Klein, M. L. *J. Chem. Phys.* **1989**, *91(8)*, 4994.

252. Chidsey, C. E. D.; Liu, G.-Y.; Rowntree, P.; Scoles, G. *J. Chem. Phys.* **1989**, *91(7)*, 4421.

253. Wilson, E. B.; Decius, J. C.; Cross, P. C., Molecular Vibrations New York: McGraw-Hill, **1955**, 285.

254. Allara, D. L.; Nuzzo, R. G. *Langmuir* **1985**, *1*, 45.

255. Joo, T. H.; Kim, K.; Kim, M. S. *J. Phys. Chem.* **1986**, *90*, 5816.

256. Widrig, C. A., Department of Chemistry, Iowa State University, **1990**, unpublished results.

257. Schultze, J. W.; Dickertman, D. *Surf. Sci.* **1976**, *54*, 489.

258. Engelsman, K.; Lorenz, W. J.; Schmidt, E. *J. Electroanal. Chem.* **1980**, *114*, 1.

259. Bewick, A.; Thomas, B. *J. Electroanal. Chem.* **1975**, *65*, 911.

260. Ulman, A.; Tillman, N. *Langmuir* **1989**, *5*, 1418.

261. Sandroff, C. J.; Herschbach, D. R. *J. Phys. Chem.* **1982**, *86*, 3277.

262. Sandroff, C. J.; Garroff, S.; Lueng, K. P. *Chem. Phys. Lett.* **1983**, *96*, 547.

263. Bain, C. D.; Whitesides, G. W. *Langmuir* **1989**, *5*, 1370.

264. Anderson, M.; Pemberton, J., Department of Chemistry, Arizona State University, private communication.

265. Riddick, J. A.; Bunger, W. B.; Sakano, T. K. Organic Solvents: Physical Properties and Methods of Purification, 4th ed., New York: John Wiley and Sons, **1986**.

266. Harris, A. L.; Rothberg, L.; DuBois, L. H.; Levinos, N. J.; Dhar, L. *Phys. Rev. Lett.* **1990**, *64(17)*, 2086.

267. Cameron, D. G.; Hsi, S. C.; Umemura, J.; Mantch, H. *Can. J. Chem.* **1981**, *59*, 1357.